NASA CR-112045
(MCR-72-51)

Final Report

INVESTIGATION OF LOW-COST ABLATIVE HEAT SHIELD FABRICATION FOR SPACE SHUTTLES

By Huel H. Chandler

Prepared under Contract No. NAS1-10793 by
MARTIN MARIETTA CORPORATION
Denver, Colorado 80201

for

NATIONAL AERONAUTICS AND SPACE ADMINISTRATION

NASA CR-112045
(MCR-72-51)

Final Report

INVESTIGATION OF LOW-COST ABLATIVE HEAT SHIELD FABRICATION FOR SPACE SHUTTLES

By Huel H. Chandler

Prepared under Contract No. NAS1-10793 by
MARTIN MARIETTA CORPORATION
Denver, Colorado 80201

for

NATIONAL AERONAUTICS AND SPACE ADMINISTRATION

FOREWORD

This report is submitted in accordance with the statement of work for Contract NAS1-10793.

The report is the result of a team effort in close cooperation with the NASA Technical Monitor, Mr. Claud Pittman. The Martin Marietta Corporation effort was managed by Mr. Daniel V. Sallis and directed by Mr. Huel H. Chandler.

CONTENTS

LIST OF ILLUSTRATIONS

LIST OF TABLES

INVESTIGATION OF LOW-COST ABLATIVE HEAT SHIELD FABRICATION FOR SPACE SHUTTLES

By Huel H. Chandler
Martin Marietta Corporation

SUMMARY

The purpose of this study was to pursue improvements in the processes and design to reduce the manufacturing costs for low density ablative panels for the Space Shuttle. The areas that were studied included methods of loading honeycomb core, alternative reinforcement concepts, and the use of reusable subpanels.

In order to determine what simplified processes and designs should be investigated, we made a review of previous studies on the fabrication of low-cost ablative panels and on permissible defects that do not affect thermal performance. From this previous work, we noted that there were considerable differences in the quoted prices for ablative panels even though the various contractors had reported similar fabrication times. This report describes how these cost differences arise from different estimating criteria, and shows which estimating assumptions and other costs must be included in order to arrive at a realistic price.

Our first area of investigation, concerned the parameters that affect loading the ablative material into the core. Our results indicate that the phenolic microspheres, which were used to reduce panel density, actually made core loading more difficult. Under normal loading pressure, they apparently deformed and interlocked, and this caused the material to resist flow, transferring the loading pressure down the core walls, rather than exerting a compacting force at the bottom of the cells. The result was improper packing of the ablative material at the bottom of the core and a density gradient through the thickness of the panel.

Composition changes generally reduced this effect and facilitated core loading, but changes in the loading method produced mixed results. Vibrating the ablator did not help move it into the core, but a sharp impact force did; and centrifugal loading produced a uniform material, but the forces judged practical for mass-production lots were apparently too low to compact the material.

Our study conclusively showed that the use of conventional honeycomb core to provide reinforcement is the largest controlling factor in establishing the cost of an ablative panel, and that the cost can be substantially reduced by using fibers, ribbons, a combination of the two, or a larger-celled core. The selected method was to reinforce the ablative panels with fiberglass ribbons, which perform the same function as the honeycomb and reduce panel fabrication costs. Phenolic impregnated ribbon provided the best overall performance.

We also found that a high concentration of fibers had a large beneficial effect in stabilizing the char, as well as in providing reinforcement. Our recommended panel constructions incorporates both fibers and ribbons for reinforcement.

The allowable strain capability of the ablator has a direct effect on the cost and weight of reusable subpanel since the subpanel design was primarily dictated by the deflection. However, to reduce the weight of the subpanel, a hogh-elastic-modulus face sheet must be used. The reusable subpanel designed under this study incorporated graphite polyimide face sheets, titanium edge members, and quick-disconnect fasteners without ablator plugs, and had a weight of 2.5 kg/m^2 (0.52 lb/ft^2).

Table 1 summarizes the panel cost per unit area for the five panel designs investigated during this study, and figure 1 shows our recommended ribbon-reinforcement configuration.

TABLE 1.- PANEL COST PER UNIT AREA

Process	Number of panels							
	1		10		100		1000	
	$/m^2	$/ft^2	$/m^2	$/ft^2	$/m^2	$/ft^2	$/m^2	$/ft^2
Baseline	2784	258.63	1492	135.58	963	89.50	648	60.26
Update	2803	260.38	1300	120.75	896	83.26	629	58.48
Pressurized core, large cell	2189	203.38	1036	96.21	708	65.75	502	46.73
No core, small glass fibers	1409	130.88	836	77.71	569	52.87	424	39.36
Ribbon construction	1472	136.75	973	90.44	666	61.86	475	44.18

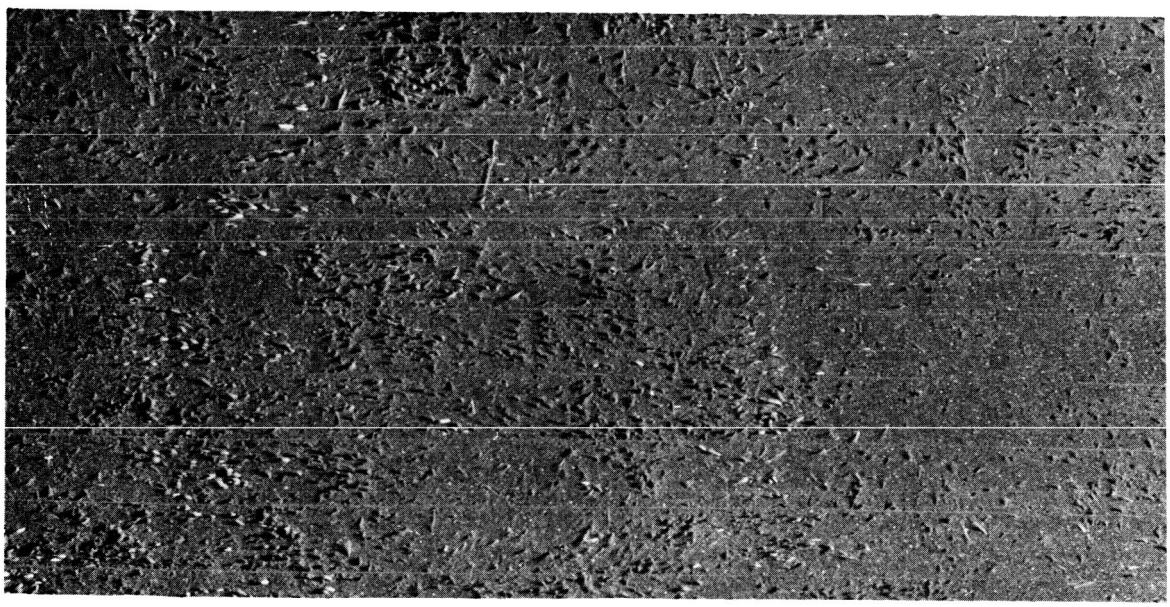

Figure 1.- Recommended Panel Construction, Ribbons

INTRODUCTION

Ablative Leaf Shields are an attractive thermal protection system for the Space Shuttle because of their high reliability and low development cost. However, since they are not a reusable system they have the disadvantage of high recurring costs. One of the primary factors contributing to this cost is the fabrication of the heat shield panels which is addressed in this study.

Under NASA Contract NAS1-9946, Low-Cost Ablative Heat Shields for Space Shuttles, costs and methodologies were developed for the present state of the art. The fabrication methods developed under that contract produced considerable cost savings over the methods used for previous vehicles like Apollo and PRIME, in which each individual cell was hand-filled with ablator.

This study showed that high manufacturing costs primarily result from the use of honeycomb core in the ablative layer. The purpose of this honeycomb is fivefold: it strengthens the ablative panel, produces a stronger attachment to the structure, bridges the pyrolysis zone, reinforces the char layer, and prevents cracks from propagating in the char. But these same design objectives can be achieved by using other types of reinforcement that will also lead to lower fabrication and material costs.

In addition we believe that panel fabrication costs can be reduced in other ways--by finding better ways to load the ablative material into the core, and by using a reusable subpanel. This latter method reduces the weight of the heat shield; and by designing the subpanel to be reusable, cost savings should result.

Under the present contract, these studies were conducted to determine if additional savings could be realized from simplifying the fabrication method and changing the panel design concept itself. The previous run and setup times recorded for each fabrication operation were analyzed to identify high-cost operations. In addition, the design concept itself was reviewed to determine what limitations and restrictions it imposed on fabrication.

The report describes the work done in investigating these areas.

COST ANALYSIS

During 1970, five contractors were awarded separate contracts to estimate the cost of producing Space Shuttle ablative panels. All of the contractors succeeded in making ablative panels that were less expensive than those for previous systems such as Apollo and PRIME. This was attributed largely to new methods that made it possible to fill all the honeycomb cells simultaneously, rather than filling each cell individually. In this study, we examined the processes used by the various contractors in order to identify the highly time-consuming steps as well as those that saved time. We knew that the operations associated with the honeycomb reinforcement were costly and, that if the core could be removed, overall fabrication costs could be greatly reduced. However, we believed that other approaches might also save time and if they could be identified.

To put all costs on a comparable basis, we assumed that they were directly proportional to the fabrication times involved. This assumption enabled us to counteract differences in labor rates, G&A rates, and overhead, and to concentrate on alternative time-saving design and fabrication concepts.

Figure 2 presents an overall cost breakdown for a typical 0.61x1.22-m (2x4-ft) low-density elastomeric ablative panel reinforced with honeycomb core (ref. 1). Raw material represents 15% of the total cost, and manufacturing, 58%. From looking at figure 3, we find that the cost of honeycomb core is more than half of the cost of all raw material. (This percentage would be much larger for panels that required a two-dimensional bending core.) Figure 4 depicts the manufacturing cost breakdown.

Three of the operations shown in figure 4--the fabrication of the subpanel, bond coating, and core loading--are operations associated with the use of honeycomb core. These three operations constitute 68% of the total manufacturing time.

All the operations involved in fabricating the subassembly and filling the honeycomb core (see fig. 5 and 6) can either be eliminated or be replaced by simply loading the ablative mix into an open mold. Obviously, by eliminating the honeycomb core and substituting a lower-cost reinforcement, panel costs can be substantially reduced.

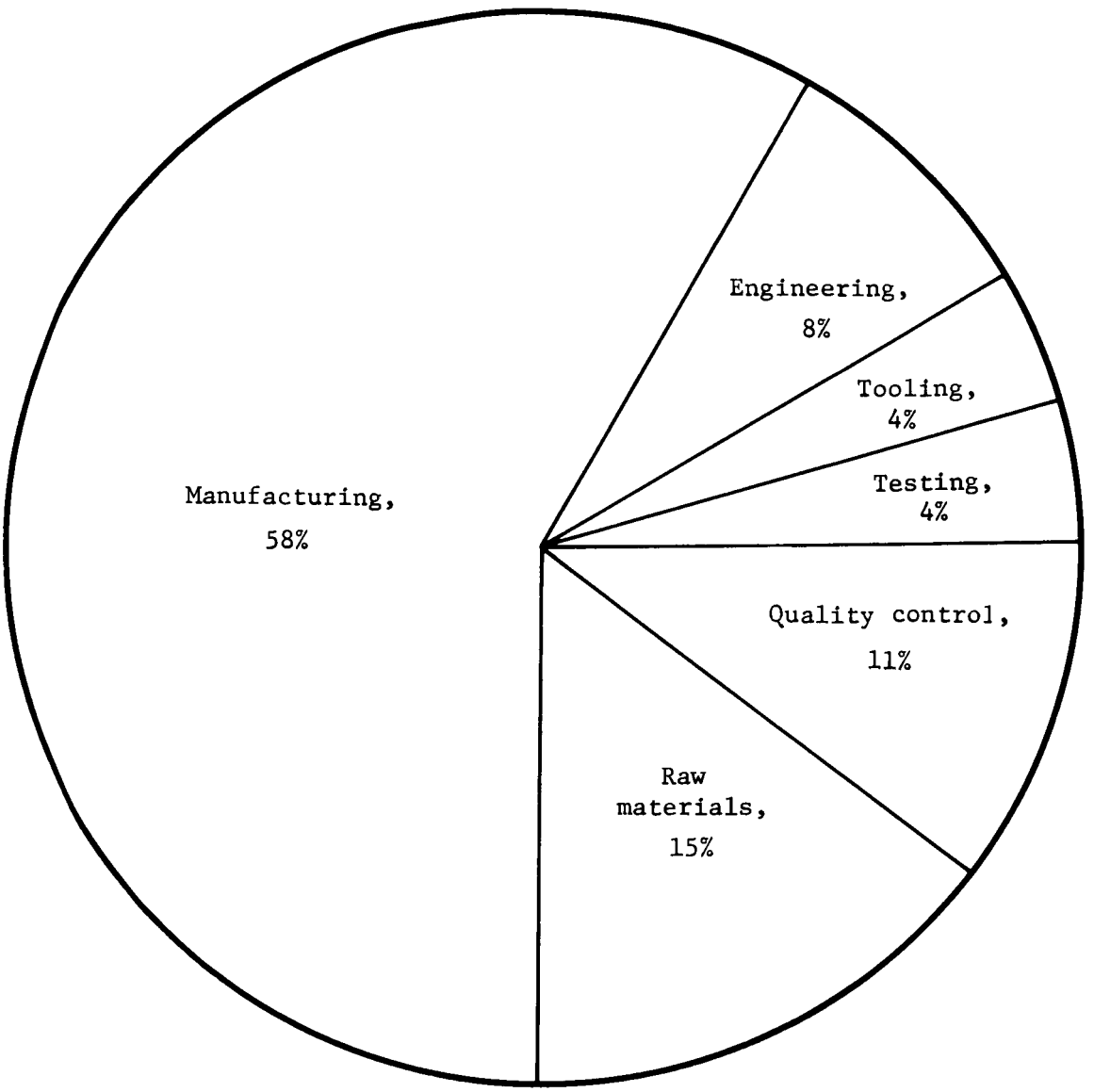

Figure 2.- Cost Breakdown for a Low-Density, 0.61x1.22-m (2x4-ft), Flat Elastomeric Ablative Panel (ref. 1)

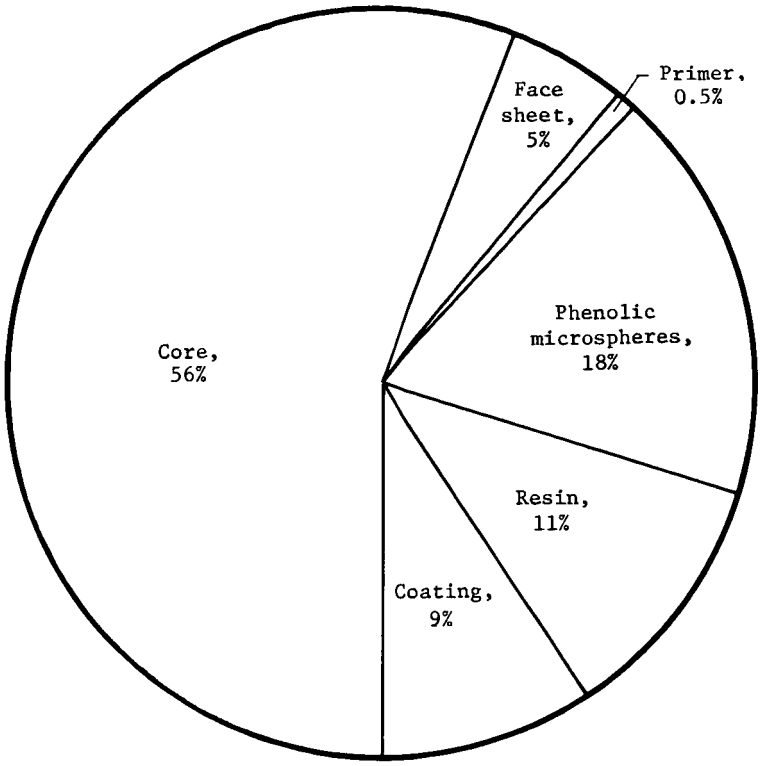

Figure 3.- Raw Material Cost Breakdown for a 90/10 (90% Phenolic Microsphere/10% Silicone Resin) Elastomeric Ablative Panel

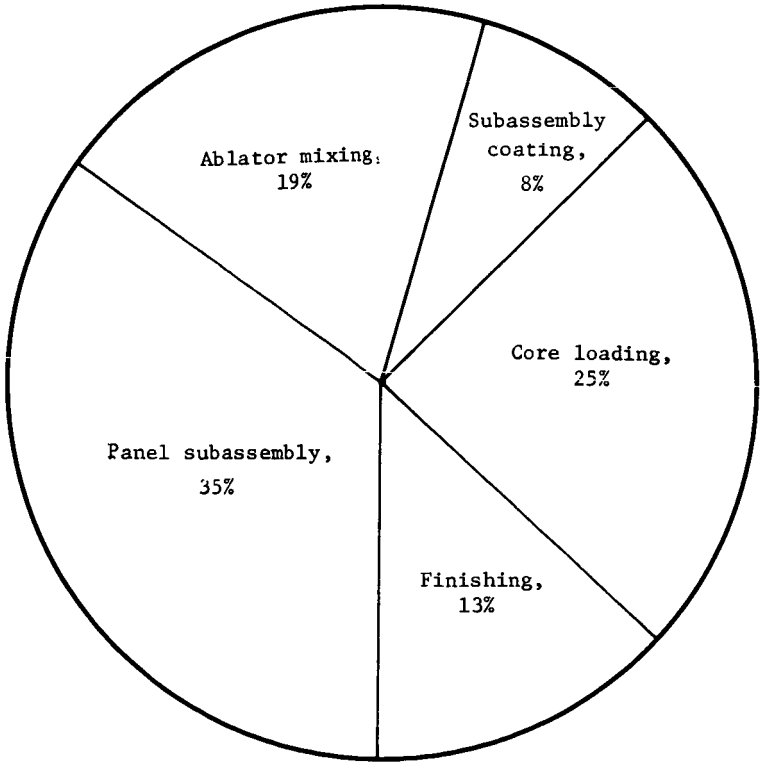

Figure 4.- Manufacturing Time Breakdown for Fabricating an Ablative Panel

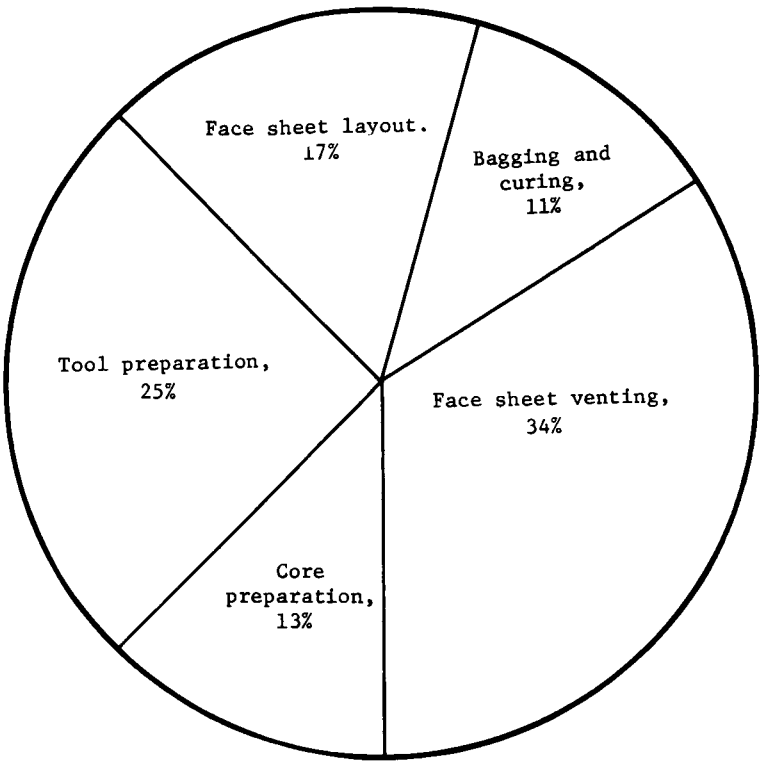

Figure 5.- Subassembly Fabrication Time Breakdown

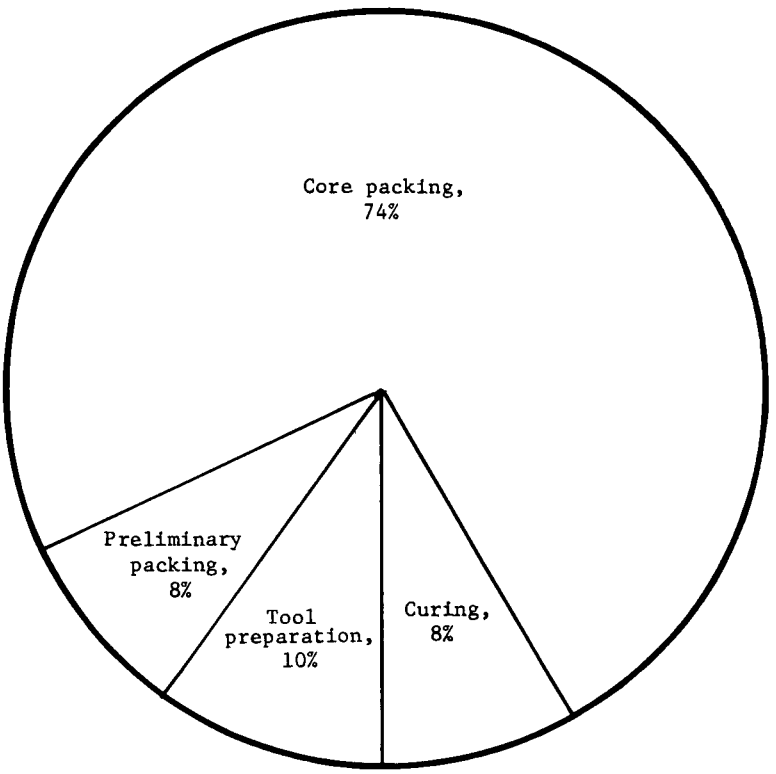

Figure 6.- Core Loading Time Breakdown

Contractors' Time Studies

To help identify other possible time-saving steps, we reviewed the fabrication times reported by the other four contractors (refs. 2 thru 5). To put each contractor's work on a comparable basis, we used only the actual times for fabricating a 0.61x1.22-m (2x4-ft) low-density elastomeric panel (see table 2). As described earlier, this eliminated the need to consider differences in the reported manufacturing support costs, inspection costs, and tooling costs, as well as these in labor rates and overhead. The analysis showed that four of the contractors' times were similar, and that North American's times were considerably higher, even though their sales prices were close to Martin Marietta's.

In reviewing these times, we discovered that several steps considered necessary for fabricating an acceptable panel had not been included by several of the contractors. The times required to complete these operations, shown in parentheses in table 2, were added to the reported times to reach an adjusted time. In addition, some of the reported times were rearranged for comparative purposes since there were basic differences in the processes used by the five contractors. Brunswick, for example, gave a single total setup time for the completed panel. Their approach was to use a match metal molding process which was not used by the other four contractors. Therefore, for comparison, the setup times were spread and some of the steps were rearranged. Because Fansteel's times were not reported in detail, only the major steps could be listed and compared.

In studying these times, we identified certain operations that took a long time to perform. These operations are listed below.

1) Preparing the honeycomb subassembly;
2) Drilling vent holes;
3) Secondary bonding of the face sheet to the core;
4) Using sprayed silicone bonding coating;
5) Loading the core with ablative material.

The time-saving steps identified from these studies were:

1) Using a tool to cut the face-sheet material;
2) Using a porous face sheet;
3) Primary bonding of face sheets;
4) Using phenolic bond coating;
5) Dip-coating the panel;
6) Using an isostatic chamber for pressing material into the core.

TABLE 2.- COMPARISON OF CONTRACTOR FABRICATION TIMES

Fabrication steps	Martin Marietta		North American		Brunswick		Fansteel		Goodrich	
	sec	hr	sec	hr	sec	hr	sec	hr	sec	hr
Subassembly										
Setup time					11 x 10^3	3.0	--- x 10^3	---		
Cut face sheet	2.9 x 10^3	0.8			4.3	1.2			6.5 x 10^3	1.8
Bag and cure			11 x 10^3	3.0					18	5.0
Cut core	2.2	0.6			5.9	1.65				
Clean core	2.2	0.6	3.6	1.0	(2.2)	(.6)*			(2.2)	(.6)*
Prepare bonding tool	6.8	1.9	11	3.0					7.9	2.2
Position assembly and vacuum bag	5.4	1.5	29	8.0					11	3.0
Cure bond	(.72)	(0.2)*	3.6	1.0					2.2	.6
Remove from assembly	.72	0.2	7.2	2.0					5.0	1.4
Drill vent holes	9.0	2.5								
Subassembly total	29	8.1	65	18.0	21	5.85	20	5.5	50	14.0
Priming of subassembly										
Setup time					1.8	0.5				
Prepare primer					4.3	1.2				
Prime core assembly										
Cure primer										
Priming total	9	2.5	14	4.0	6.1	1.7	3.6	1.0	(3.6)	(1.0)*
Filler treatment										
Setup time										
Dry microspheres	1.8	0.5					1.8	0.5	5.4	1.5
Screen microspheres	(1.8)	(0.5)*					(1.8)	(0.5)*		
Store microspheres	1.8	0.5					(1.8)	(0.5)*	1.8	.5
Filler treatment total	3.6	1.0	(5.4)	(1.5)*	(5.4)	(1.5)*	1.8	0.5	7.2	2.0
Mixing of ablator										
Setup time					2.7	0.75				
Weigh batch										
Mix resin										
Mix microspheres					7.0	1.95				
Mixing total	14.8	4.1	12.2	3.4	9.7	2.7	7.2	2.0	14.4	4.0
Core filling										
Setup time	2.5	0.7	18	5.0	7.2	2.0				
Prepare tooling	2.5	0.7	18	5.0	5.9	1.65	25.0	7.0	4.3	1.2
Weigh batch	(1.8)	(0.5)*	36	10.0	1.4	.38				
Load panel	19	5.4	43	12.0	12.4	3.45			18.7	5.2
Install vacuum bag			22	6.0	---	---	11	3.0	7.2	2.0
Cure	.7	0.2	22	6.0	2.7	.75	3.6	1.0	7.2	2.0
Remove part	.7	0.2	3.6	1.0	1.1	.30			5.0	1.4
Postcure	---	---	---	---	5.4	1.5	---	---	---	---
Core filling total	23	6.5	162	45.0	36	10.03	39.6	11.0	42.5	11.8
Machining										
Machine edges	3.2	0.9					7.2	2.0		
Machine top	5.0	1.4	3.6	1.0						
Machine attachment holes	1.4	0.4	3.6	1.0	(4.5)	(1.25)*	5.4	1.5	(7.5)	(1.25)*
Machining total	9.7	2.7	7.2	2.0	(4.5)	(1.25)*	12.6	3.5	(7.5)	(1.25)*
Prepare for shipment total	3.2	0.9	3.6	1.0	7.2	2.0	3.6	(1.0)*	(6.0)	(1.0)*
Total times reported	92.9	25.8	356	99	80.2	22.28	84.6	23.5	114.5	(31.8)
Total times adjusted†	97.2	27.0	?	?	95.9	26.63	91.8	25.5	128.3	(35.65)

*Times in parentheses were not reported but are considered necessary. They are included only in the adjusted totals.

†The adjusted total includes the times in parentheses.

Learning Curves and Other Estimating Assumptions

When a repetitive operation is performed, it tends to be done a little more efficiently each time. This can be represented by an improvement curve, which is simply a graph that expresses this in a measurable and predictable manner. If the improvement is expressed in terms of cost, the curve forecasts the extent to which the costs required to produce an item will decrease each time the item is produced. Thus, using a 95% improvement curve, the second panel takes 5% less fabrication time than the first, the fourth takes 5% less time than the second, and so on.

The use of improvement curves is based on a generalization that, within certain reasonable limits, the knowledge, skills, and techniques employed in producing a product will improve as production continues, even if there are no substantial changes in the method of production. This gradual improvement will continually reduce the time and material required to produce the product and will therefore reduce the cost of the product. A basic assumption in using improvement curves is that the rate of improvement is relatively regular and constant for any given product.

The primary use of improvement curves is to predict the cost of operation. However, any prediction is subject to error, especially when it is based on the operation of a complex industrial organization. Factors not known when the original curve is developed, such as strikes, slowdowns by employees, machinery breakdowns, and design problems, are only a few items that can cause actual improvement curves to vary from projected ones. The more skillful a person becomes in using improvement curves, the better he anticipates and allows for these unknowns; but because they are unknowns, they can never be completely accounted for. Because of this, improvement curves have to be recognized for what they are--valuable tools--but ones that involve a great deal of subjective judgment.

Effect of various learning curves.- Because predicted costs for producing ablative panels for the Space Shuttle can be based on different learning curves, we must be aware of the differences that can result. To show this, we will use three different cost improvement curves for an ablative panel and assume that the first panel costs $100 to fabricate.

We can then apply a factor, obtained from an improvement curve table, to calculate the cost reduction due to learning and skill improvement. The following tabulation illustrates the effect each improvement curve has on the initial cost of $100 per panel.

Curve	Number of panels			
	1	10	100	1000
90%	$100.00	$70.46	$49.66	$34.99
92%	100.00	75.80	57.47	43.56
95%	100.00	84.33	71.12	59.98

Note that the higher the improvement curve, the greater the cumulative average cost.

Improvement curves have a tendency to be relatively high in machine shops because there are limits on the improvement that can be realized. These limits arise from the regular use of standard shop procedures and numerically-controlled machines, and because the operators generally have an extensive knowledge of machinery and techniques. Based on our experience with machine shop operations involving numerically-controlled machines, we have used an improvement curve of 97%.

In contrast to the fabrication area, the assembly, or ablative panel fabrication, area tends to have a lower improvement curve. This is because the many operations associated with assembly allow a wider range of improvement and skill development. Our assembly operation has been giving us an overall improvement curve of 85%.

We estimate that the learning curve for fabricating ablative panels will lie between these two extremes. In view of this and past ablative heat shield production experience we recommend a learning curve of 92%.

Figure 7, which is plotted on log-log paper, shows the affect, on average times of using three different improvement curves to predict the direct times required to fabricate an ablative panel. The times are based on the time study conducted under Contract NAS1-9946 (ref. 1).

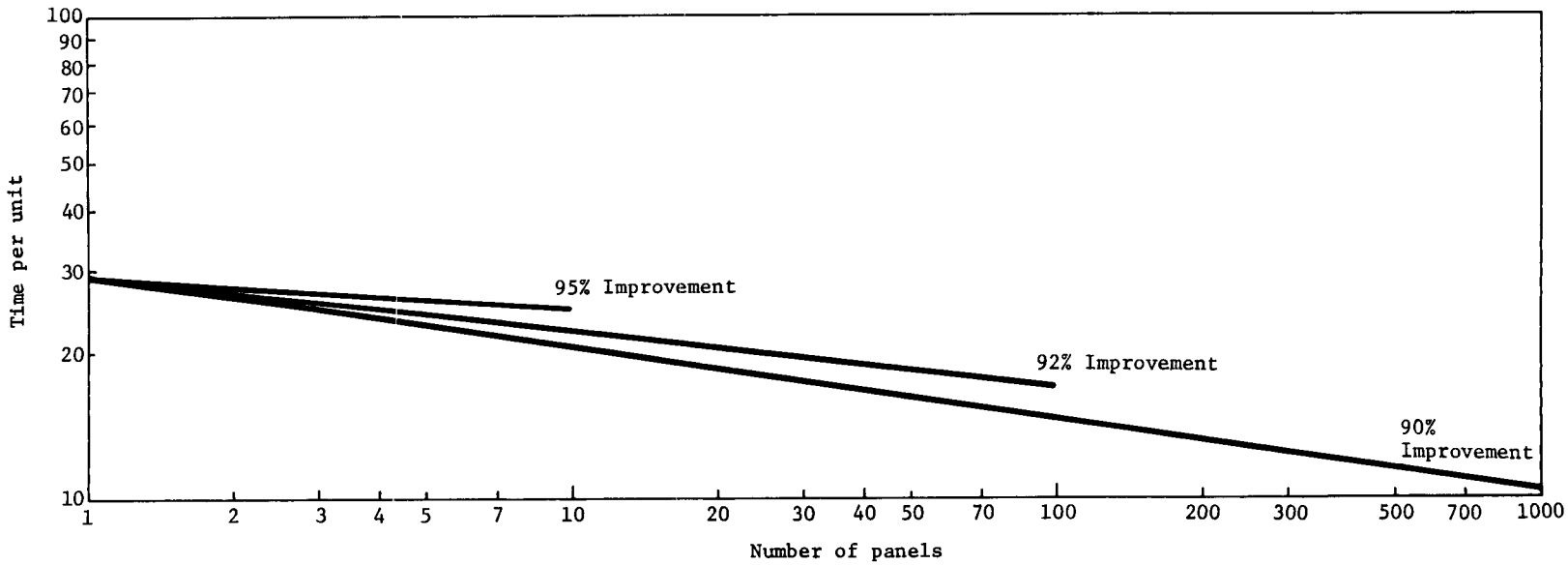

Figure 7.- Improvement Curves for Fabricating Ablative Heat Shields

Other cost factors.- Other factors besides the learning curve affect the final cost. Even though ablative panels have never been fabricated in large, mass-production lots, we can use our experience with metal working, subassembly, and final assembly to estimate how mass production affects fabrication costs. The primary effect is on the rejection rate. The factors that have the greatest influence on the rejection rate are the skill level, the availability and adequacy of tooling and facilities, and the quality of materials. Depending on these factors, the rejection rate can be as high as 10%, or as low as 7%.

Estimations of Panel Cost

During this study, we developed and priced five different methods for fabricating an ablative heat shield. The fabrication methods are described in Appendix A; the pricing methods are described in the next section. To establish a basis for comparing costs, we took the actual times shown in reference 1 for fabricating a low-density, 61x122x5-cm (2x4-ft x 2-in.) elastomeric panel, and factored in the new process times. The five methods and their code designations are listed below.

Code	Method
A	This is the old method reported in reference 1. The cost breakdown for material was adjusted to correspond to the cost of an 80/20 (80% phenolic microspheres, 20% silicone resin) elastomeric mixture, but the manufacturing times were assumed to remain the same.
B	This panel uses SS-41* ablator, a phenolic bond coating over the core, and a porous face sheet.

*SS-41 is an ablative composition developed by NASA-LRC. However, in this study we used a modification of their original formulation, and refer to this modified composition as SS-41. This change was made to improve the handling properties of the material by substituting GE 655 for GE 602 resin, and to lower the material's cost by using IG-101 in place of the Si microspheres. The following tabulation compares the two formulations.

NASA's SS-41	SS-41 as used in this study
50% Phenolic microspheres, BJO-0930	50% Phenolic microspheres, BJO-0930
25% Silicone resin, GE 602	25% Silicone resin, GE 655
15% Glass microspheres, EC Si	15% Glass microspheres, EC IG-101
10% Nylon powder, 66D	10% Nylon powder, 66D

C This process uses the SS-41 composition in a large-celled honeycomb core without a face sheet.

D This material uses fibers to replace the honeycomb reinforcement and also does not have a face sheet.

E This panel is of the ribbon construction without a face sheet.

The times shown in Appendix A are based on 30.4x30.4x5-cm (12x12x2-in.) panels and have been extrapolated to determine the equivalent times for a 61x122x5-cm (2x4-ft x 2-in.) flat panel. Figure 8 depicts the process simplifications developed under this study and summarizes the data presented in Appendix A.

Pricing Method

Because the panel sizes and phases have not been clearly defined for the Space Shuttle Orbiter and not conventionally included, we elected to omit tooling costs from the total panel cost. These tooling costs are shown separately in table 3.

TABLE 3.- TOOLING COST PER LOT

Material	Number of panels			
	1	10	100	1000
A, B, C, D, E	$3550	$3550	$7083	$10 000

Once the configurations are defined, these costs can be adjusted by using a panel complexity factor. Only the 61x122x5-cm (2x4-ft x 2-in.) flat panels were priced. In pricing them, we reviewed our previous rejection and rework percentage, 25%, which was based on the eight panels fabricated under Contract NAS1-9946. The new cost now contains a 10% rejection and rework factor, which is more in line with our present fabrication records and experience. Also, our overhead rates, G&A rates, and wages have changed since the original prices were quoted. The net result is that whereas 100 panels cost $1326/m^2 ($124/ft^2), the price is now $963/m^2 ($89.50/ft^2).

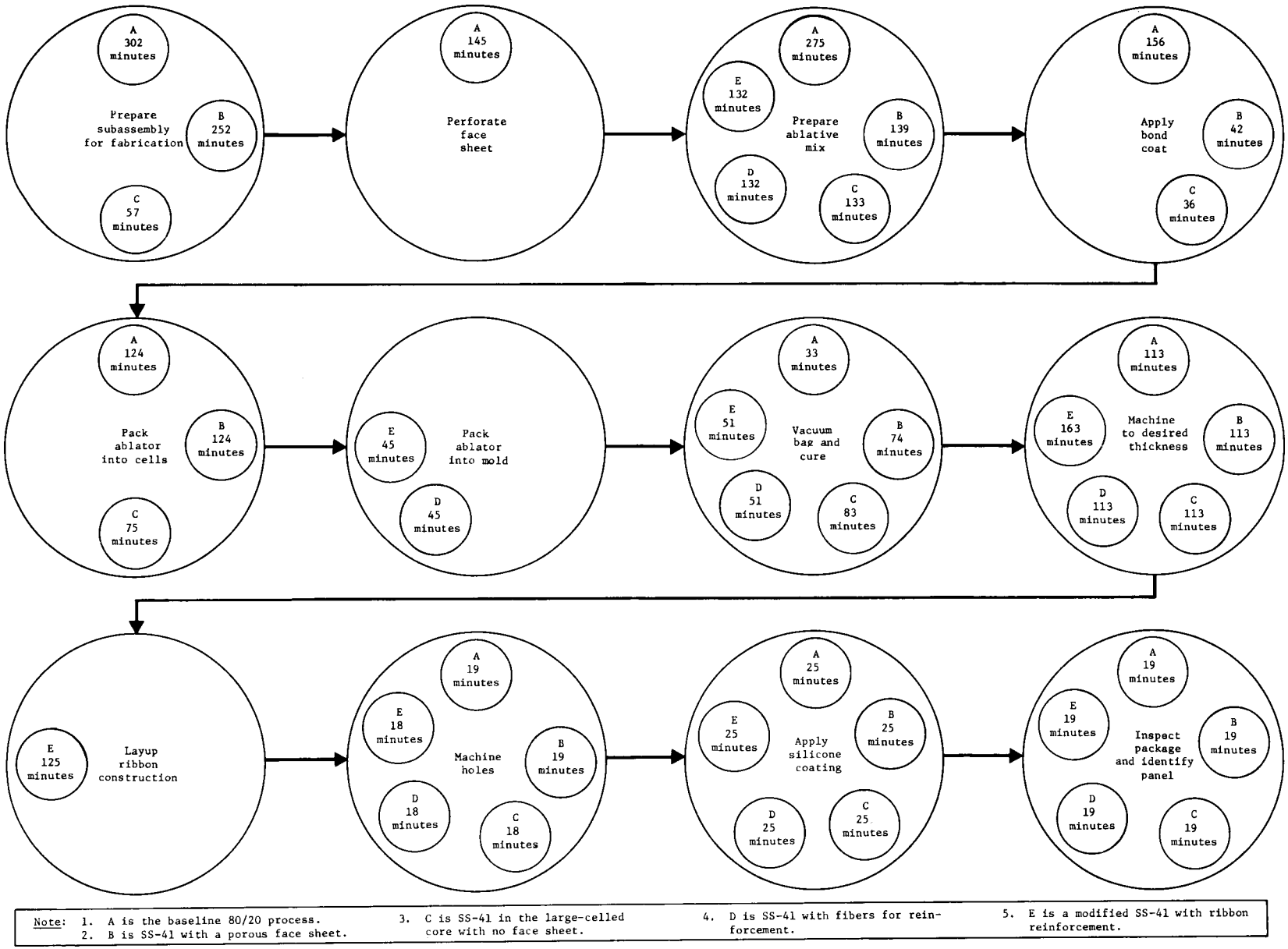

Figure 8.- Process Simplification

Pricing Assumptions

1. All estimated fabrication times are based on run times measured in the Engineering Plastics Laboratory when fabricating the 61x122x5-cm (2x4-ft x 2-in.) panels.

2. Baseline production times were derived from the actual Engineering Laboratory run times by adding a 25% factor to account for differences in skill level, motivation, etc.

3. A 95% learning curve was used for production runs for lots of 10 panels. Lots of 100 and 1000 panels were given 92% and 90% learning curves, respectively.

4. The manufacturing support factor, which is added to the direct manufacturing times, includes rejection and rework, in-scope design changes, shop supervision, production control, project support, and industrial engineering.

5. Quality control activities were estimated at 26% of the total manufacturing time, excluding the manufacturing support factor.

6. Engineering support was estimated at 20% of the manufacturing times, excluding the manufacturing support factor.

7. A limited tooling concept (nonautomated tooling) has been assumed. Under this concept, tooling is accomplished by laboratory technicians using shop aids, and without process plans. Tooling costs are priced separately.

8. All panels are to be shipped, 25 per container, in nonreusable containers.

9. All costs are based on January 1972 labor rates, and no escalation factors are added to reflect future costs.

10. No costs are added for overtime.

11. Quality assurance testing costs are based on nondestructive (radiographic) tests of each and every panel.

12. All costs exclude travel, computer time, contract data documentation, and reproduction.

13. All costs are exclusive of any fee or profit.

14. All costs include raw materials.

Tables 3 through 7 depict the various subcosts associated with the panel fabrication methods.

TABLE 4.- PANEL COST PER UNIT AREA

Process	Number of panels							
	1		10		100		1000	
	$/m^2	$/ft^2	$/m^2	$/ft^2	$/m^2	$/ft^2	$/m^2	$/ft^2
A	2784	258.63	1492	135.58	963	89.50	648	60.26
B	2803	260.38	1300	120.75	896	83.26	629	58.48
C	2189	203.38	1036	96.21	708	65.75	502	46.73
D	1409	130.88	836	77.71	569	52.87	424	39.36
E	1472	136.75	973	90.44	666	61.86	475	44.18

TABLE 5.- RAW MATERIAL COST PER UNIT AREA, UNBURDENED

Process	Number of 61x122-cm (2x4-ft) panels							
	1		10		100		1000	
	$/m^2	$/ft^2	$/m^2	$/ft^2	$/m^2	$/ft^2	$/m^2	$/ft^2
A	1214	112.75	239	22.20	182	16.94	137	12.22
B	1430	132.88	306	28.48	235	21.82	188	17.49
C	1072	99.63	230	21.36	175	16.32	141	13.12
D	487	45.25	139	12.93	111	10.32	105	9.78
E	391	36.30	144	13.40	117	10.85	106	9.83

TABLE 6.- COST PER 61x122-cm (2x4-ft) PANEL

Process	1	10	100	1000
A	$2069.00	$1084.60	$ 716.01	$ 482.09
B	2083.00	966.00	666.09	467.84
C	1627.00	769.70	526.02	373.80
D	1047.00	621.70	422.98	314.89
E	1094.00	723.50	494.91	353.41

TABLE 7.- MATERIAL COST PER PANEL, UNBURDENED

Process	Number of 61x122 cm (2x4 ft) panels			
	1	10	100	1000
A	$ 902.00	$177.60	$135.55	$101.72
B	1063.00	227.80	174.59	139.92
C	797.00	170.90	130.59	104.94
D	362.00	103.40	82.58	78.21
E	291.00	107.20	86.80	78.68

Refurbishment Cost

Tables 8 through 12 show the refurbishment cost calculated for reusable subpanels. These costs are based on a time study recorded in Appendix B. Two methods are priced: the first is our shop method, which is based on the use of only limited hand tools; the second method would require optimum tooling and a power plane that could remove more spent ablator than our present hand-held power plane.

Details of the actual refurbishment method are described in a later section of this report.

TABLE 8.- REFURBISHMENT COST PER PANEL

Process	Number of panels			
	1	10	100	1000
A, B, C, D, or E	$129.00	$109.80	$81.76	$54.55

TABLE 9.- REFURBISHMENT COST PER UNIT AREA

Process	Number of panels							
	1		10		100		1000	
	$/m^2	$/ft^2	$/m^2	$/ft^2	$/m^2	$/ft^2	$/m^2	$/ft^2
A, B, C, D, or E	174	16.13	148	13.73	110	10.22	73.40	6.82

TABLE 10.- REPLACEMENT COST PER PANEL, USING OPTIMUM TOOLING

Process	Number of panels			
	1	10	100	1000
A, B, C, D, or E	$79.00	$64.60	$46.85	$32.82

TABLE 11.- REPLACEMENT COST PER UNIT AREA, USING OPTIMUM TOOLING

Process	Number of panels							
	1		10		100		1000	
	$/m^2	$/ft^2	$/m^2	$/ft^2	$/m^2	$/ft^2	$/m^2	$/ft^2
A, B, C, D or E	106	9.88	87	8.08	63	5.86	44	4.10

TABLE 12.- TOOLING COST, USING OPTIMUM TOOLING REPLACEMENT

Process	Number of panels			
	1	10	100	1000
A, B, C, D or E	$7470	$7470	$7470	$7470

HONEYCOMB REPLACEMENT

The most effective cost-reduction method is to replace the honeycomb with other materials that will perform its basic functions. Our approach was to consider other types of reinforcement on the basis of their estimated equivalent reinforcement and to evaluate their thermal performance and their fabrication and raw material costs. The estimated equivalency approach was used because of a lack of definitive heat shield performance criteria that would clarify ablator reinforcement requirements. We feel this approach provides a realistic evaluation of alternative reinforcement methods and realistically assesses their applicability to heat-shield design and fabrication processes.

During this study, we developed three configurations that we feel meet the requirements of char and pyrolysis-zone reinforcement. The first is a panel that contains glass-phenolic ribbons on 1.3-cm (0.5-in.) centers. These ribbons extend through the depth of the panel for reinforcement. The second is a panel with larger cells. Using 1.9-cm (0.75-in.) cells instead of the conventional 0.9-cm (0.37-in.) cells facilitates core loading, and results from thermal tests show that there is essentially no difference between the two configurations. The third panel uses a high percentage of long glass fibers to stabilize the char and provide reinforcement. We believe that all three configurations are satisfactory for Space Shuttle use.

All three reinforcement concepts were evaluated thermally by plasma-arc tests. To further prove out these concepts, we also tested them in the plasma-arc large wedge configuration using 20x35-cm (8x14-in.) specimens. The ribbon-panel configuration was tested with the ribbons running parallel to the flow, as well as perpendicular to the flow. The other configurations that were tested were the fiber composition panel and the Langley SS-41 composition in the 0.9-cm (0.37-in.) cell core. We did not believe it necessary to test the large-cell core in the wedge configuration because the splash tests showed that the difference in cell size did not affect performance.

Fabrication time studies were also made for these panel configurations. The estimated fabrication costs are reported in the Cost Analysis section of this report.

Ribbon Reinforcement

During the study, we fabricated and tested several kinds of panels that used glass cloth ribbons instead of honeycomb core. Our first attempts were to cure the ablative material and the prepreg ribbons together to form the panel. Because of the springback of the compressed material and its high debulking factor, such attempts have not been successful. We then envisioned that a low-cost panel could be fabricated by first extruding the ablative material between layers of prepreg, and then cutting the ribbons produced in this continuous operation into lengths and laminating them together to form an ablative panel. The following tabulation lists the attempts that were made and their end results.

Fabrication method	Results
1. Preform prepared fiberglass into U-shaped channels and fill with ablator. Laminate together under pressure and heat.	The high debulking factor resulted in buckling of the channel legs. Difficulty in uniformly filling the channels was also experienced.
2. Preform ablator into slabs by pressing and slip the preforms into the formed channels. Cure into panel.	Springback of ablative preforms prevented sufficient material from being placed in channels. This caused the channels to buckle during curing.
3. Place layers of prepreg with alternate layers of loose ablative material. Apply molding pressure to sides of panel.	This resulted in insufficient pressure in the center of the panel, very low density, and distortion of the prepreg.

Next, work was directed toward fabricating panels from precured ablative billets. Precuring the ablative material eliminated the problems due to springback and high debulking factors, produced uniform ablative material, and enabled us to eliminate the core subassembly, the core, and the need to fill the core with ablator.

The basic procedure for fabricating these panels was as follows:

1) Mix ablative composition.

2) Place mix in mold and vacuum-bag.

3) Apply isostatic pressure to compact mixture.

4) Place mix in oven and cure under vacuum pressure.

5) Saw cured billet into strips.

6) Slice prepreg and cut to length.

7) Laminate alternating layers of ablator and prepreg.

8) Cure adhesive/prepreg according to resin used.

The first ablative mixtures that were fabricated into billets and formed into ribbon panels had the following compositions. All of these compositions could be fabricated into ribbon-type ablative panels.

Silicone resin with catalysts, pbw	Phenolic microspheres, pbw	Glass microspheres, pbw	Glass fibers, pbw
10	90	--	--
20	80	--	--
20	60	20	--
20	40	40	--
20	60	20	15
20	80	--	10

Several prepreg ribbon systems were studied to determine which was the best. Preliminary investigations revealed that a high-temperature epoxy prepreg system lacked sufficient adhesion. Consequently, all additional work was directed toward phenolic and silicone systems. Both of these systems provide enough adhesion to cause the ablative material to fail cohesively, rather than causing an adhesive failure between the ablator and ribbons. The silicone systems have an additional advantage in that they can be cured at room temperature under low contact pressure, but on the other hand, they invariably produce high-density panels because of the large amount of resin required to obtain a satisfactory bond.

To initially evaluate the feasibility of using ribbon panels, a 36x20x5-cm (14x8x2-in.) plasma-arc wedge test specimen was prepared and tested. This specimen was composed of 80 pbw of phenolic microspheres, 20 pbw of DC 182 silicone resin, and 15 pbw of 1.3-cm (0.5-in.) E-glass fibers. The ablative billet was isostatically compacted at 7 kg/sq cm (100 psi), then cured under vacuum pressure at 398°K (250°F) for 58×10^3 sec ($\sim$16 hr) and cut into 1.3-cm (0.5-in.) wide strips.

The panel was prepared by impregnating catalyzed RTV60 into strips of 181 glass cloth. The impregnated ribbons and ablative strips were laminated together under C-clamp pressure and allowed to cure overnight. The panel was then cut to the test wedge configuration.

The forward section was made with the ribbons running transverse to the flow. The last 5.6-cm (2.2-in.) strip was cut with the ribbons running perpendicular to those in the first sections in order to evaluate parallel as well as perpendicular flow during the plasma-arc tests.

A closed-circuit television record showed that the ribbons reinforced the char and prevented it from cracking during the test. However, during a subsequent inspection, some cracking was observed at the back end of the model where lower heat fluxes were present. These cracks probably occurred during cooldown, since previous tests have shown that surface cracks can be seen using the TV system.

Approximately 500 sec into the run, small molten droplets originating at the ribbons could be seen forming on the surface. A posttest examination of the panel revealed that the melting was due almost entirely to surface effects and that the amount of ribbon melted was insignificant since its recession did not exceed the shrinkage of the ablative material packed between the ribbons (see fig. 9). Based on this inspection, we concluded that the ribbons were at least as resistant as the ablative matrix.

Even though the phenolic prepreg ribbons must be cured using both heat and pressure, we recommend them over silicone resins. The system we selected consisted of phenolic resin 91LD impregnated into a 181 glass cloth fabric. This system performed well and could be cured under moderate pressure. Although we could have used lighter cloth and other phenolic compositions, the system worked well and met our goals on the program, so we used it rather than conduct a materials survey for a better system.

At first we used a heated platen press to laminate the phenolic ribbons to the ablator. However, this method could not be used for large panels, so we made an isostatic laminating tool to bond the phenolic ribbon panels together. This tool allows 0.205x0.305x0.051-m (12x12x2-in.) panels to be made using an autoclave cure.

Figure 9.- 80/20 Ablative Composition with Silicone Prepreg Ribbons

The first panel made by adding fibers to the SS-41 composition and by using phenolic laminating resin had a density of 0.378 gm/cm^3 (23.5 lb/ft^3). This was reduced to the present density of about 0.25 gm/cm^3 (15.0 lb/ft^3) by changing the SS-41 composition and reducing the packing pressure. Our final composition was:

Silicone resin (GE 655)	20%
Phenolic microspheres (BJO 0930)	35%
Nylon powder (66D)	10%
Glass microspheres (IG 101)	25%
E-glass fibers, 1.3 cm (0.5 in.) long	10%

To compact and cure the billet, the above mixture was placed in a mold and vacuum bagged. Only 48 kN/m^2 (7 psia) was used for compaction and curing. The laminating pressure was reduced from 340 kN/m^2 (50 psia) to 206 kN/m^2 (30 psi). This procedure and composition are identical to the ones used for the plasma-arc wedge specimen described later in this report, and are the ones we recommend for panel construction.

Fiber Reinforcement Concept

An ablative panel that contains only fiber reinforcement provides the lowest-cost panel. A satisfactory panel can be produced by increasing the fiber content until the reinforcement is equivalent to that provided by honeycomb core. This concept reduces fabrication costs since it eliminates the raw material used in the core--as well as the time spent in loading the ablative materials into the core--and it also produces a gain in thermal efficiency due to the lower density and the absence of conduction down the core cell walls. To date, in plasma-arc tests, we have not found evidence of detrimental cracking in the pyrolysis and char zones. We feel that this material can be shown to perform well in lower-heat-flux regions, but that extensive additional tests would be required before it can be considered for the high-heat-flux, high-shear areas.

After evaluating several compositions that used glass fiber reinforcement, we selected the SS-41 composition to which 15 pbw of glass fibers have been added as our recommended mixture. To fabricate a panel, the mixed material is spread evenly into a mold, vacuum bagged, and cured, and the cured panel is then machined to final dimensions.

We also examined the feasibility of spraying an ablator composition containing short reinforcing fibers directly onto an aluminum skin. This approach proved impractical for thick sections because the spraying operation was very time consuming and because the resulting material had a high density [0.40 gm/cm^3 (25 lb/ft^3)].

Fiberglass Thread Reinforcement

During the study, we also made and tested a panel to evaluate the use of vertical fiberglass threads for reinforcement. To fabricate the panel, an 80/20 mixture of ablative material was prepared and sandwiched between two face sheets of uncured glass phenolic prepreg. Threads of E fiberglass were then sewn through the panel using a hand awl. Next the panel was vacuum-bagged and cured, and the top face sheet was cut off, leaving the back face sheet attached by interlocking threads and by the prepreg bond to the ablator. Plasma-arc tests showed that the vertical glass fibers did not provide the necessary reinforcement.

Reduced Core Depth

A panel was made in which the honeycomb core extended down from the outer surface half-way through the ablative panel. This shallow core still provided the necessary char and pyrolysis-zone reinforcement, and made it considerably easier to fill the panel with ablator. Plasma-arc tests indicated that there was a slight improvement in thermal efficiency, which was attributed to the reduced conductivity of the core. However, the core terminated in the approximate region of the pyrolysis zone, which could provide an undesirable stress concentration that could result in spallation and loss of the char layer.

HONEYCOMB LOADING INVESTIGATION

During this task, we investigated the parameters that affect the loading of the ablative material into honeycomb core. We also studied various loading methods, as well as the effect of composition changes to facilitate loading. This task assumes that, for some reason, it is desirable to retain the core for reinforcement rather than to use reinforcing fibers or ribbons.

Past experience has demonstrated that the most difficult and time-consuming single operation in fabricating an ablative panel is that of filling the core with ablator. This is especially true when the panel is thick. What happens is that the force applied to the ablative mix is not completely transmitted to the bottom of the core, but is transferred, through friction, down the cell walls. The result is a density gradient throughout the thickness of the panel.

Analytical Investigation

To measure the effects of composition changes on the extrudability of the ablative mixture (fig. 10), we constructed an extrusion device from 5.08-cm (2-in.) pipe, using a contoured plasma-arc nozzle for the extrusion nozzle. An 80/20 mixture was placed in the extruder. It was necessary to increase the extrusion pressure to 13 800 kN/m^2 (2000 psi) in order to produce an extrusion. An examination of the extrudate revealed that, as it emerged from the nozzle, it expanded and its density decreased to 0.15 gm/cm^3 (9.1 lb/ft^3).

Because we felt that the force required to extrude the material was excessive and might possibly fracture the microspheres, and because we also felt that this technique did not accurately simulate the movement of the material into the core, these experiments were discontinued.

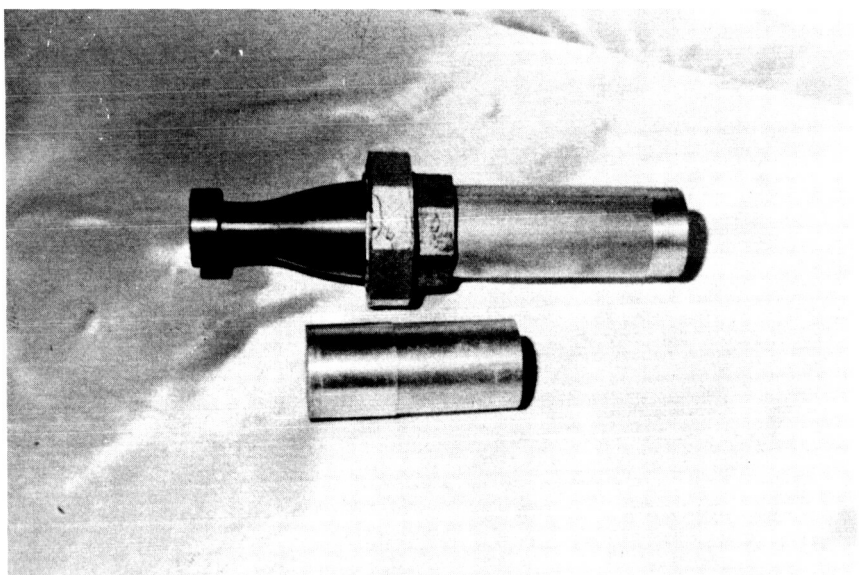

Figure 10. - Extrusion Device

Material Springback Investigation

Springback occurs when a compacted material relaxes to a lower density when the compacting pressure is removed. The springback phenomenon noted above was considered a problem because, if the pressure was not kept on a panel after it was loaded, the material would expand to a lower density. To investigate this problem we constructed a 5.08-cm (2-in.) diameter compression mold and placed an 80/20 mixture with an initial bulk density of 0.11 gm/cm^3 (6.7 lb/ft^3) into the mold. The mold's top punch was positioned and the unit was placed in a press. The material was then compressed to a density of 0.22 gm/cm^3 (14 lb/ft^3), as determined by piston travel. After the pressure was released, the movement of the piston was measured. Our calculations revealed that the mixture sprung back 19%, to a density of 0.18 gm/cm^3 (11.3 lb/ft^3).

We concluded that this high a springback must be caused by the compression of a gas, rather than a solid. Because the volume of entrapped air should be very minute and almost entirely evacuated under vacuum, the only gas available is that in the microspheres. Consequently, the microspheres must compress under pressure, and then expand back to their original shape when the pressure is released. We believe that these microspheres essentially act like a roomful of rubber balloons: when pressure is applied, they deform and interlock with each other. This makes the material act like a solid rather than a liquid. Thus, the force applied to the top of the panel no longer exerts a hydraulic pressure, but transfers itself by friction into the cell wall. As a result, the material closer to the bottom does not experience compressive forces.

If this theory is true, then substituting a microsphere with a more rigid wall should reduce the springback. Table 13 shows the effect on springback when glass microspheres, which have a higher wall rigidity, are substituted for some of the phenolic microspheres.

TABLE 13. - EFFECT OF MICROSPHERE RIGIDITY ON SPRINGBACK

Resin, pbw	Phenolic microspheres, pbw	Glass microspheres, pbw	Springback	
			cm	in.
20	60	20	1.4	0.54
20	40	40	1.1	0.43
20	20	60	.71	0.28
20	--	80	.35	0.14

In another test, designed to measure the amount of residual springback, a 25.4x25.4-cm (10x10-in.) panel was made by loading the 80/20 ablative composition into conventional honeycomb core. The panel was then vibration-impacted to a thickness of 5.7 cm (2.25 in.). A dial gauge was placed over the panel to read the amount of springback that occurred when the vacuum pressure was released and reapplied. The following data were obtained.

	Relative change of thickness, %
Impacted to 0.22 gm/cm (14 lb/ft^3)	0
Vacuum released at end of 300 sec (5 minute)	19
Vacuum reapplied	7.1
Vacuum released	15.5
Vacuum reapplied	6.7

Resin Cure Inhibition

During our efforts to establish the springback of material containing glass microspheres, we encountered another problem. An examination of the panels that had been cured revealed that the panels containing 100% and 75% glass microspheres did not cure. After checking with 3M, we learned that their microspheres contained sulfur. To remove the sulfur, a new batch of microspheres was washed with MEK. The broken spheres were allowed to settle, and were then vacuum-dried in a V-blender. This time the all-glass microsphere filler composition cured.

I-G 101 glass microspheres, an equivalent product from Emerson & Cuming, Inc., were checked for compatibility with the silicone resin. They were found to be compatible, and were used during the remainder of the program.

Vibration Loading

In another phase of the study, we conducted a series of tests using a magnetic shake table (fig. 11) to determine if vibration would assist in moving the ablative material into the honeycomb core while under vacuum pressure.

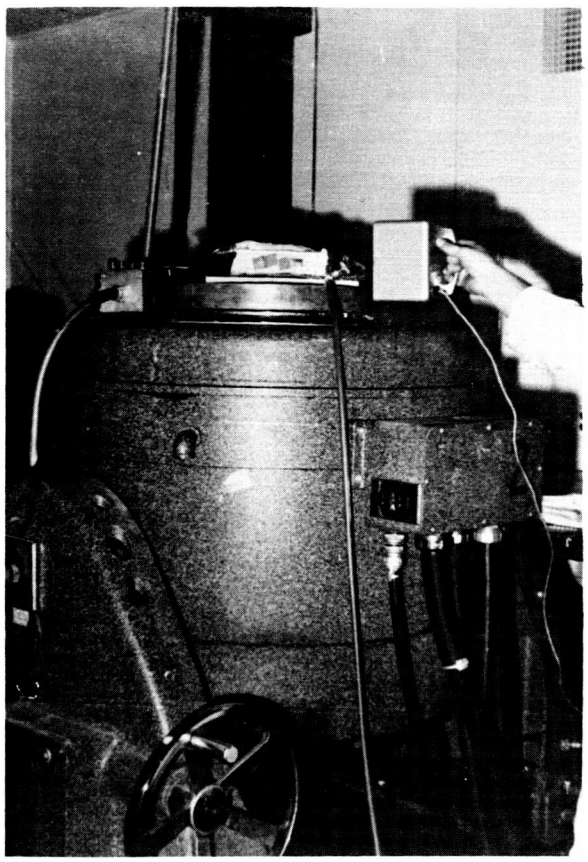

Figure 11. - Vibration Loading Fixture

TABLE 14. - VIBRATION TEST RESULTS

Panel No.	Amplitude	g level	Vacuum, mm Hg	Result
1	0.25 cm (0.1 in.), 5 to 36 Hz	10 g, 36 to 500 Hz	610	No effect
2	0.76 cm (0.3 in.), 5 to 36 Hz	20 g, 36 to 2000 Hz	610	No effect
3	0.76 cm (0.3 in.), 20 to 36 Hz	20 g, 36 to 2000 Hz	305	No effect
2	Resonance frequency survey; 3 g, 20 to 2000 Hz Audible resonance found at 230, 326, 560, and 2000 Hz			
2		20 g, 230 Hz, 1 min	0	No effect
2		20 g, 326 Hz, 3 min	0	No effect
2		20 g, 560 Hz, 3 min	0	No effect

The aluminum base of the test panel was bolted to an adapter plate, and the table was oscillated in the vertical direction, parallel to the honeycomb cells. The shaker was energized in a sine-wave mode. Two accelerometers were attached to the adapter plate to monitor and control g-loading.

A strobe light was connected to the signal generator so it would remain synchronized with the table at all frequencies.

The panels used in the vibration loading study were constructed as follows.

Honeycomb - 15.2x15.2x5.1-cm (6x6x2-in.) phenolic-glass honeycomb with 0.95-cm (3/8-in.) cells

Bond coat - Dip coat of Monsanto SC1008 phenolic bonding compound, staged for 5.4×10^3 sec (1.5 hr) at 340°K (150°F)

Base plate - 30.5x30.5x1.26-cm (12x12x1/2-in.) aluminum base plate, drilled to match the shake table adapter

Loading frame - Wood frame, 5.08-cm (2-in.) deep, attached to the base plate with wood screws

Ablative filler - 80% phenolic microspheres, 20% Sylgard 182

The method of controlling the vibration table was to use an amplitude mode for frequencies up to 36 Hz and a g-loading mode for frequencies above 36 Hz.

As shown in table 14, the vibration did not assist in moving the ablative material into the core.

Impact Loading

Next, a series of impact loading tests were conducted to determine whether they facilitated core loading. The purpose of impact loading is to force the honeycomb up while overcoming the resistive inertia of the ablative filler. A gas-operated high-g table (fig. 12) was used for testing. This device was programmed to give alternate 5-msec high-acceleration pulses and 15-msec slow-deceleration pulses. An accelerometer attached to the table was used to monitor acceleration, and a storage oscilloscope was used to record load time curves. The test panel was bolted to the high-g table so the load would be parallel to the cells.

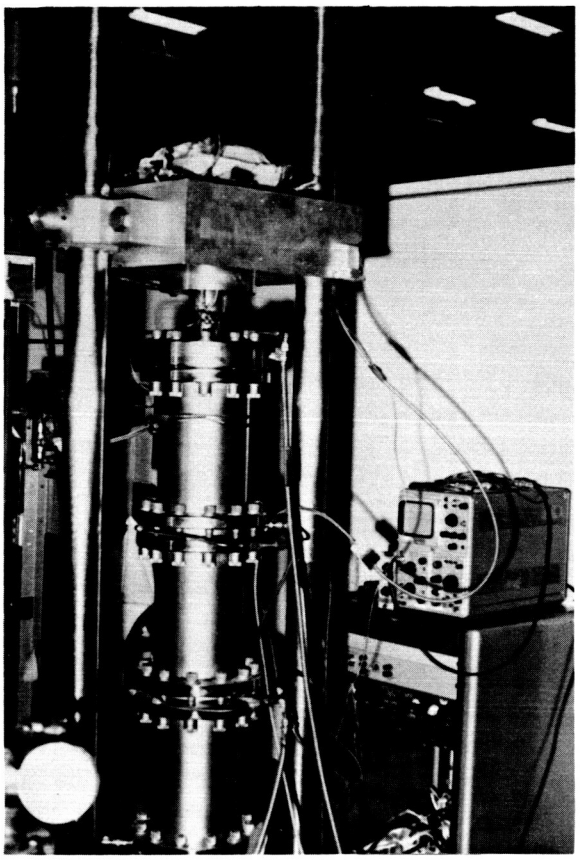

Figure 12. - Impact Loading Device

One panel was impacted five times. A vacuum of 610 mm of Hg was pulled prior to each impact; the valve was then closed and the vacuum hose was disconnected before making the test. Five separate tests were conducted: one at an impact load of 75 g, one at 77 g, and three at 88 g.

No measurable settling was observed during these tests. It was felt that this technique would be effective if a much higher g-loading could be produced.

Since rivet guns have been successfully used for loading panels, we wanted to find out if the movement they produced was due to impact or vibration. Tests were run to determine the waveform and to see if it could be duplicated on a large scale. The test was set up with an ablative panel bolted to the shake-table adapter plate, which was shock-mounted on polyurethane foam.

Using the rivet gun on the ablative head produced a 5-g load on the adapter plate. In contrast, a direct impact on the plate gave a reading of 50 g. The impact duration was 60 msec.

The rivet gun produces the type of loading we are looking for: a high impact--in one direction only--for a relatively long duration. These pulses occur about 30 times per sec.

Centrifugal Force Loading

We felt that, if a body force could be applied to the ablative material through centrifugal means, the microsphere interlocking could be overcome and the material would move down into the honeycomb core. This centrifugal force would then more closely represent a hydraulic pressure force, and would give a more uniformly dense panel because the material at the bottom of the cells would also experience the same compacting pressure.

In addition, we wanted to know whether to apply vacuum pressure on the panel while using the centrifugal loading, or whether to remove the vacuum pressure to prevent interlocking of the microspheres.

Because there are several large centrifuges available throughout the country, 300-g levels could probably be achieved economically on large panels. Therefore, our tests were limited to 300-g levels.

Six panels, each 15.2x15.2x5.08-cm (6x6x2-in.), were fabricated by using centrifugal force to load SS-41 material into 9-mm (3/8-in.) core. After being filled, the vacuum-bagged panels were evacuated to full vacuum and placed in the centrifuge, and the centrifuge was brought up to the desired g level while still under vacuum pressure. For panels 1, 3, and 6, the vacuum was applied during the entire test.

After panels 2, 4, and 5 had reached the desired g level, the vacuum pressure was released. The vacuum pressure was reapplied on panels 2 and 4 just before slowing down the centrifuge, so as to hold the material in the core; vacuum was reapplied to panel 5 sixty seconds before the centrifuge was slowed down. All panels were kept under full vacuum pressure until they cured.

Table 15 gives the test conditions and the resultant densities.

TABLE 15. - CENTRIFUGAL LOADING RESULTS

Panel no.	g level	Density		Vacuum time applied, sec	Total time, sec
		gm/cm^3	lb/ft^3		
1	175	0.222	13.9	150	150
2	175	0.228	14.2	--	150
3	300	0.218	13.6	150	150
4	300	0.219	13.7	--	150
5	300	0.221	13.8	60	300
6	300	0.219	13.7	300	300

All of the centrifugally-loaded panels were completely filled. Even though the filler material compacted slightly during the centrifugal loading, the resultant densities were still considered low. There was no apparent effect from varying the g level or from applying vacuum during the run or not.

To determine whether the loading method affected the uniformity of the ablator that had been loaded into the core, we conducted another test to compare one impact-loaded panel with one centrifugally-loaded panel. Both panels were filled with SS-41 ablator and cured for 16 hr at 394°K (250°F). The centrifugally loaded panel was cured under vacuum at sea level in Orlando, Florida, and the rivet gun-loaded panel was cured at Denver, Colorado, which has a nominal barometric pressure of 81 kN/m^2 (24 in. of Hg). Each original 5.08-cm (2-in.) thick panel was cut into four 12.7-cm (1/2-in.) thick sections, and each section was weighed separately. Both panels were found to be uniformly loaded, but the centrifugally loaded panel had a lower overall density (see table 16).

TABLE 16. - COMPARISON OF CENTRIFUGAL LOADING VS RIVET GUN LOADING

	Centrifugal panel density		Rivet gun panel density	
	gm/cm^3	lb/ft^3	gm/cm^3	lb/ft^3
Top surface layer	0.221	13.74	0.252	15.7
Second layer	0.239	14.90	0.225	14.04
Next layer	0.222	13.85	0.225	14.04
Bottom layer	0.217	13.54	0.233	14.54

Hydrostatic Loading

Vacuum bagging, isostatic compaction, and pressure compaction are all hydrostatic loading methods. Each of these methods essentially uses a unidirectional external force to push the ablative mixture into the cells of the honeycomb core. Since vacuum bagging is the simplest method, we ran a test to determine if the panels could be filled using vacuum pressure only by merely increasing the resin content.

Six 5.08-cm (2-in.) thick sections of 9-mm (3/8-in.) cell size honeycomb core were placed in loading frames and filled with different ablative compositions. The proportions (by weight) of phenolic microspheres to silicone resin, were 90/10, 80/20, 70/30, 60/40, 50/50, and 33/67, respectively. The mixtures were first hand-pressed into the core, excess material was then placed on top, and the panels were vacuum bagged.

We were unable to completely fill the core using vacuum pressure only. However, we had previously noted that adding carbon powder to silicone ablative compositions tended to make the mixture more workable. Thus, to make loading the core even easier, we also substituted silica microspheres, which have a higher modulus of elasticity, for part of the phenolic microspheres.

Two new compositions were prepared.

	Mixture 1	Mixture 2
Resin (GE 655), pbw	25	25
Phenolic microspheres, pbw	37	37
Silica microspheres, pbw	37	37
Carbon powder, pbw	--	9

We found that the second mixture could be loaded by using vacuum-bagging pressure first, and then rolling a roller over the surface. However, the first mixture would not fill the core unless it was impacted. When the two mixtures were tested in the plasma-arc, they both produced a stable char, but had lower thermal efficiencies than SS-41 materials.

Next, we investigated the effect of adding 10% carbon powder to the 80/20 and SS-41 compositions. Both materials could now be rolled down, even though a great amount of pressure was required. The carbon powder had less effect on ease of loading than in the previous composition.

Hydraulic pressure and isostatic loading methods were also investigated. Both methods proved satisfactory once the baseline composition was switched from the 80/20 mixture to the SS-41. However, the isostatic method (autoclave without heat) is preferred because the material is held in place through vacuum-bagging pressure after being compacted, which eliminates the springback problem. In using the hydraulic pressure method, we found it necessary to recompact the material with a rivet gun after vacuum bagging the panel in order to bring the panel to the desired density.

At this time, we believe that it is necessary to impact the material into the core to give a uniform density gradient from front to back. However, the present method of moving a rivet gun head over the surface is not desirable for a production-type operation since it depends too much on the individual operator for control.

In comparison the isostatic method of pressing the material into the core is the quickest and cheapest fabrication method however, it produces a high density variation through the thickness. From a theoretical standpoint it appears to be desirable to have a high density at the front of the panel and decreasing density to the backside such as that produced by this method. On this basis the isostatic-pressure loading method would be recommended since it is cheaper and appears to be thermally more efficient. However this is contingent on the ability to produce acceptable density gradients for various thickness requirements and the ability of this method to re-produce these density gradients. To-date the accepted approach has been to pursue procedures which produce the most uniform density panels. This simplifies the quality control, the design, and allows machining to desired contours. In line with this approach, which requires the most uniform panels, we recommend the impacting loading method.

PLASMA ARC TESTING

A series of screening tests were conducted in the plasma arc to thermally evaluate methods for replacing the honeycomb core and to determine the effect of compositional variations on char residue and integrity. Twenty-six specimens, each 12.7 cm (5 in.) in diameter and 5.08 cm (2 in.) thick, were tested with their surface normal to the flow (splash test). Two thermocouples were installed on each specimen. These were nominally located 1.27 and 2.54 cm (0.5 and 1.0 in.), respectively, from the heated surface. Each specimen was bonded (without face sheets or simulated structure) to an uncooled nonablating base that was then mounted to an arm mechanism for insertion into the arc jet. The specimens were tested in simulated air at the nominal test conditions listed below.

	Test condition 1	Test condition 2
Heating rate, Btu/ft^2-sec	12	25
MW/m^2	0.14	0.28
Heating time, sec	2000	1000
Steam enthalpy, Btu/lb	3000	3800
MJ/kg	6.9	8.7
Stagnation pressure, atm	0.005	0.005
N/m^2	50.6	50.6
Initial temperature of ablator, °F	80	80
Initial temperature of ablator, °K	300	300

The results of the screening test were evaluated by examining the charred specimens (surface and cross-section) and by computing the insulation efficiency for each specimen. The insulation efficiency is given by

$$E_i = \frac{\dot{q}_{cw}\, t}{\rho\, \Delta L_t},$$

where

$\dot{q}_{cw}$ = cold-wall heat flux, MW/m^2 or Btu/ft^2-sec,

t = heating time, sec,

ρ = density of uncharred material, kg/m^3 or lb/ft^3,

ΔL_t = distance from heated surface to the 422°K (300°F) isotherm, cm or in.,

and is defined as the total heat applied to the surface unit area divided by the mass unit area traversed by the 422°K (300°F) isotherm. The efficiency was determined for each specimen after 500 sec of heating by cross-plotting the thermocouple distance versus time required for each thermocouple to reach 422°K (300°F). Then the value of ΔL_t to be used in the above equation was determined by reading the distance-time curve at 500 seconds, and E_i was calculated.

The results of these temperature calculations are presented in table 17 and in figures 13 and 14. Visual observations are presented in figures 15 through 40, along with photographs of the tested specimens. These visual data are summarized in table 18. The following discussion describes the rating system used to help interpret these results.

TABLE 17.- PLASMA ARC DATA

Model data	2-1	3-1	5-1	5-2	6-1	6-2	12-1	12-2	15-1	16-1	16-2	17-1	17-2
Composition													
Resin DC 182, pbw													
Resin GE 655, pbw	25	25	25	25	25	25	25	25	25	25	25	25	25
Phenolic microspheres, pbw	37	37	37	37	50	50	50	50	50	50	50	50	50
Silica microspheres, pbw	37	37	37	37									
Glass microspheres, pbw					15	15	15	15	15	15	15	15	15
Nylon power, pbw					10	10	10	10	10	10	10	10	10
P-33 carbon powder, pbw		9											
1.3-cm glass fiber, type E, pbw			13	13								15	15
Sewn fiber threads													
Urethane foam, pbw													
Ribbon resin													
Phenolic 91LD							✓	✓					
Silicone RTV60									✓			✓	✓
0.95-cm (0.375-in.)-cell core	✓	✓			✓	✓				1 in. deep	1 in. deep		
1.90-cm (0.75-in.)-cell core													
Packing method	1	2	3	3	1	1	3	3	3	3	3	3	3
Panel density, gm/cm^3	.24	.24	.25	.25	.26	.26	.27	.27	.30	.26	.26	.40	.40
lb/ft^3	15.1	15.0	15.3	15.3	16.1	16.1	16.6	16.6	18.5	16.2	16.2	25.1	25.1
Heat flux, kW/m^2-sec	280	280	280	140	280	140	280	140	280	280		280	
Btu/ft^2-sec	24.45	24.45	25.3	12.8	24.45	12.8	25.3	12.8	25.3	25.4	12.2	25.6	12.2
Enthalpy, Btu/lb	3 724	3 724	3 915	2 942	3 724	2 942	3 915	2 942	3 915	3 947	2 267	3 772	2267
Pressure, atm	.0058	.0058	.0056	.0064	.0058	.0064	.0056	.0064	.0056	.0057	.0059	.0057	.0059
Run time, sec	1 000	1 000	1 000	2 000	1 000	2 000	1 000	2 000	1 000	1 000	2 000	1 000	2000
Ablation efficiency, J/gm	19 000	19 200	22 100	11 400	22 300	13 700	22 300	13 100	21 300	23 500	14 400	16 300	9400
Btu/lb	8 200	8 290	9 100	4 920	9 590	5 890	9 620	5 640	9 170	10 100	6 190	7 030	4050
Model recession, in.	-.069	-.074	-.106	-.100	-.068	-.066	-.074	-.067	-.031	-.079	-.074	-.005	-1.21
cm	.18	.19	.27	.25	.17	.17	.19	.17	.08	.20	.19	.01	.05
Char depth, in.	.830	.700	.560	.960	.740	1.140	.820	.940	.820	.850	.730	.700	.460
cm	2.11	1.78	1.42	2.44	1.88	2.09	2.08	2.39	2.08	2.16	1.66	1.78	1.17
Pyrolysis depth, in.	.350	.240	.320	.240	.100	.120	.100	.200	.530	.170	.190	.200	.350
cm	.89	.61	.81	.61	.25	.31	.25	.51	1.35	.43	.48	.51	.89
Time for TC 1 to reach 300°F, sec	117	93	125	139	148	238	581	182	133	124	220	181	244
Distance, TC 1 to surface, in.	.500	.465	.515	.500	.495	.520	1.025	.420	.435	.440	.425	.500	.480
cm	1.27	1.18	1.31	1.28	1.26	1.35	2.60	1.22	1.10	1.12	1.08	1.27	1.22
Time for TC 2 to reach 300°F, sec	382	386	496	526	556	812	1 296	682	596	524	840	625	885
Distance, TC 2 to surface, in.	1.050	1.030	1.080	1.045	1.000	1.045	1.55	.960	.975	.955	1.080	.975	1.010
cm	2.67	2.62	2.74	2.66	2.54	2.66	3.94	2.44	2.48	2.42	2.74	2.48	2.57

TABLE 17.- PLASMA ARC DATA - Concluded

Model data	18-1	18-2	19-1[a]	23-1	24-1	24-2	25-1	31-1	31-2	32	33	34-1	34-2
Composition													
Resin DC 182, pbw				20									
Resin GE 655, pbw	25	25			25	25	20	25	25	23	25	20	20
Phenolic microspheres, pbw	50	50		80	50	50	80	50	50	50	30	35	35
Silica microspheres, pbw													
Glass microspheres, pbw	15	15			15	15		15	15	15	25	25	25
Nylon powder, pbw	10	10			10	10		10	10	10	10	10	10
P-33 carbon powder, pbw										10	10		
1.3-cm glass fiber, type E,	15	15	5		15	15							
Sewn fiber threads				✓								10	10
Urethane foam, pbw			100										
Ribbon resin													
Phenolic 91LD	✓	✓										✓	✓
Silicone RTV60													
0.95-cm (0.375-in.)-cell core							✓			✓	✓		
1.90-cm (0.75-in.)-cell core								✓	✓				
Packing method[b]	3	3	self blown	3	3	3	5	5	5	4	4	1	1
Panel density, gm/cm^3	.39	.39	.06	.22	.27	.27	.24	.27	.27	.26	.27	.26	.26
lb/ft^3	23.5	23.5	3.8	13.9	17.0	17.0	15.1	16.7	16.7	16.2	17.0	15.8	15.8
Heat flux, kW/m^2-sec	280		280	280	280								
Btu/ft^2-sec	25.4	12.2		25.6	25.4	12.0	12.0	25.0	11.4	25.0	11.4	25.0	11.4
Enthalpy, Btu/lb	3 947	2267		3 772	3 947	2 640	2 640	4 510	2 570	4 510	2 570	4 510	2 570
Pressure, atm	.0057	.0059		.0057	.0057	.0054	.0054	.0051	.0056	.0051	.0056	.0051	.0056
Run time, sec	1 000	2000		1 000	1 000	2 000	2 000	1 000	2 000	1 000	2 000	1 000	2 000
Ablation efficiency, J/gm	18 100	9700		24 200	27 200	13 300	14 100	22 700	12 100	23 100	12 600	22 500	11 700
Btu/lb	7 810	4180		10 400	11 700	5 720	6 070	9 760	5 220	9 960	5 440	9 690	5 030
Model recession, in.	-.043	-.026		-.231	-.032	-.139	.038	-.166	-.074	-.036	-.137	-.037	-.162
cm	.11	.07		.59	.08	.03	.10	.42	.19	.09	.35	.09	.41
Char depth, in.	.665	.675	1.390	0.830	.700	.615	1.040	.775	.920	.770	.720	.570	.985
cm	1.69	1.72	3.53	2.11	1.78	1.56	2.65	1.97	2.34	1.96	1.85	1.45	2.51
Pyrolysis depth, in.		.210		.140	.250	.300	.320	.130	.190		.100	.270	.280
cm		.53		.36	.64	.76	.81	.33	.48		.25	.69	.71
Time for TC 1 to 300°F, sec	163	237		No Data	193	No Data	218	169	217	175	212	128	150
Distance, TC 1 to surface, in.	.475	.530		.545	.520	.515	.500	.490	.500	.505	.510	.490	.480
cm	1.21	1.35	1.4	1.38	1.32	1.31	1.28	1.25	1.28	1.28	1.30	1.25	1.22
Time for TC 2 (to 300°F), sec	794	977		476	947	960	798	595	834	653	850	530	600
Distance, TC 2 to surface, in.	1.065	1.060		1.045	1.020	1.035	1.030	1.010	1.060	1.070	1.050	1.020	1.030
cm	2.70	2.69	2.56	2.65	2.59	2.63	2.62	2.57	2.69	2.72	2.67	2.59	2.62

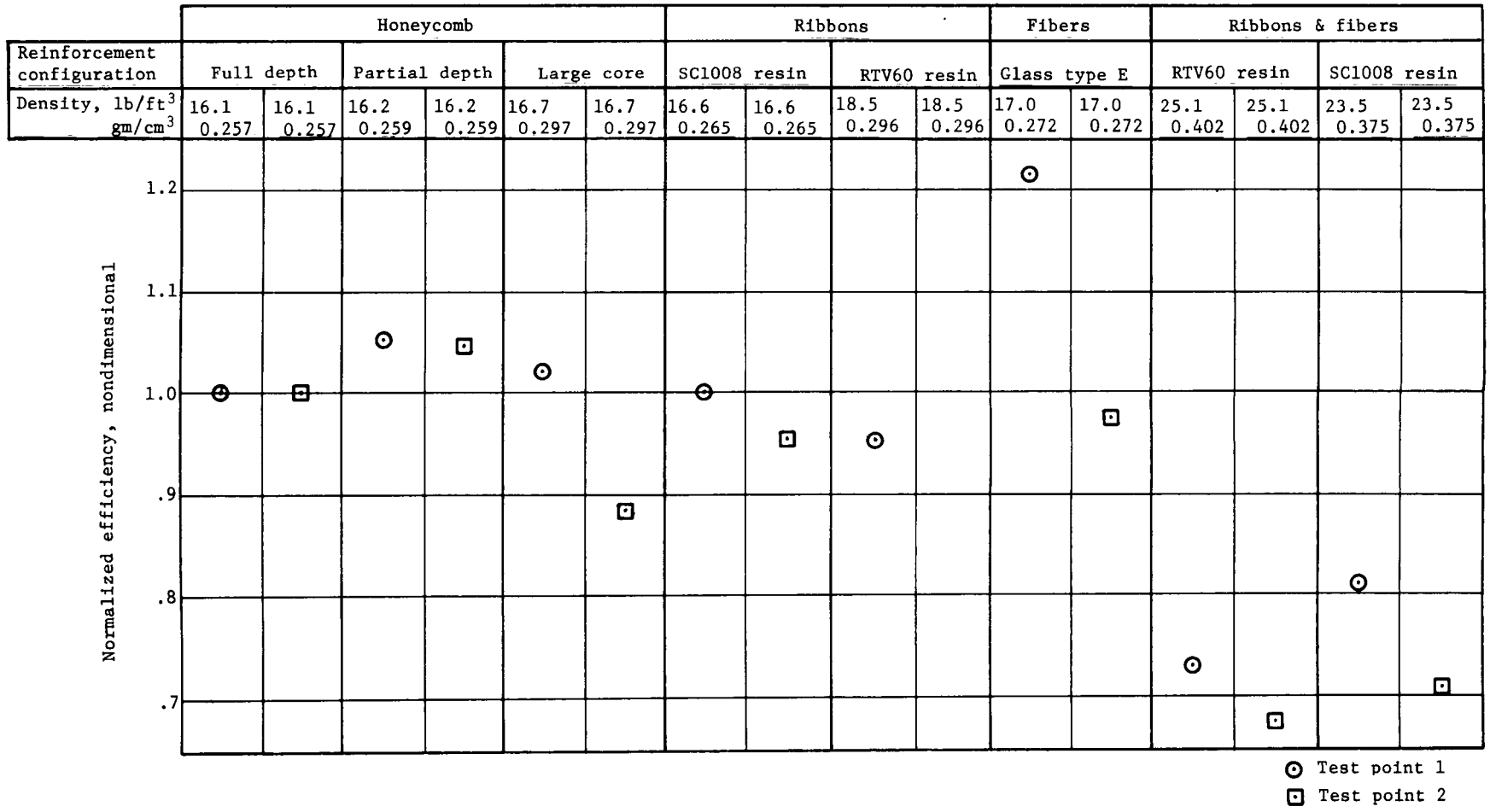

Figure 13.- Effect of Reinforcement on Thermal Performance

Composition	SS-41			High silica		High silica with carbon powder	SS-41 with carbon powder	80/20	SS-41 mixture 1	SS-41 mixture 2	
Reinforcement configuration	Core	Fibers	Ribbons & fibers	Core	Fibers	Core	Core	Core	Threads	Core	Ribbons & fibers
Density, lb/ft^3 gm/cm^3	16.1 0.257	17.0 0.272	23.5 0.376	15.1 0.242	15.3 0.245	15.0 0.240	16.2 0.259	15.1 0.242	13.9 0.222	17.0 0.272	15.8 0.253

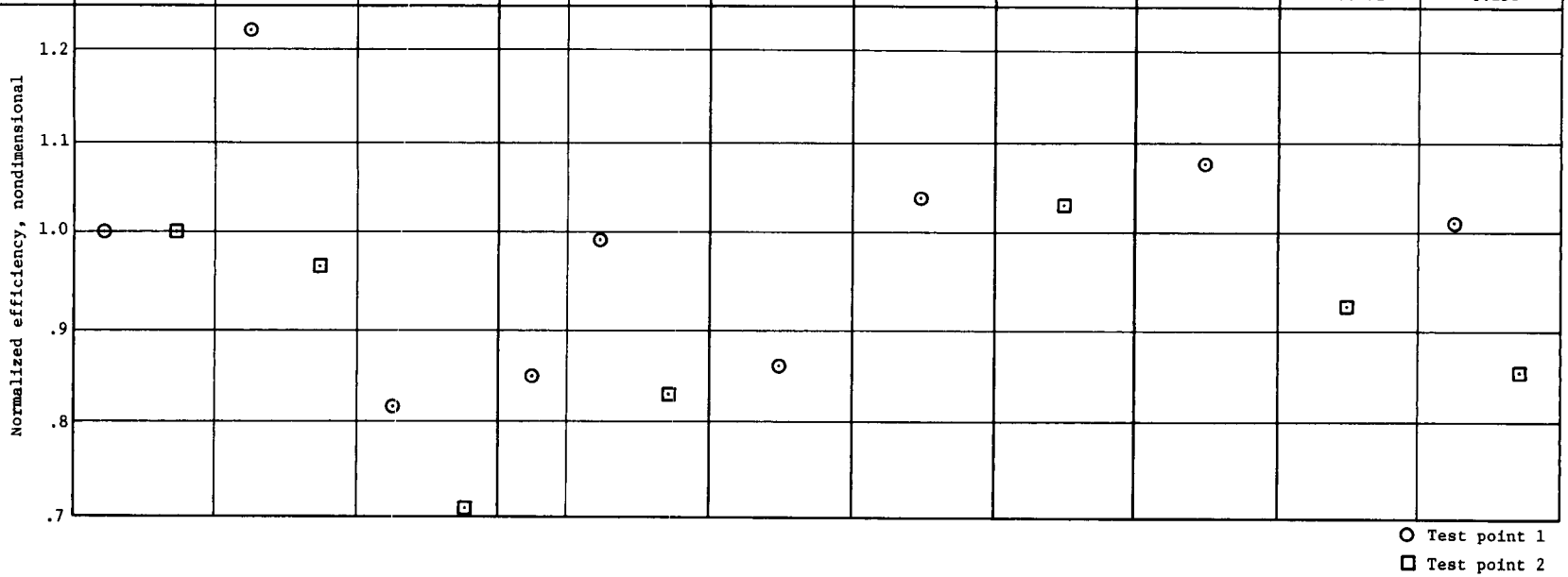

Figure 14.- Effect of Composition on Thermal Performance

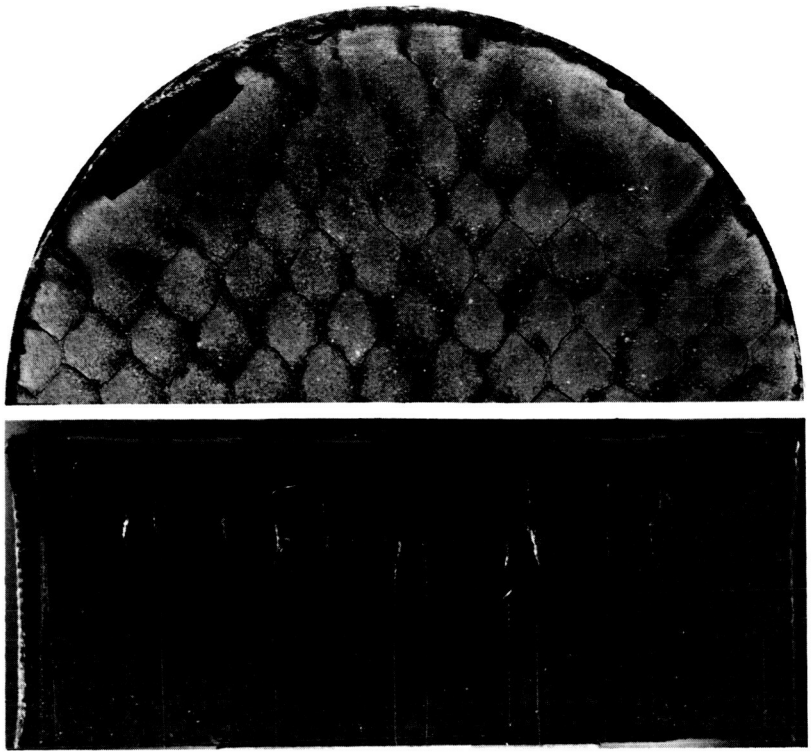

Char Surface

Toughness.- Hard surface crust firmly bonded to core, despite shrinkage cracks at cell walls (one side only).

Color.- Dull reddish-brown.

General Comments.- Surface crust blistered around edges of specimen, and was uniformly coated with a whitish (silica) deposit. Black deposits also present, and concentrated around core.

Cross-Sectional View

Char Integrity. Very low strength, with voids and cracks throughout.

Char Shrinkage.- Char pulled away from surface crust and core.

Pyrolysis Zone and Virgin Interface.- Some horizontal cracking, but interface generally appears satisfactory.

General Comments.- Char has low porosity, but is rated poor because it crumbled in many cells and pulled loose from surface crust.

Figure 15.- SS-41 in Core, Specimen 6-1

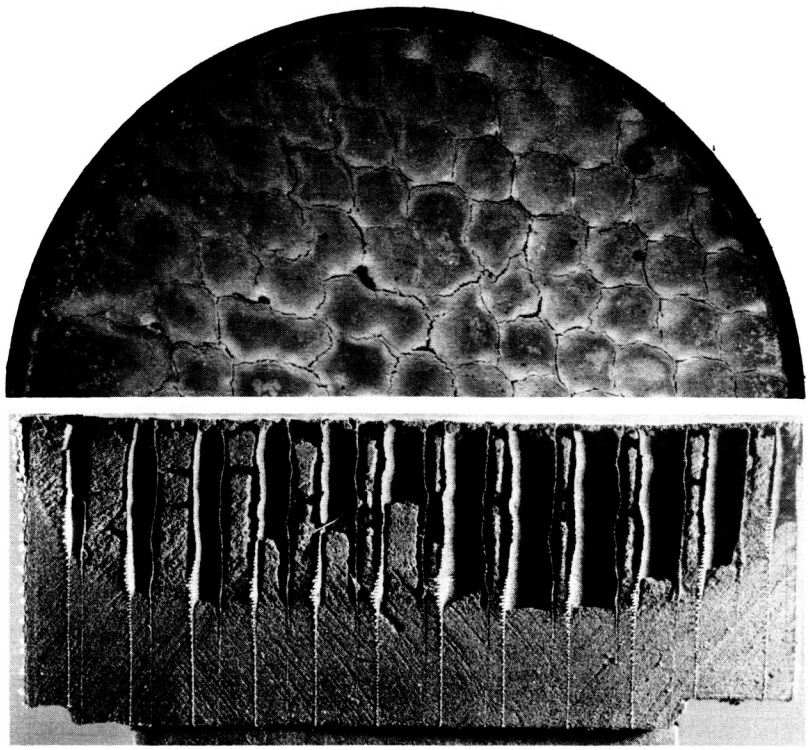

Char Surface

Toughness.- Hard surface crust firmly bonded to core, although shrinkage cracks appear around each cell (one side only).

Color.- White over a reddish-brown background.

General Comments.- Whitish-blue deposits in evidence around core. On one side of specimen, core was short of surface, which caused "mud" cracking of char. High concentrations of blowing noted.

Cross-Sectional View

Char Integrity.- Porosity uniform and low, but char was completely disbonded, cracked, and fell out of many cells upon sectioning.

Char Shrinkage.- Shrinkage apparent in both char and pyrolysis zones along cell walls. Char pulled away from surface crust, leaving a void space.

Pyrolysis Zone and Virgin Interface.- Normal pyrolysis zone and virgin interface.

General Comments.- Very poor char integrity.

Figure 16.- SS-41 in Core, Specimen 6-2

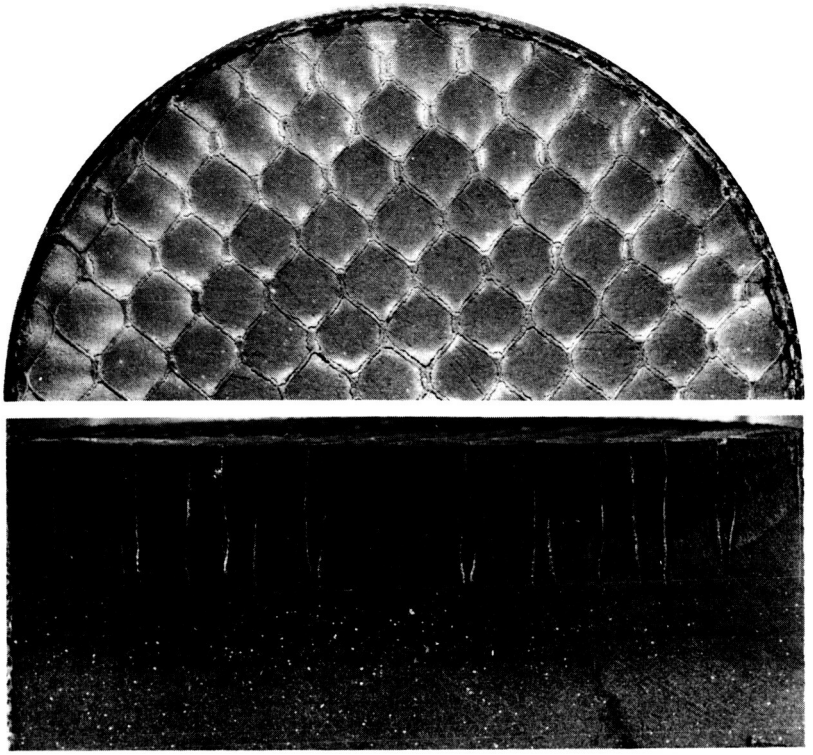

Char Surface

Toughness.- Hard surface, with very little overall shrinkage.

Color.- Reddish-brown.

General Comments.- Shrinkage cracks developed on both sides of core ribbon and left a hard char deposit on ribbon itself.

Cross-Sectional View

Char Integrity.- Very poor char, cracked throughout.

Char Shrinkage.- Char fractured in all directions, but predominantly normal to surface.

Pyrolysis Zone and Virgin Interface.- Pyrolysis zone not as badly cracked as char. Interface happened to coincide with depth of core, and appears normal.

General Comments.- Char looks essentially same as with full-depth core. Strain mismatch did not noticeably affect virgin interface.

Figure 17.- SS-41 in Partial-Depth Core, Specimen 16-1

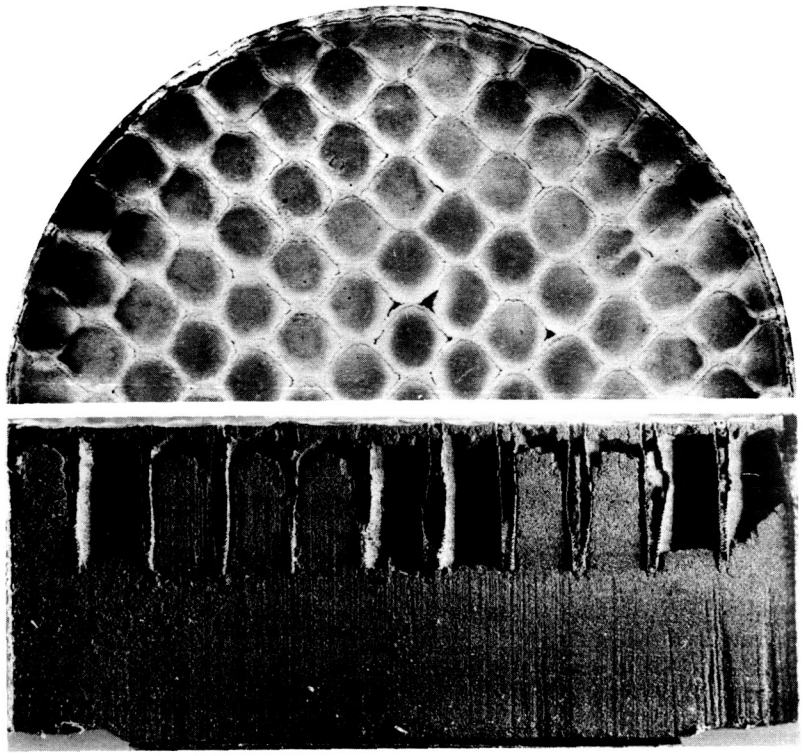

Char Surface

Toughness.- Hard surface, with very little overall shrinkage.

Color.- Nontypical gray, with bluish tint and reddish-brown background.

General Comments.- Surface is crusty looking, but hard.

Cross-Sectional View

Char Integrity.- Weak char, although not as badly cracked as at higher heating rate.

Char Shrinkage.- Typical shrinkage, with void below surface and bonding failure along both sides of core.

Pyrolysis Zone and Virgin Interface.- No cracking, but weak virgin interface.

General Comments.- Weakness at virgin interface may have been aggravated by core discontinuity.

Figure 18.- SS-41 in Partial-Depth Core, Specimen 16-2

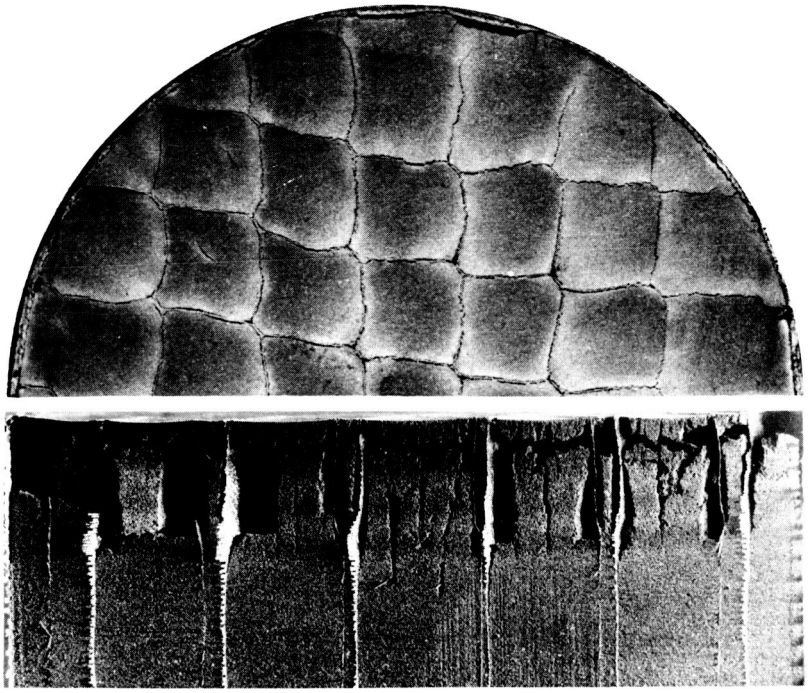

Char Surface

Toughness.- Hard surface crust with typical shrinkage cracks at core ribbons.

Color.- Very uniform light reddish-brown.

General Comments.- Surface appears fairly normal, and shows only very minor cracking.

Cross-Sectional View

Char Integrity.- Rated low because of extensive char cracking and disbonding from core, which resulted in some char loss upon sectioning.

Char Shrinkage.- Large shrinkage, void below surface char, and disbonding from core.

Pyrolysis Zone and Virgin Interface.- Only visible means of char support is through pyrolysis zone and virgin interface, and char is, therefore, rated only as fair.

General Comments.- Larger-celled core has not significantly affected char stability. Apparent cracks in virgin material of center cell actually resulted from cutting through thermocouple wires.

Figure 19.- SS-41 in Large Core, Specimen 31-1

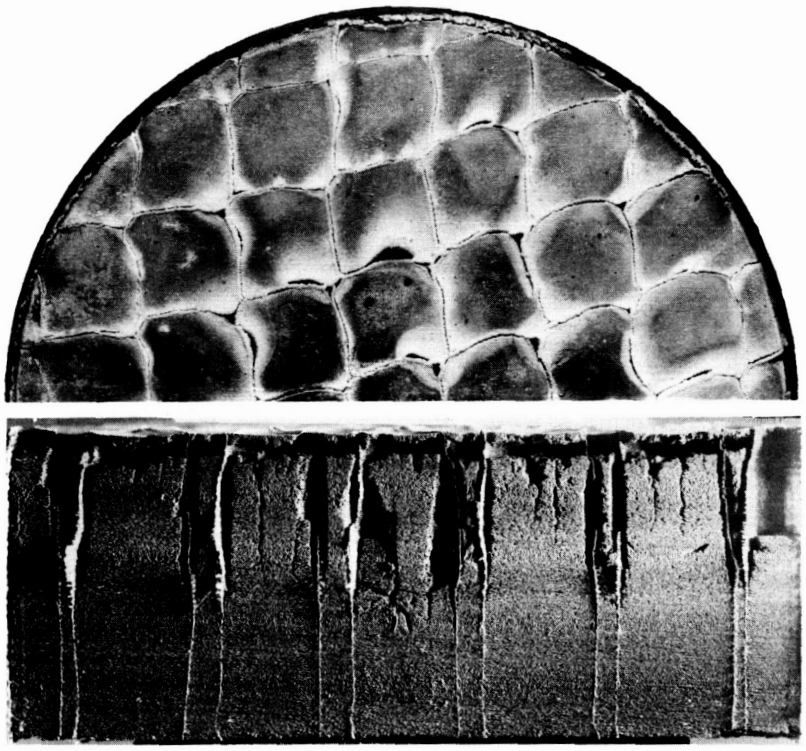

Char Surface

Toughness.- Hard surface, very thin and weak with typical shrinkage cracks at core ribbons.

Color.- Wine-colored, with white, yellow-green, and bluish deposits.

General Comments.- Char slumping left dimpled surface.

Cross-Sectional View

Char Integrity.- Rated low due to char cracking, subsurface voids, and disbonding.

Char Shrinkage.- Char characterized by large shrinkage, voids below surface char, and disbonding from core.

Pyrolysis Zone and Virgin Interface.- Pyrolysis zone appears fairly strong and is only visible means of support for char.

General Comments - Char zone appears identical to char formed at the higher heating rate (fig. 19) and for smaller core (fig. 15).

Figure 20.- SS-41 in Large Core, Specimen 31-2

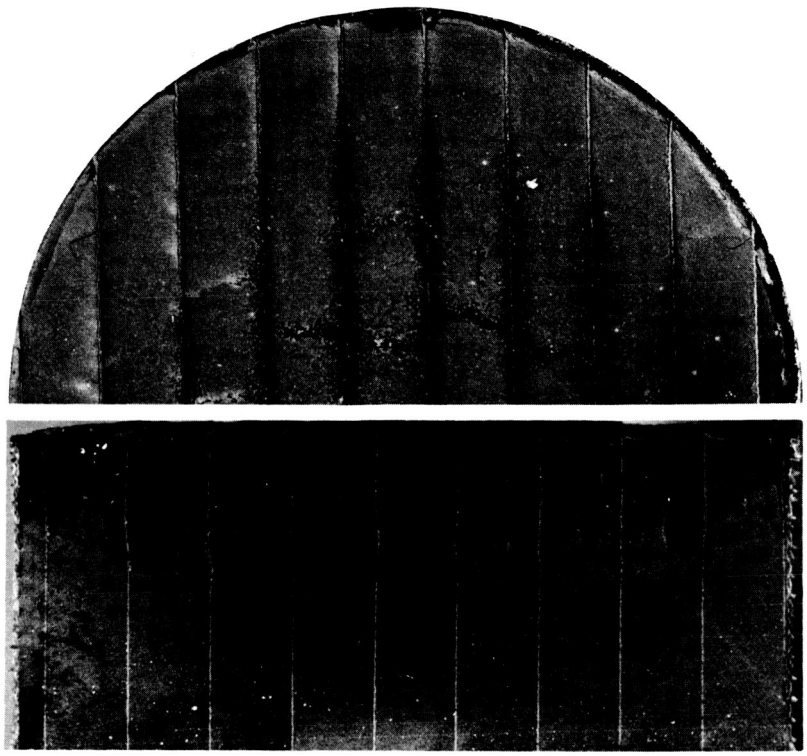

Char Surface

Toughness.- Hard char surface, with some cracks running normal to ribbons.

Color.- Dull uniform reddish-brown surface.

General Comments.- Carbonaceous deposition along ribbons.

Cross-Sectional View

Char Integrity.- Rated poor due to bond failure at core, some char loss on sectioning, and many vertical shrinkage cracks running through char and pyrolysis zone.

Char Shrinkage.- Char and pyrolysis-zone shrinkage have pulled apart char layer just below surface, leaving a large subsurface void.

Pyrolysis Zone and Virgin Interface.- Pyrolysis zone is badly cracked, but exhibits typical strength for this composition. No horizontal cracks at virgin interface.

General Comments.- Char formed integrally in ribbon direction; this lateral restraint prevented major char loss from sectioned specimen.

Figure 21.- SS-41 with Phenolic-Coated Ribbons, Specimen 12-1

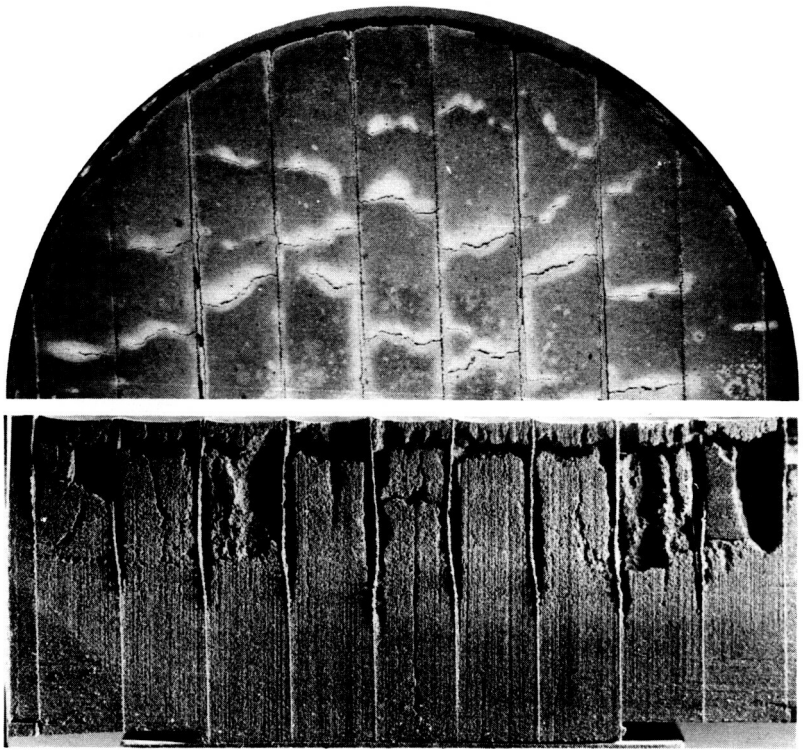

Char Surface

Toughness.- Hard char surface, with many cracks normal to ribbons.

Color.- Reddish-brown background with large amount of whitish silica residue along cracks.

General Comments.- Typical shrinkage cracks along ribbons.

Cross-Sectional View

Char Integrity.- Very weak, with some disbonding from ribbons and cracking within char layer.

Char Shrinkage.- Large shrinkage cracks below char surface and along ribbons.

Pyrolysis Zone and Virgin Interface.- Typically friable pyrolysis zone, but not as badly cracked as in Specimen 12-1 (fig. 21).

General Comments.- Rated poor due to large gaps between char and ribbons, deflection of ribbons, and extreme char shrinkage, which resulted in bond failure.

Figure 22.- SS-41 with Phenolic-Coated Ribbons, Specimen 12-2

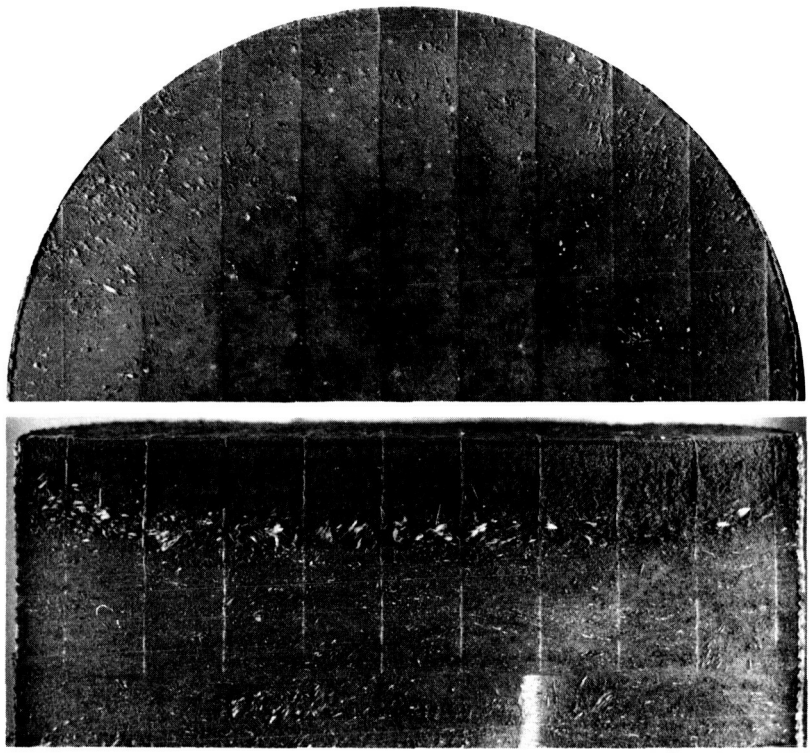

Char Surface

Toughness.- Very hard char surface. No cracking or disbonding.

Color.- Dull reddish-brown.

General Comments.- Surface appears rough due to fiber ends and some carbonaceous deposits, but seems very good. Bonding with ribbons is excellent.

Cross-Sectional View

Char Integrity.- Strong char, but highly porous.

Char Shrinkage.- None observed. Very good bond with ribbons.

Pyrolysis Zone and Virgin Interface.- Typical soft pyrolysis zone, but fibers bridge interface and reduce shrinkage and cracking.

General Comments.- Fibers doing an excellent job in breaking up thermal strains to reduce shrinkage and cracking. This configuration is our recommended type of construction and composition.

Figure 23.- SS-41 with Fibers and Phenolic-Coated Ribbon Reinforcement, Specimen 18-1

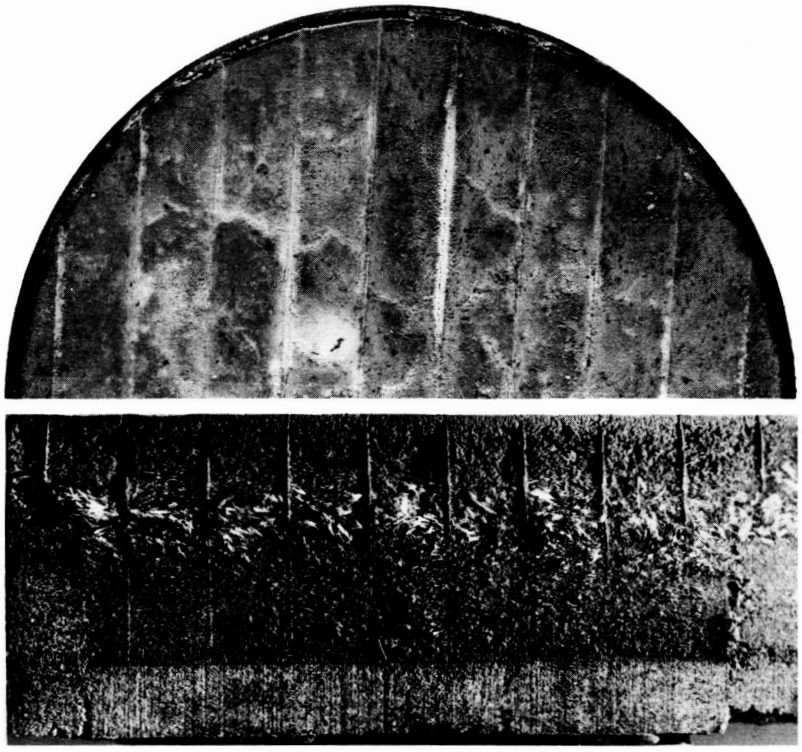

Char Surface

Toughness.- Very hard char surface and intact ribbon bond. Some extremely small cracks, generally across ribbons.

Color.- Light reddish-brown.

General Comments.- Good char surface, but somewhat rough.

Cross-Sectional View

Char Integrity.- Strong char, but friable and porous, with absence of fibers. Fibers on surface melted.

Char Shrinkage.- None observed. Very good bond with ribbons.

Pyrolysis Zone and Virgin Interface.- Typical soft pyrolysis zone, but fibers bridge interface. Interface appears normal.

General Comments.- Good cross-sectional appearance, but fibers are unbonded in pyrolysis zone.

Figure 24.- SS-41 with Fibers and Phenolic-Coated Ribbon Reinforcement, Specimen 18-2

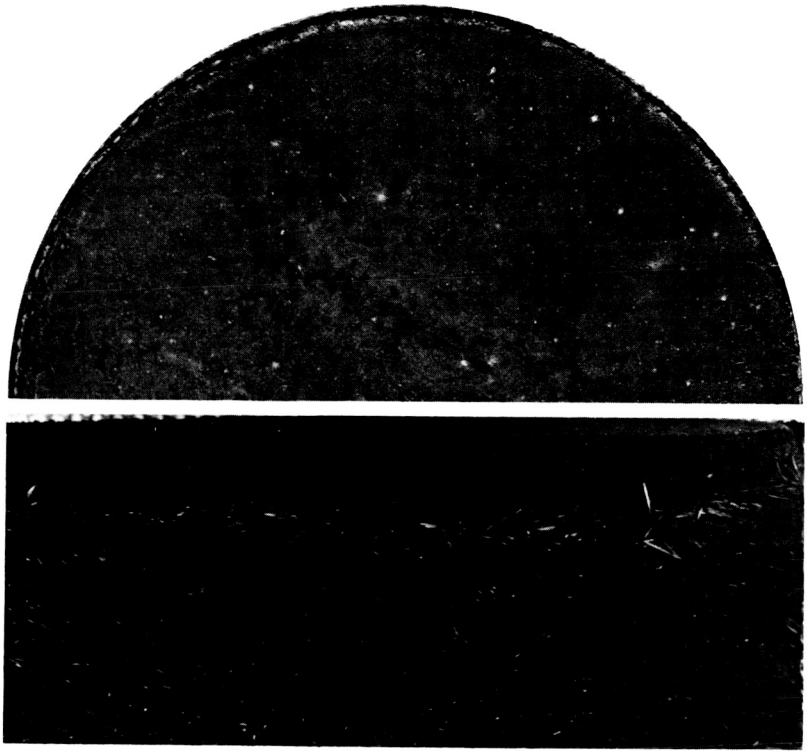

Char Surface

Toughness.- Very hard char surface.

Color.- Reddish-brown and very uniform.

General Comment.- Glass melting from fibers tended to leave a somewhat rough surface.

Cross-Sectional View

Char Integrity.- Very good carbonaceous char.

Char Shrinkage.- Only evidence was slight concavity of surface.

Pyrolysis Zone and Virgin Interface.- Typical soft pyrolysis zone, but holds together well. Interface appears good.

General Comment.- Melting of fibers in char enhances char strength.

Figure 25.- SS-41 with Fiber Reinforcement, Specimen 24-1

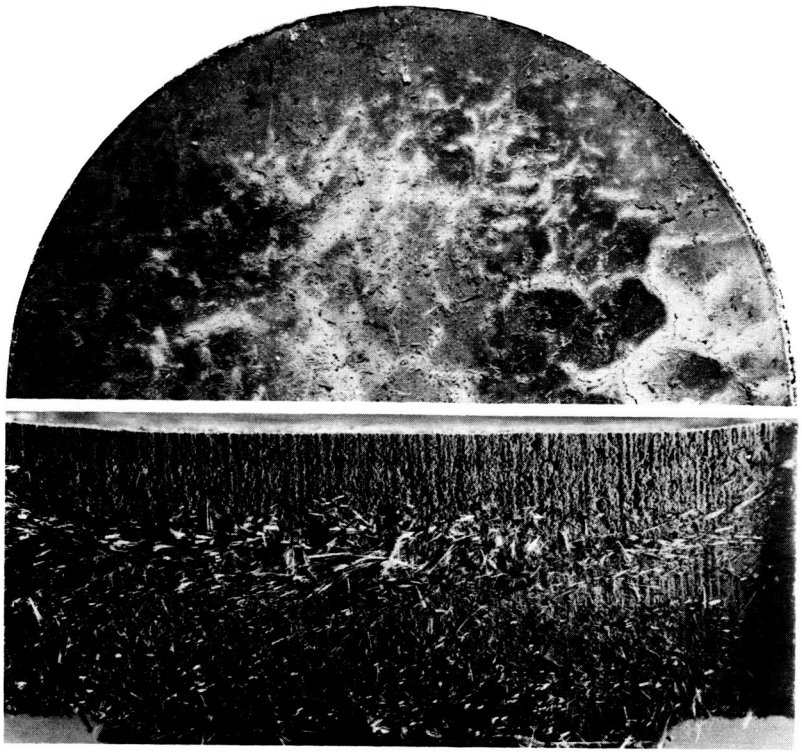

Char Surface

Toughness.- Very hard char surface with some "mud" cracking.

Color.- Multicolored--reddish-brown, green, white, and yellows.

General Comments.- Some surface roughness due to fiber melt and offgassing residues.

Cross-Sectional View

Char Integrity.- Very good carbonaceous char.

Char Shrinkage.- Only evidence of shrinkage was slight concavity of surface.

Pyrolysis Zone and Virgin Interface.- Typical pyrolysis zone, with fibers well dispersed. Interface appears normal.

General Comments.- Cross-section appears normal.

Figure 26.- SS-41 with Fiber Reinforcement, Specimen 24-2

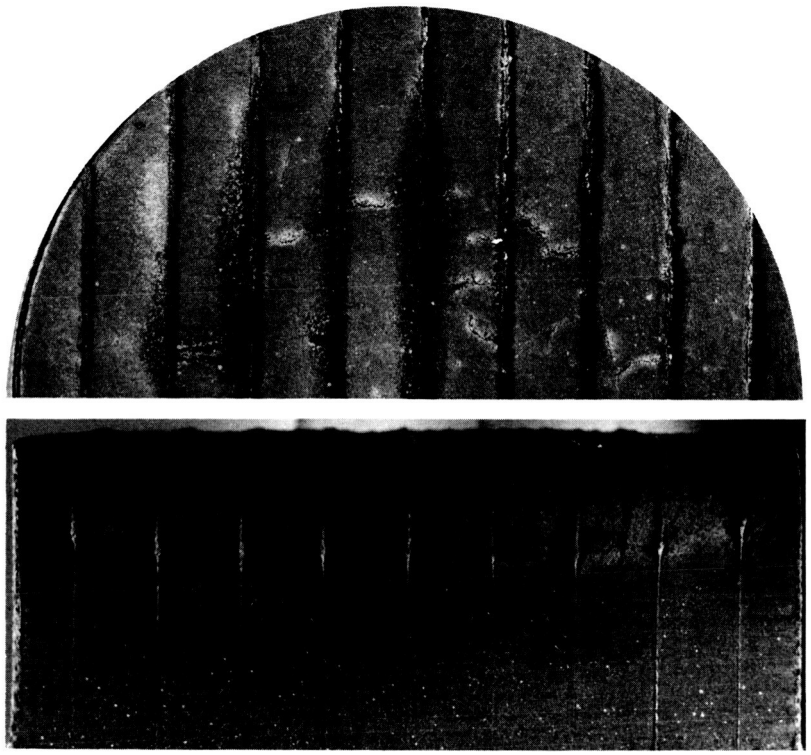

Char Surface

Toughness.- Hard surface with some char cracking.

Color.- Dull reddish-brown, with some hard black deposits along ribbons.

General Comments.- Slight protrusion of ribbons above surface may be caused by expansion of RTV 60 or by char "slippage" and rebonding.

Cross-Sectional View

Char Integrity.- Char is bonded to core, has good strength and low porosity near surface.

Char Shrinkage.- Appreciable shrinkage and bond failure in pyrolysis zone.

Pyrolysis Zone and Virgin Interface.- Weak pyrolysis interface, with some cracking.

General Comments.- Char separated (pulled apart) below the surface, as evidenced by char loss from pyrolysis zone on sectioning.

Figure 27.- SS-41 with Silicone-Coated Ribbons, Specimen 15-1

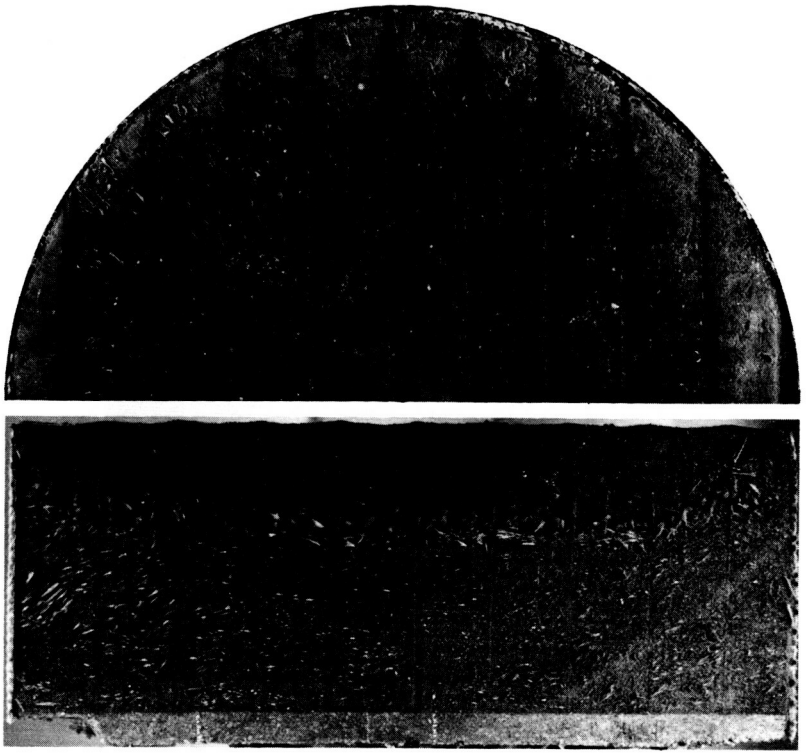

Char Surface

Toughness.- Hard char surface formed. No significant cracking or disbonding.

Color.- Black, with reddish-brown edges.

General Comments.- Some char slumping between ribbons.

Cross-Sectional View

Char Integrity.- Very rigid char with excellent ribbon bonding and very low porosity.

Char Shrinkage.- No bond failure or char cracking.

Pyrolysis Zone and Virgin Interface.- Pyrolysis zone and interface appear very good.

General Comments.- Fibers and ribbons working together very well to reduce thermal strains and cracking.

Figure 28.- SS-41 with Fibers and Silicone-Coated Ribbon Reinforcement, Specimen 17-1

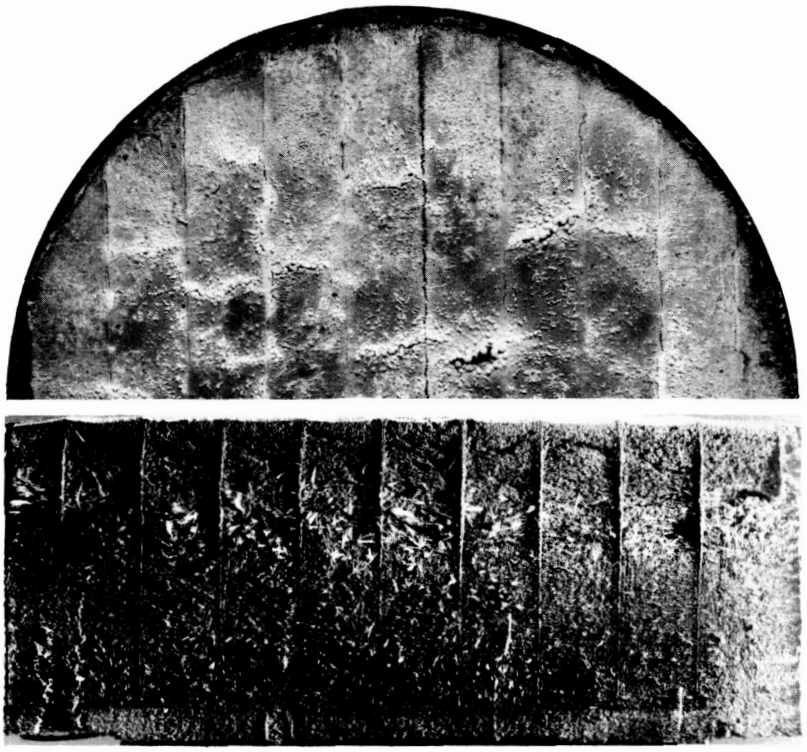

Char Surface

Toughness.- Hard char surface, with significant cracking across ribbons.

Color.- Cinnamon colored.

General Comments.- Silica globules highly concentrated around surface cracks. Surface generally very rough.

Cross-Sectional View

Char Integrity.- Char has fair strength and is well bonded to ribbons, but is friable, cracked, and rather porous.

Char Shrinkage.- Evidence of subsurface cracks.

Pyrolysis Zone and Virgin Interface.- Both appear good.

General Comments.- Char layer is very distinctive (1/2-in. thick) and absent of fibers.

Figure 29.- SS-41 with Fibers and Silicone-Coated Ribbon Reinforcement, Specimen 17-2

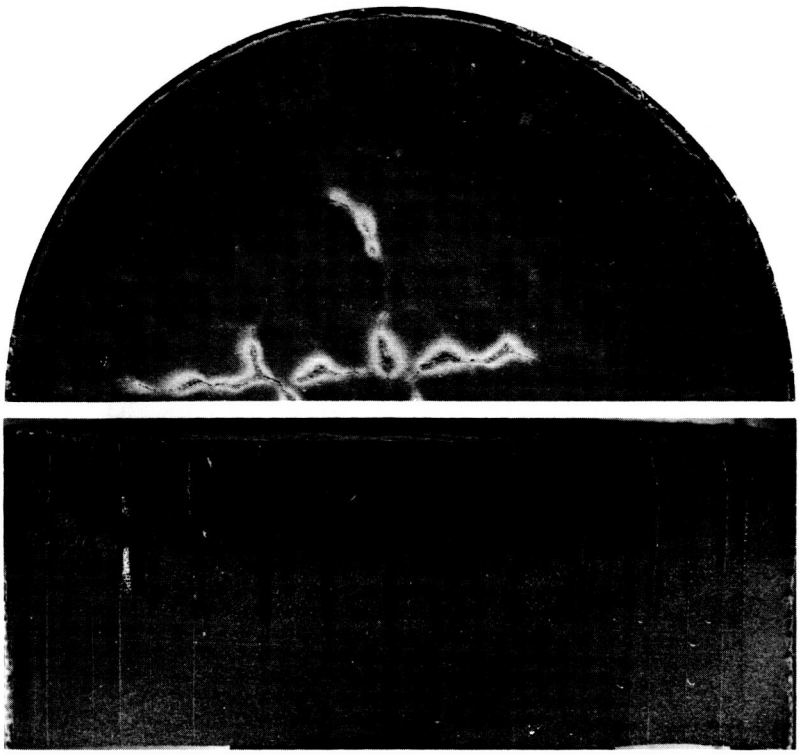

Char Surface

Toughness.- Good hard, smooth char, with some cracking along cell ribbons.

Color.- Reddish-brown center, with darker carbonaceous edges and silica residue concentrated along cracks.

General Comments.- Surface was generally smooth because core was slightly below surface and there was very little surface shrinkage.

Cross-Sectional View

Char Integrity.- Strong char with low porosity.

Char Shrinkage.- Very little shrinkage. Bond with core rated fair to good.

Pyrolysis Zone and Virgin Interface.- No major weaknesses such as cracks, disbonding, or friability.

General Comments.- Char and pyrolysis zone appear fairly good.

Figure 30.- High-Silica-Microsphere Composition, Specimen 2-1

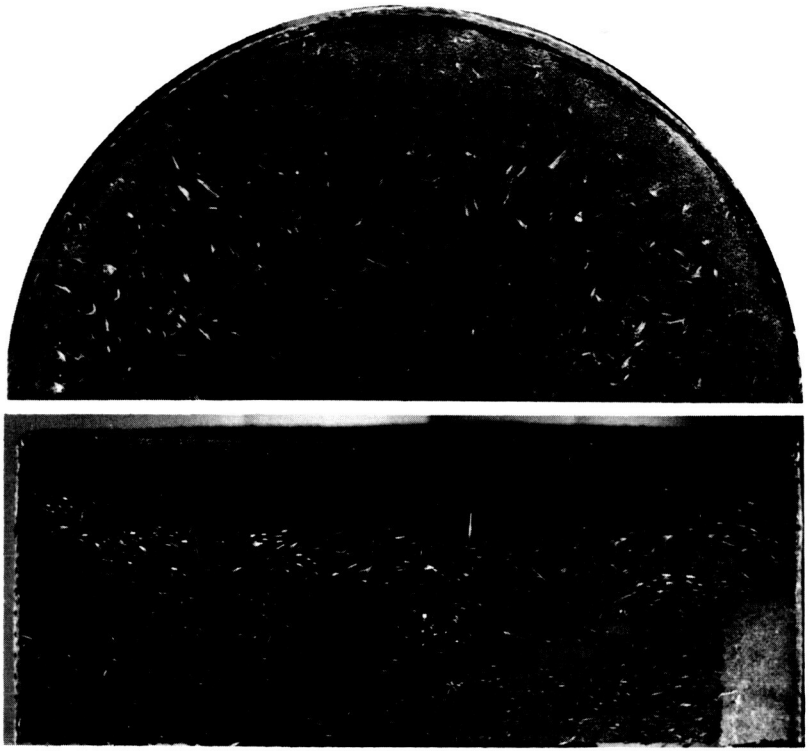

Char Surface

Toughness.- Very strong char surface, with no cracking.

Color.- Dull reddish-brown.

General Comments.- E-glass fibers are prominent at surface, and are very brittle.

Cross-Sectional View

Char Integrity.- Very strong char with low porosity.

Char Shrinkage.- No cracking or other indications of char shrinkage.

Pyrolysis Zone and Virgin Interface.- Typically soft, but appear good.

General Comments.- The char integrity is very good.

Figure 31.- High-Silica-Microsphere Composition with Fiber Reinforcement, Specimen 5-1

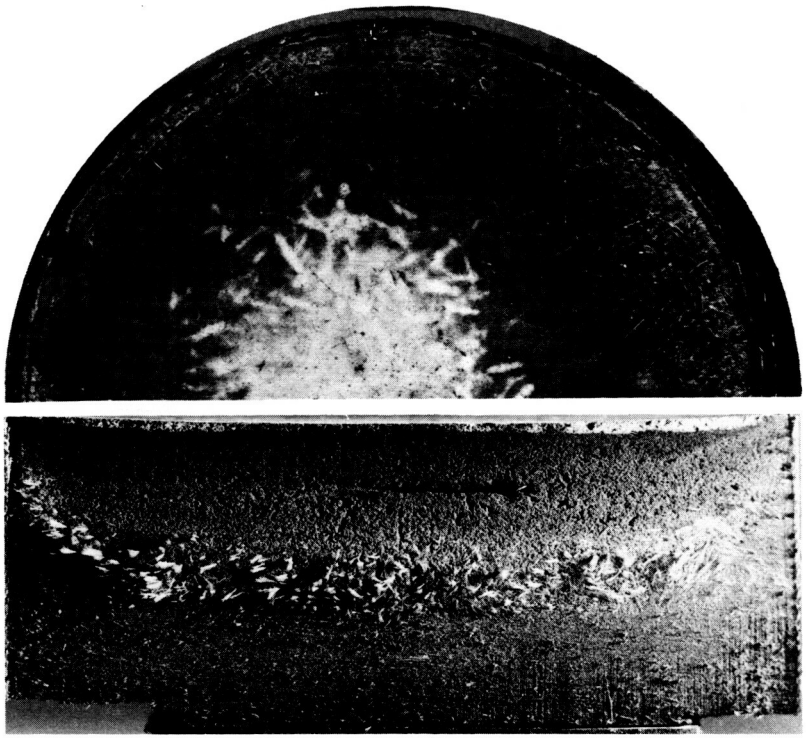

Char Surface

Toughness.- Very strong char, with no surface cracking.

Color.- Reddish-brown at edges, but whitish, blue-green near center.

General Comments.- Char surface looks very good.

Cross-Sectional View

Char Integrity.- Highly stable char with low porosity.

Char Shrinkage.- No cracking or other indications of char shrinkage.

Pyrolysis Zone and Virgin Interface.- Appear good, but there is no chemical bonding of fibers.

General Comments.- E-glass fibers are apparently melting at a very low temperature (below 1500°F) and combining with silica melt to form a very strong char layer.

Figure 32.- High-Silica-Microsphere Composition with Fiber Reinforcement, Specimen 5-2

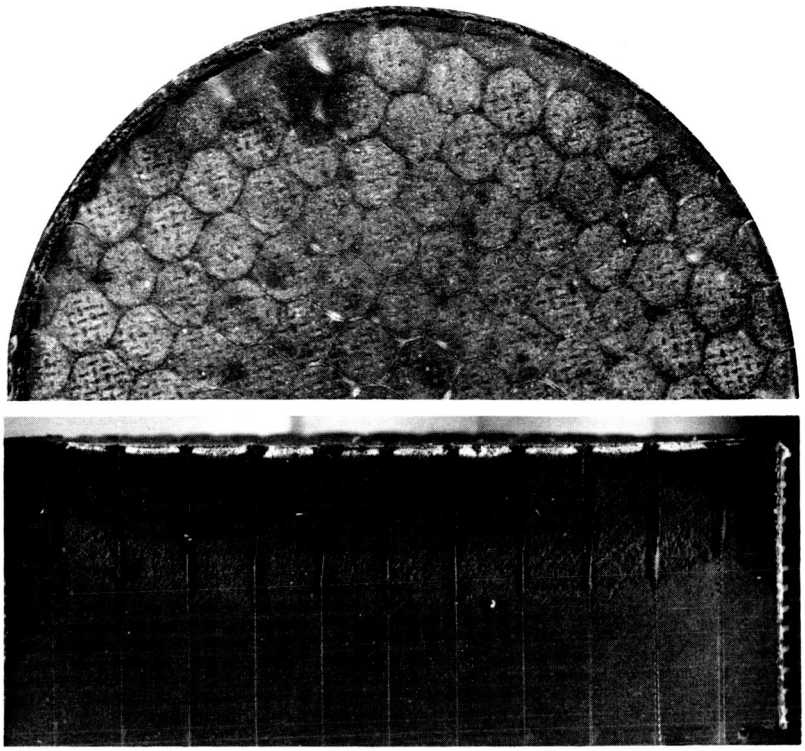

Char Surface

Toughness.- Good char surface.

Color.- Gray with traces of brown.

General Comments.- Unusual cross-hatched surface pattern resulted from fabrication. Surface was dry looking and somewhat porous.

Cross-Sectional View

Char Integrity.- Moderately porous char. Remained intact upon sectioning.

Char Shrinkage.- Some core node bonds were pulled apart, but bonding generally good.

Pyrolysis Zone and Virgin Interface.- Very powdery pyrolysis zone, and a very distinct virgin interface.

General Comments.- Significant silica deposit present just below surface, indicating possible subsurface oxidation. Otherwise, a good char and pyrolysis zone.

Figure 33.- High-Silica-Microsphere Composition with Carbon Powder, Specimen 3-1

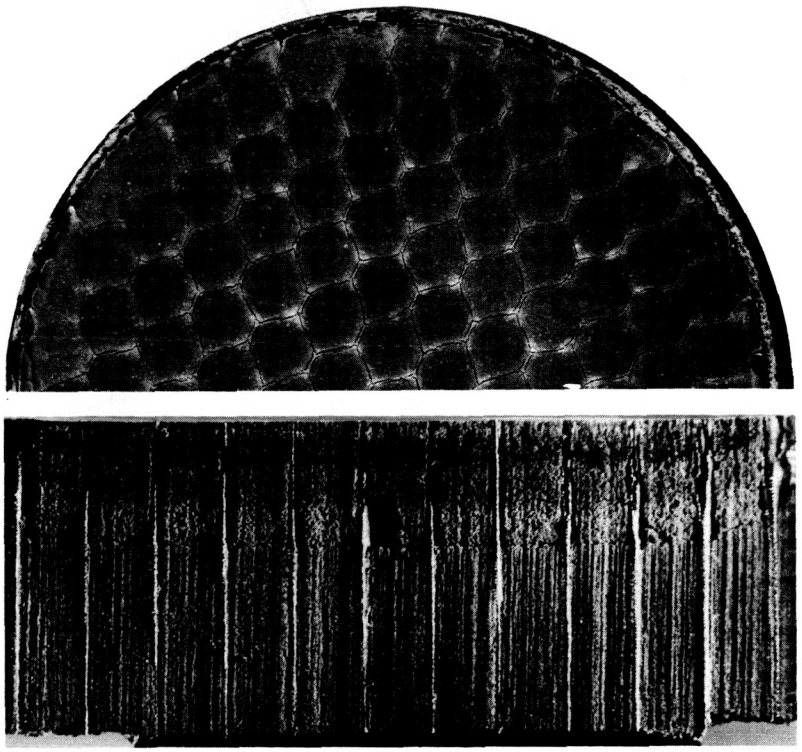

Char Surface

Toughness.- Very hard surface. No char cracks or disbonds, although shrinkage cracks present along core.

Color.- Reddish-brown and very uniform.

General Comments.- Surface appears very good. Only minimal char shrinkage and no blistering.

Cross-Sectional View

Char Integrity.- Good char strength and homogeneous porosity.

Char Shrinkage.- Some char shrinkage noted along ribbons.

Pyrolysis Zone and Virgin Interface.- Friable pyrolysis zone. Crack apparent at interface.

General Comments.- Adding fibers should reduce char porosity and strengthen virgin interface.

Figure 34.- SS-41 with Carbon Powder, Specimen 32

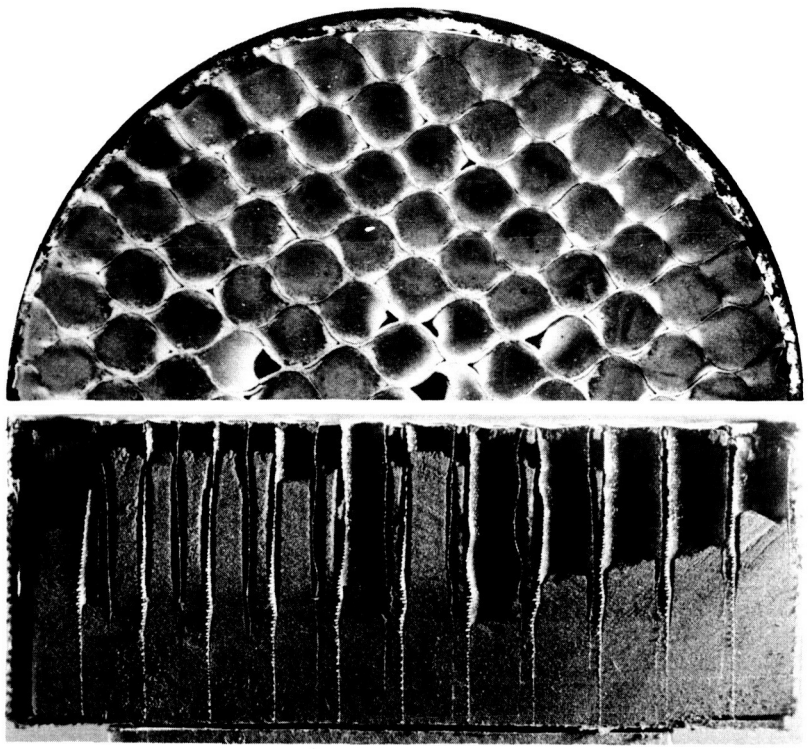

Char Surface

Toughness.- Very thin "film" crust, but no filler cracks.

Color.- Reddish-brown, with silica residue around core.

General Comments.- Char shrunk within each cell, leaving a dimpled surface.

Cross-Sectional View

Char Integrity.- Actual char had good strength and very low porosity. However, except for surface crust, there was no evidence of bonding with core.

Char Shrinkage.- Very significant char shrinkage, leaving large cracks between char and core that ran from surface to virgin material.

Pyrolysis Zone and Virgin Interface.- Appeared very good on visual inspection, but in reality, were very fragile.

General Comments.- Char was completely unbonded and supported only by its attachment through pyrolysis zone. Upon sectioning, much char lost due to weakness of this attachment.

Figure 35.- 80/20 Composition, Specimen 25-1

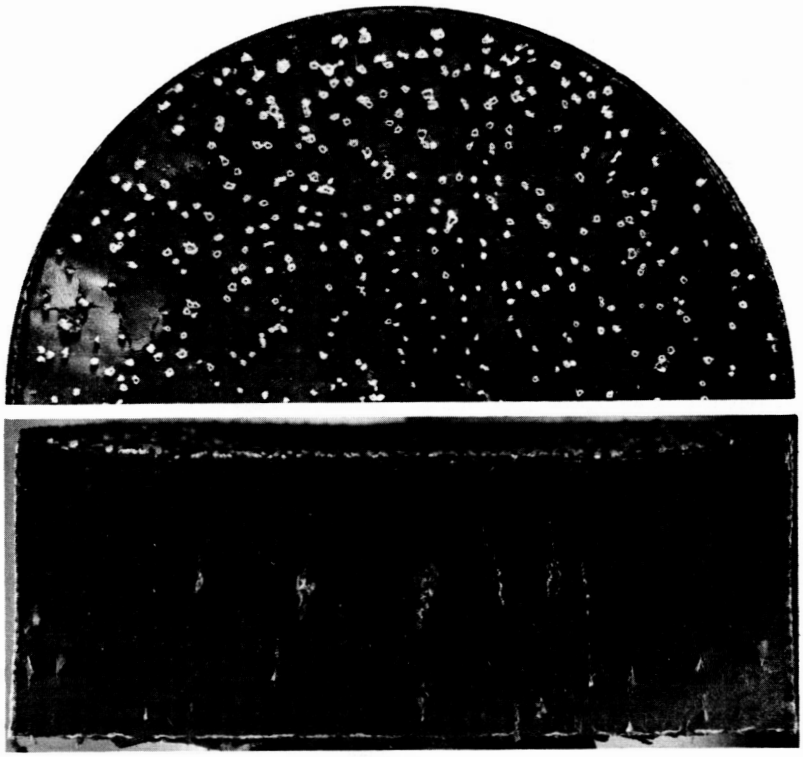

Char Surface

Toughness.- Below average in hardness; some cracking between thread ends.

Color.- Reddish-brown.

General Comments.- Formulation shrunk badly, leaving a very concave surface. Glass fiber melt present on charred surface.

Cross-Sectional View

Char Integrity.- Poor char with extensive cracking normal to surface.

Char Shrinkage.- Very deep vertical cracks, indicating significant char shrinkage.

Pyrolysis Zone and Virgin Interface.- Relatively weak, with some horizontal cracking near interface.

General Comments.- Fibers did not melt, and their strength was retained within char layer. However, for this technique to be effective, chemical bonding of fibers and a strong char layer are needed.

Figure 36.- 80/20 Composition with End-Oriented Threads, Specimen 23-1

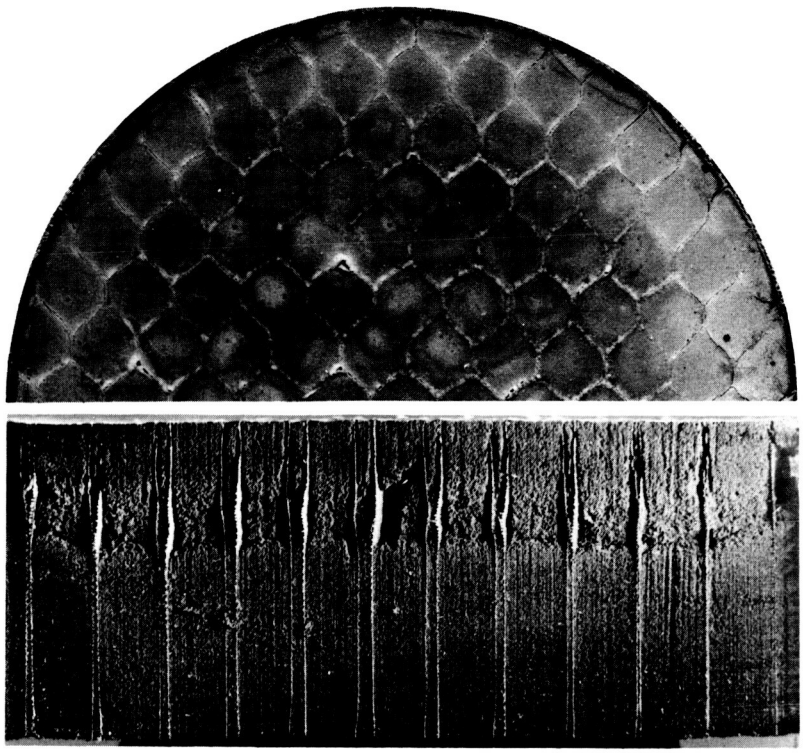

Char Surface

Toughness.- Very hard surface with good core bond.

Color.- Reddish-brown, with blue and orange at edges.

General Comments.- No appreciable char shrinkage, and only very minor cracking at core.

Cross-Sectional View

Char Integrity.- Good char and fair bonding strength near surface, but strength decreases in pyrolysis zone.

Char Shrinkage.- Significant char shrinkage and disbonding in pyrolysis zone.

Pyrolysis Zone and Virgin Interface.- Pyrolysis zone and plastic interface are weak even though very little char was lost on sectioning.

General Comments.- Adding fibers should significantly improve plastic interface, pyrolysis zone, and char strength.

Figure 37.- SS-41 Mixture 1 in Core, Specimen 33

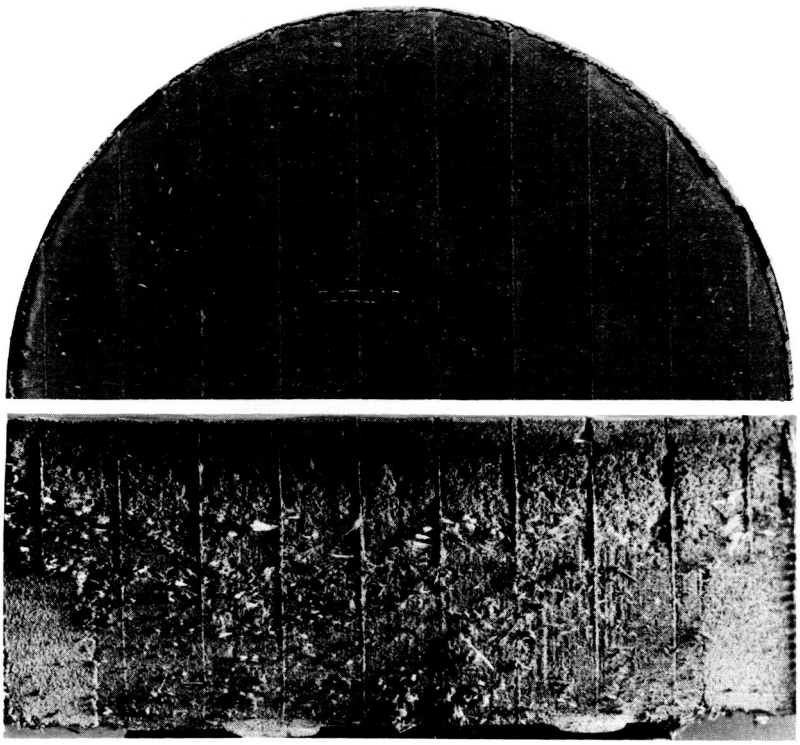

Char Surface

Toughness.- Very good surface strength.

Color.- Uniform reddish-brown.

General Comments.- Ribbon bond appears very good; very little cracking along the ribbons due to shrinkage.

Cross-Sectional View

Char Integrity.- Porous char, but of good strength.

Char Shrinkage.- Very little char shrinkage, and no significant cracking or disbonding.

Pyrolysis Zone and Virgin Interface.- Pyrolysis zone and interface appear good.

General Comments.- Adding some carbon powder should strengthen char layer by reducing its porosity.

Figure 38.- SS-41 Mixture 2 with Fibers and Phenolic-Coated Ribbon Reinforcement, Specimen 34-1

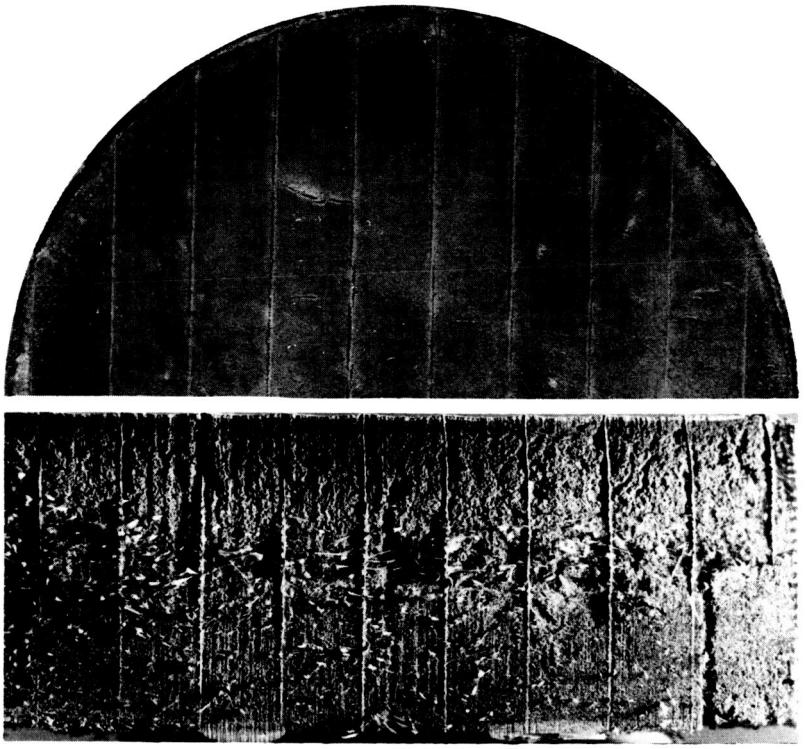

Char Surface

Toughness.- Very good surface strength.

Color.- Reddish-brown.

General Comments.- Ribbon bond seems very good; very little cracking along the ribbons due to shrinkage.

Cross-Sectional View

Char Integrity.- Char is porous, but has good strength and is well bonded to ribbons.

Char Shrinkage.- No significant shrinkage.

Pyrolysis Zone and Virgin Interface.- Both appear good.

General Comments.- Addition of carbon powder should strengthen char layer by reducing porosity.

Figure 39.- SS-41 Mixture 2 with Fibers and Phenolic-Coated Ribbon Reinforcement, Specimen 34-2

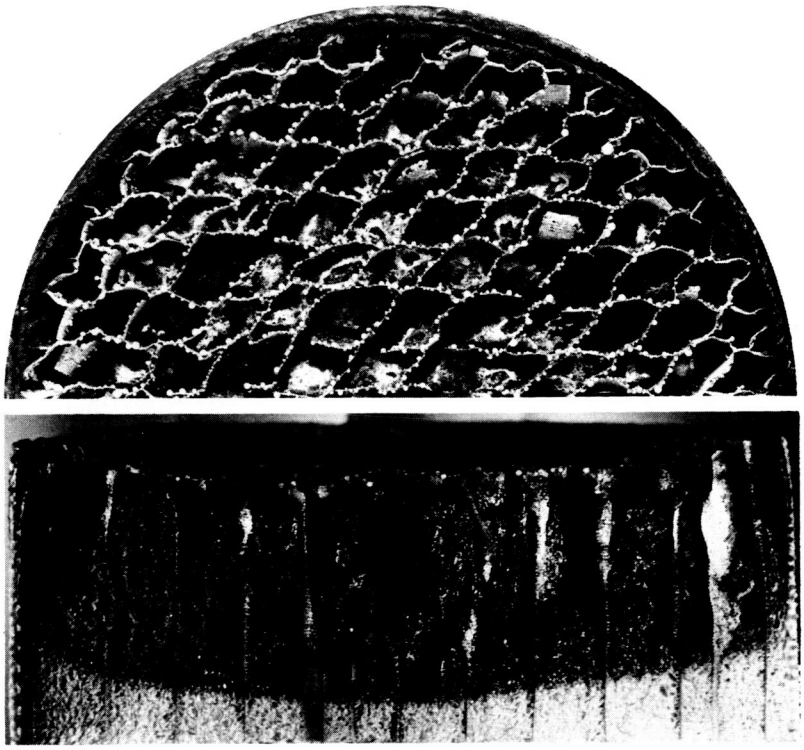

Char Surface

Toughness.- No char surface *per se* existed, just empty core.

Color.- Black.

General Comment.- Material was incapable of sustaining test environment.

Cross-Sectional View

Char Integrity.- Highly porous cinder.

Char Shrinkage.- Unable to evaluate.

Pyrolysis Zone and Virgin Interface.- No particular weakness at interface, but pyrolysis zone is a very porous carbon matrix.

General Comment.- Material not considered a candidate for the Shuttle Orbiter at the heat-flow level tested.

Figure 40.- Urethane Foam, Specimen 19-1

TABLE 18. - SUMMARY OF VISUAL DATA

Composition	Specimen no.	Char surface	Core bond	Char layer	Pyrolysis zone	Virgin interface	Char visual rating, %	Insulation efficiency rating, %
Honeycomb core reinforcement								
SS-41 (baseline)	6-1	G	F	P	F	F	67	100
SS-41 (baseline)	6-2	F-G	F	P	F	P	50	100
SS-41 (baseline)	16-1	G	F	P	F	F	67	105
SS-41 (baseline)	16-2	F-G	P	P	F	P	50	105
SS-41 (baseline)	31-1	G	P	P	F	F	60	102
SS-41 (baseline)	31-2	F-G	P	P	F	F	70	88
High silica	2-1	G	F-G	G	F	F	83	85
High silica with carbon powder	3-1	G	G	G	F	F	87	86
80/20	25-1	F	P	G	P-F	P-F	60	103
SS-41 with carbon powder	32-1	G	F	G	F	P	73	103
SS-41, mixture 1	33-1	G	F	G	F	P	73	92
Fiber reinforcement								
SS-41 (baseline)	24-1	G	---	G	G	G	100	122
SS-41 (baseline)	24-2	F	---	G	G	G	92	97
High silica	5-1	G	---	G	G	G	100	99
High silica	5-2	G	---	G	G	G	100	83
80/20	23-1	P	---	P	P	P	33	108
Ribbon reinforcement								
SS-41 (baseline)	12-1	G	P-F	P	F	F	60	100
SS-41 (baseline)	12-2	F	P-F	P	F	F	60	95
SS-41 (baseline)	15-1	G	F-G	F	P-F	P-F	70	95
Ribbons and fiber reinforcement								
SS-41 (baseline)	17-1	G	G	G	G	G	100	73
SS-41 (baseline)	17-2	F	G	F	G	G	87	69
SS-41 (baseline)	18-1	G	G	G	G	G	100	81
SS-41 (baseline)	18-2	F-G	G	G	G	G	97	71
SS-41, mixture 2	34-1	G	G	G	F	G	93	101
SS-41, mixture 2	34-2	G	G	G	F	G	93	86

Note: 1. All specimens generally exhibited some length change or thickness decrease. This "recession" of the charred surface is attributed to pyrolysis zone settling and char shrinkage during cooldown.

2. All specimens retained their surface char during exposure to the two test conditions. Some specimens did lose some surface char upon posttest handling, but this was the result of accidental damage and is not considered to be a valid measure of char strength.

3. The following assignments were made in determining the visual char rating.

Letter	Definition	Value
G	Good	3
F	Fair	2
P	Poor	1

Therefore, the minimum visual rating was 33% out of a possible 100%.

Discussion of Test Results

The thermal efficiency values shown in table 17 have been normalized by using the SS-41 composition (in core) as the baseline, and are plotted in figures 13 and 14.

Figure 13 shows the effect on efficiency of using several alternative char-reinforcement compositions. Figure 14 presents the results of using compositional variations to improve char residue.

Core Replacement by Ribbons

The ribbon laminating technique proved effective in reinforcing the char (fig. 21 and 22). A good char-ribbon bond was formed at the surface, and internally, the char seemed to be more intact. This probably had to do with the lower restraint in the direction of the ribbons, which allowed the char to strain in this direction without cracking. Thermally, the results in figure 13 show that the cloth and spacing selected did not significantly affect the insulation efficiency.

During these tests, we also investigated coating the ribbons with phenolic resin (SC1008) and silicone resin (RTV60) to improve the bond between the ribbons and the ablative material.

The use of the silicone coating (fig. 27 thru 29) was subsequently discontinued because of its high density [0.32 gm/cm^3 (20 lb/ft^3)] and weaker ribbon bond.

Fiber addition.- The addition of fibers to the ribbon-construction panel was found to greatly improve char stability, as seen by comparing specimens 12-1 and 12-2 (fig. 21 and 22) with specimens 18-1 and 18-2 (fig. 23 and 24). This improvement was manifested in two ways: (1) the fibers apparently melted at about 1090°K (1500°F) and joined with the carbon to form a very strong char matrix, and (2) the fibers reduced the thermal strains and, thus, minimized char shrinkage and the corresponding cracks, subsurface voids, and disbonds.

The same intact char was found when fibers alone were used for reinforcement. Posttest calculations showed that the insulation efficiency (fig. 14) was generally improved. This can be seen by comparing specimens 24-1 and 5-1 (fig. 25 and 31) with specimens 6-1 and 2-1 (fig. 15 and 30).

Unfortunately, the first ribbon panels that were fabricated had high densities. Generally, the higher the density of a panel, the lower its thermal efficiency. The decrease in thermal efficiency due to a higher density masks out the effect of the added fiber.

Large core.- Thermally, the test results (fig. 13) for the two specimens with 1.9-cm (3/4-in.) honeycomb cells were inconclusive: a slight improvement was observed for one specimen, but the other showed a reduced efficiency. A visual examination showed that the char integrity was unaffected by the larger cell size (fig. 19 and 20).

Partial-depth core.- Posttest sectioning revealed that the pyrolysis zone penetrated to the core discontinuity (fig. 17 and 18) without noticeably affecting the char-virgin material interface (see fig. 15 and 16). The tests also demonstrated that some thermal improvement can be expected from a partial core depth since the insulation efficiency was consistently 5% higher than that of the full-depth core specimens.

Composition Studies

The remaining test specimens generally served to evaluate techniques for facilitating core loading and for reducing the density of the ribbon- and fiber-reinforced material. These techniques have been discussed in a previous section. Here the discussion emphasizes the effect of composition on char residue, stability, and thermal performance.

In total, six compositions, including the SS-41, were evaluated in the 0.9-cm (0.37-in.) honeycomb core. In general, all formed a strong char surface, but typically had weak virgin material-pyrolysis zone interfaces.

Microspheres.- The integrity of the char layer was significantly improved by splitting the total percentage of microspheres between phenolic and silica (fig. 30 thru 32). This apparently reduced the char strain in such a way that a degree of core bonding was maintained. This improvement in char integrity, however, was obtained at the expense of the insulation efficiency (fig. 14), which was reduced by approximately 15%. It is quite possible that cooldown shrinkage is responsible for the poor char integrity of the higher-percentage phenolic microsphere compositions.

Carbon Powder

In every instance, the addition of carbon powder seems to have resulted in a minor improvement in char integrity without reducing thermal efficiency. This can be seen by comparing specimens 2-1 (fig. 30) and 3-1 (fig. 33), and 6-1 (fig. 15) with 3-2 (fig. 34).

Nylon Powder

The addition of nylon powder should also improve thermal efficiency by increasing blockage. In these tests it was not our intent to investigate this particular aspect. However, it is interesting to note that adding 10 pbw of nylon has effectively offset the redistribution of phenolic and glass microspheres between the SS-41 (fig. 15) and the 80/20 (fig. 35) compositions, as illustrated by specimens 6-1 and 25-1 (fig. 14). The char integrity was not noticeably altered by this formulation change: subsurface voids, cracks, and disbonds were common in both specimens.

80/20 Composition

The 80/20 ablative mixture was also used to evaluate the use of fiberglass threads as a replacement for the honeycomb. These threads were stitched through the specimen, perpendicular to the surface. Surface cracks were noted during the test and subsurface cracks formed after sectioning the specimen. The surface cracks generally ran between the thread ends, and the internal cracks ran parallel to the threads (fig. 36).

SS-41 Modification

As a culmination of this study, the SS-41 composition was modified to produce more char residue and to incorporate the ribbon and fiber without increasing density. The first step was to reduce the phenolic microspheres to 30% and increase the glass microspheres to 25% and add 10% carbon powder. This produced a slightly higher density and a much better char (fig. 37).

As we saw previously (fig. 13), replacing the honeycomb core with fibers and phenolic laminating resin (specimens 18-1 and 18-2) increased the density of the SS-41 to 0.378 gm/cm^3 (23.5 lb/ft^3). Now, to reduce the density, we made an additional slight alteration to this composition and reduced the packing pressure. The results of these iterations were that a density of 0.25 gm/cm^3 (15.5 lb/ft^3) was obtained with the following composition:

Silicone resin (GE 655)	20%
Phenolic microspheres	35%
Glass microspheres	25%
Nylon powder	10%
E-glass fibers	10%

To compact and cure the billet, the above mixture was placed in a mold, vacuum bagged at 48 kN/m^2 (7 psia), and the laminating pressure was reduced to 206 kN/m^2 (30 psi). No cracks, disbonds, or subsurface voids were found upon posttest sectioning (fig. 38 and 39), and the thermal efficiency was essentially the same as that of the original SS-41 composition used in this study (fig. 14).

Plasma Arc Test Conclusions

1. The addition of E-glass fibers is considered the single most significant factor in improving the performance of the char. These fibers had a very positive effect on relieving shrinkage strain (a most serious problem), and the glass melt they produced was very beneficial in forming good strong char layers. Using a fiber treatment (such as silicone silane surface coating) that would promote chemical bonding with the elastomeric mixture would further strengthen the pyrolysis zone.

2. The laminated ribbon layup is considered at least as good as honeycomb core for reinforcing the char. Generally, a good chemical bond between the char layer and the ribbons or core was obtained for all compositions.

3. No clear-cut physical advantage was found between the SC1008 and RTV60 adhesive coatings. The RTV60-coated specimens exhibited 5 to 10% higher densities, and this accounted for the slight difference in thermal efficiency.

4. A small (5%) thermal improvement was found for the partial-depth core and, physically, no problems developed at the core discontinuity. In these tests, the pyrolysis depth coincided with the bottom of the core. This is undesirable. The core should extend into the virgin material for some distance, but this would reduce the thermal advantage.

5. Enlarging the core size from 0.95 cm (3/8 in.) to 1.9 cm (3/4 in.) did not significantly affect thermal or physical performance.

6. None of the five composition variations from the SS-41 baseline composition (25% RTV655 resin, 50% phenolic microspheres, 15% glass microspheres, and 10% nylon powder) significantly improved the thermal performance.

7. Reducing the percentage of phenolic microspheres and increasing that of the glass microspheres until both were equal, while holding the percentages of all other constituents constant, reduced the insulation efficiency of the char by 10 to 15%.

8. A clear tradeoff was found between char integrity and thermal performance. Maximum thermal efficiency requires a high percentage of phenolic microspheres; however, the low percentage of residue left by this constituent results in a poor char. Using the SS-41 composition or its second modified version (see p. 36) seems to be a good compromise between adequate char residue and good thermal performance.

9. The addition of fibers did not reduce thermal performance for any of the three compositions that were evaluated. Their addition to the base composition significantly increased the integrity of the char.

10. Adding carbon powder also improved char integrity without reducing thermal efficiency.

Wedge Test Results

The plasma-arc test program included four SS-41 composition wedge panels, each 20.3x35.6x5.04 cm (8x14x2 in.). Thermocouples were placed on the back face sheet of the models, as well as on the specimen holder. These thermocouples were used only to indicate that the holder did not overheat during the test. The purpose of these tests was to evaluate, in a more realistic flow environment, the char-reinforcement methods discussed previously.

The original test plan was to test all panels at the 0.33-MW/m^2 (30-Btu/ft^2-sec) test condition. However, after successfully testing the SS-41/honeycomb core panel, tests on the next two panels had to be aborted because the equipment failed. At this

point, testing was stopped. An analysis of the problem revealed that the high operating current required to achieve the desired heating condition was affecting the reliability of the facility. In concurrence with the NASA technical monitor, it was decided that the test objectives could be met by dropping back to a lower heating condition.

The reinforcement configurations and plasma-arc wedge test conditions are defined in table 19. Figure 41 shows the variation in heating rate along the centerline of the model for the 20-deg wedge angle test setup.

After the test, each wedge specimen was first inspected for surface cracks, strength, and general appearance, and then sectioned along its centerline. There were no visual differences in the char structures for the wedge or splash models tested at similar rates and times and having equivalent reinforcement. The SS-41 composition in honeycomb core (fig. 42) exhibited a typical hard, intact char surface, and subsurface cracks, voids, and disbonding from the core. In the fiber-reinforced specimen (fig. 43), there were several large surface cracks running across the face of the panel normal to the flow direction. These cracks, however, were confined to the surface and did not impair the overall char strength since, internally, the char was strong and free of cracks and voids.

The remaining two panels contained both ribbons and fibers, and were constructed with the ribbons running with the flow (fig. 44) and perpendicular to it (fig. 45). As with the splash models, some char cracks were found between the ribbons, but these were not continuous, as the ribbons were effective in restraining crack propagation.

The splice at the trailing edge of the model (fig. 44) was a manufacturing convenience and was not intended as a joint evaluation, although it did perform quite satisfactorily. Internally, the char performance was typical for the splash-test models: no cracks or subsurface voids were found, and a good ribbon bond was formed, although in this particular view the bond is not shown.

TABLE 19. - WEDGE PANEL TEST MATRIX

Test conditions	SS-41 in honeycomb core, 35	SS-41 with fibers		SS-41 with fiber and phenolic-coated ribbons parallel to flow		SS-41 with fibers and phenolic-coated ribbons perpendicular to flow, 38
		36*	36-1	37*	37-1	
Heating rate† Btu/ft^2-sec	30	30	12	30	12	12
MW/m^2	.34	.34	.14	.34	.14	.14
Heating time, sec	1 000	577	2000	100	2000	2000
Stream enthalpy, Btu	11 700	11 700	3900	11 700	3900	3900
MJ/kg	27.2	27.2	9.1	27.2	9.1	9.1
Pitot pressure, atm	.018	.018	---	.018	---	---
N/m^2	182.5	182.5	---	182.5	---	
Test gas	Air	Air	Air	Air	Air	Air

*Test 36 aborted at 577 seconds because the arc heater failed. Test 37 aborted at 100 seconds because the arc heater failed.

†This measurement is made approximately 5.04 cm (2 in.) aft of the water-cooled leading edge.

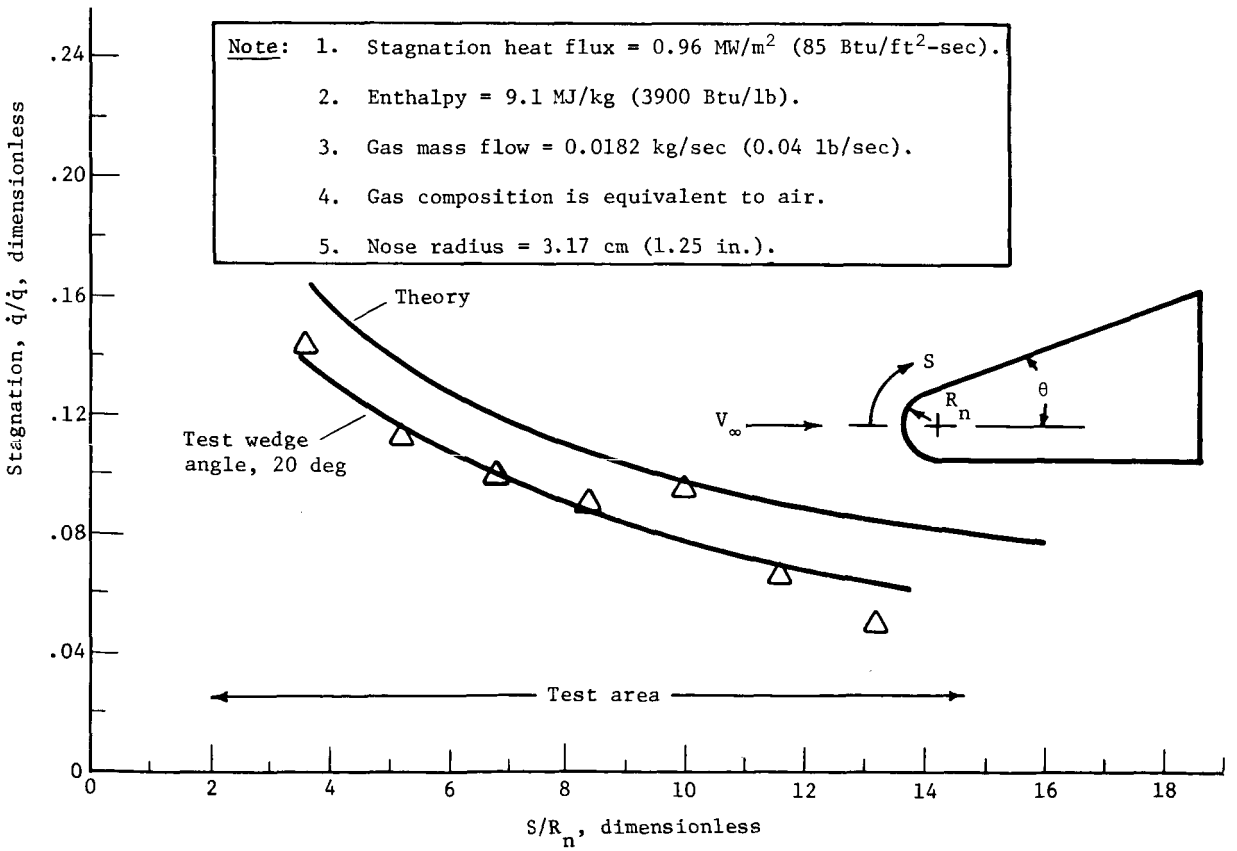

Figure 41.- Experimental Heating Distribution over Cylinder-Wedge

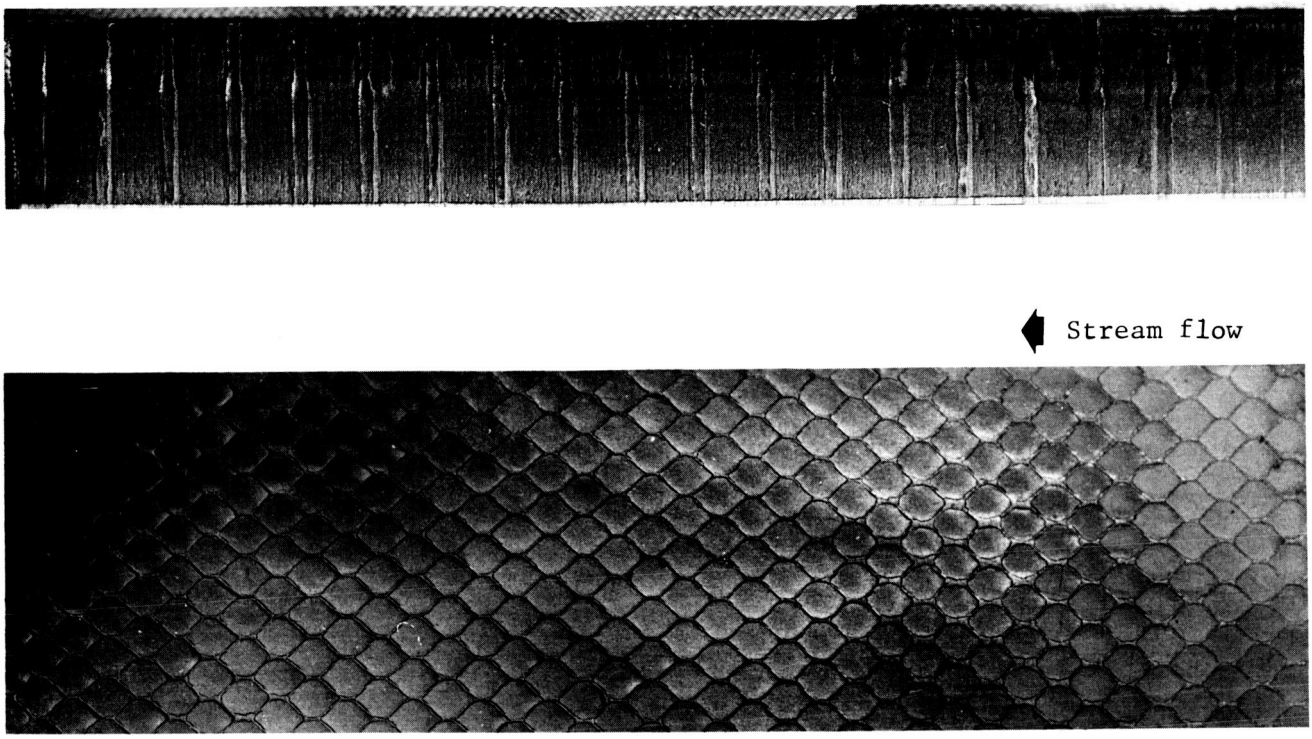

Figure 42.- SS-41 in Honeycomb Core, Wedge Model

Figure 43.- SS-41 with Fibers, Wedge Model

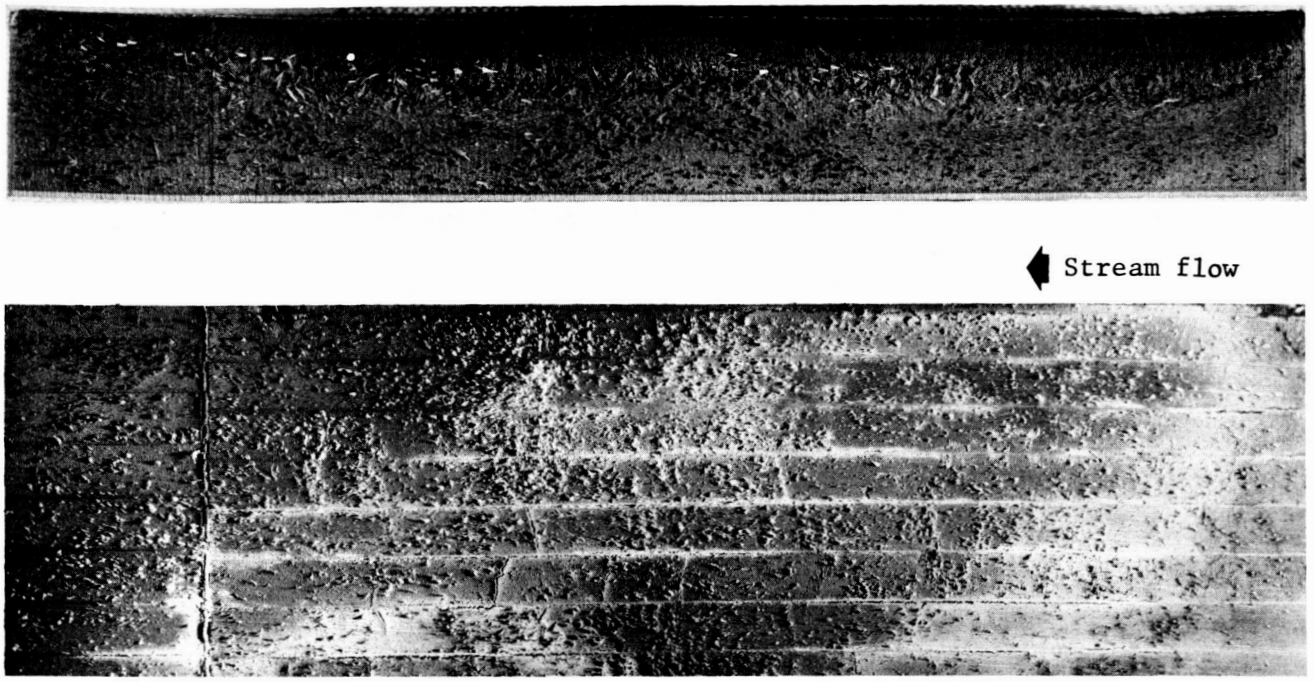

Figure 44.- SS-41 with Fibers and Phenolic-Coated Ribbons Parallel to Flow, Wedge Model

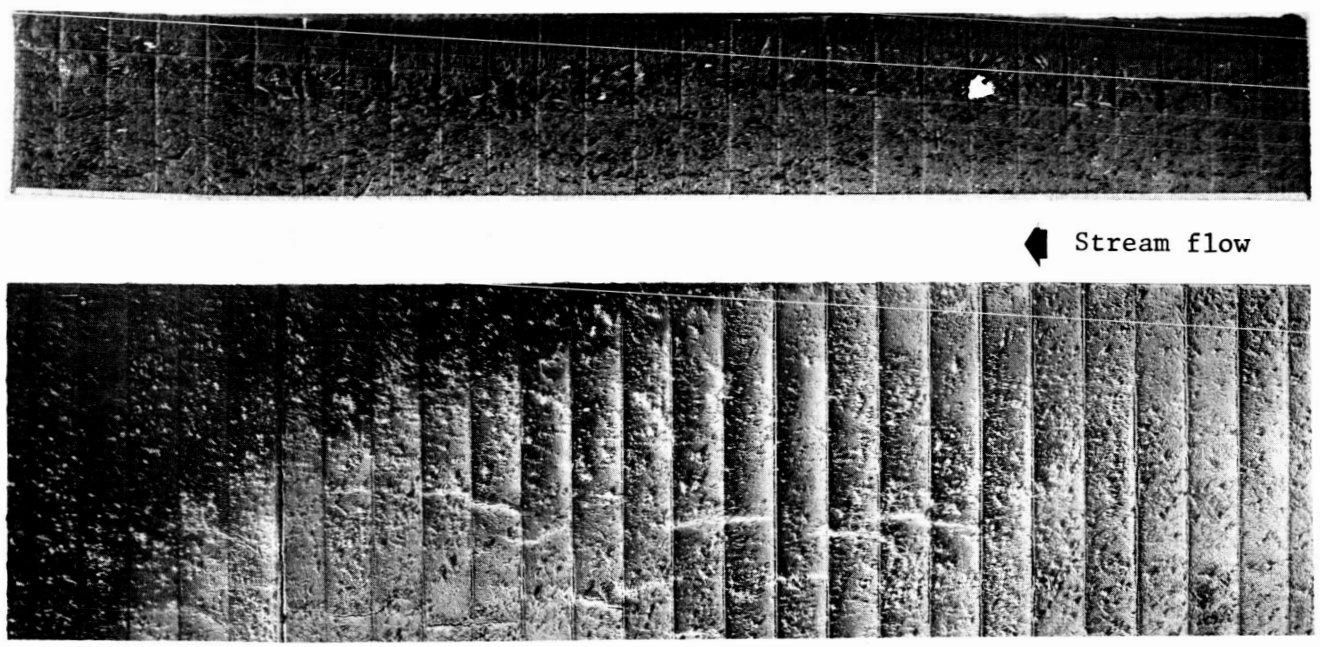

Figure 45.- SS-41 with Fibers and Phenolic-Coated Ribbons Perpendicular to Flow, Wedge Model

REUSABLE SUBPANEL

Incorporating a reusable subpanel under the ablative portion of a thermal protection system reduces weight, cost, and refurbishment time.

In this concept, the ablative material is bonded to a structural subpanel. After a flight, refurbishment in the field would consist of removing the panel and replacing it with a new panel. The first panel would be sent to a refurbishment center where the spent ablative material would be stripped off and a new ablative panel would be bonded on. (A spare panel would be required to serve one or more ships.)

Calculations indicate that, as the operating temperature of a subpanel increases, the overall weight decreases. For example, if an aluminum subpanel is used and operated at 421°K (300°F), its overall weight, including ablator, subpanel, and insulation, is 3.61 lb/ft^2 (17.63 kg/m^2). However, a titanium panel operating at 644°K (700°F) has an overall weight of 2.83 lb/ft^2 (13.81 kg/m^2). This weight saving results from using thermal insulation having a lower density and conductivity than the ablator to resist the heat flow to the primary structure. Figure 46 depicts the unit weight of ablator versus total heat for three subpanel operating temperatures.

In this study, we limited the peak operating temperature of the subpanel to 533°K (500°F). We feel that this is the highest practical temperature if the subpanel is to be reused. Higher temperatures would require the honeycomb to be bonded to the subpanel with a polyimide film adhesive before being filled with ablative material. Polyimide adhesives do not fillet well to the core; therefore, the panels would require more adhesive, and more weight, than if they were made using a silicone adhesive. In addition, polyimide adhesive would be very difficult to remove for refurbishment.

Materials

The proper choice of facing and core material is of prime importance in selecting a competitive subpanel design. Since preliminary studies show that ablator strain is one of the most critical design criteria, a stiff subpanel is needed to keep the ablator strain to a minimum. This may be achieved either by using a thick core section or a high-elastic-modulus facing material.

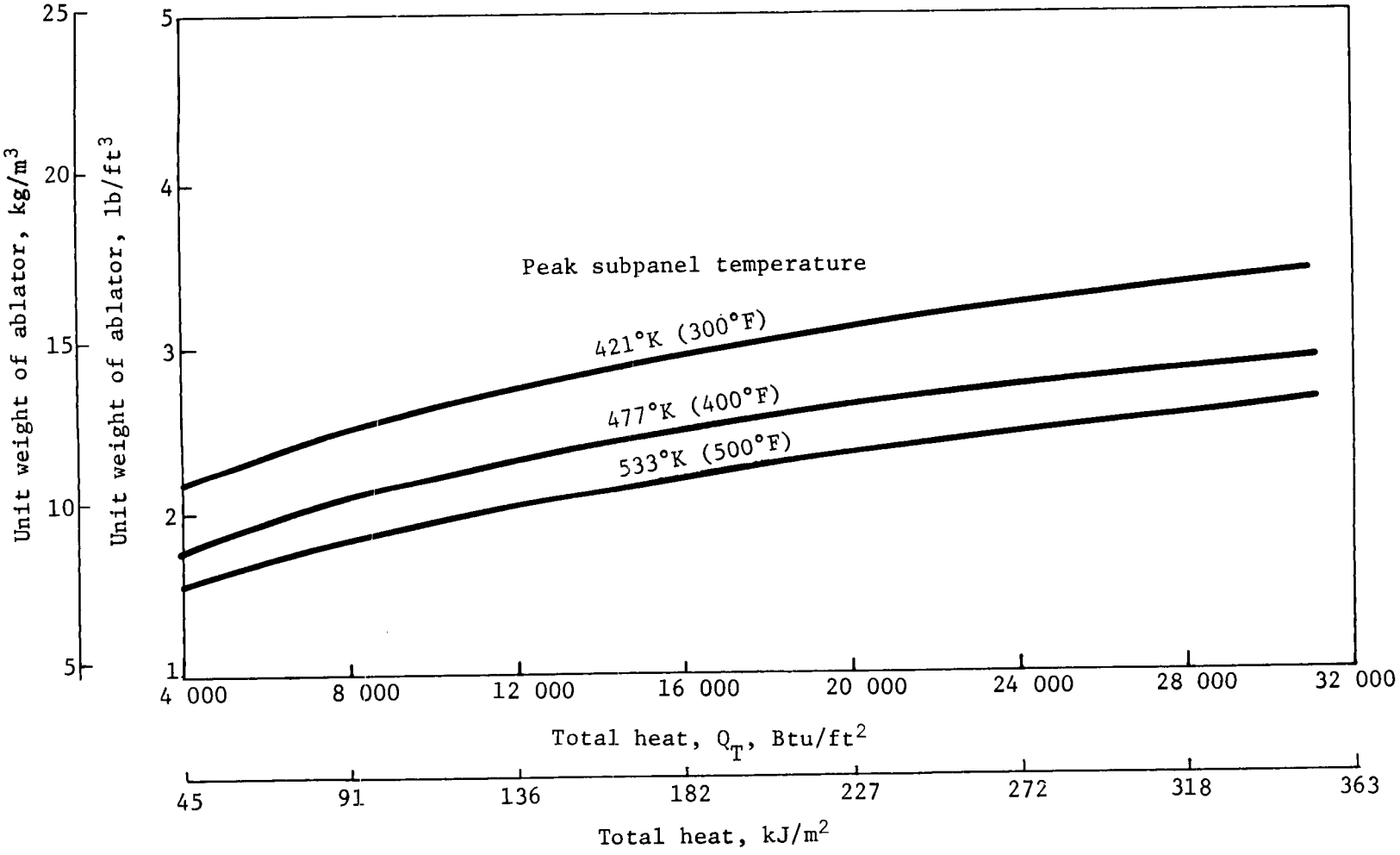

Figure 46.- Ablator MG-36 Design Curve for Entry Orbiter

Because increasing the core thickness adds weight and expense, it is desirable to choose a facing material with as high a modulus as is economically and practically feasible. In this study, we examined a wide variety of possible facing materials, ranging from high-modulus, high-cost materials to low-modulus, low-cost materials (see table 20).

HTS-Gemon L is composed of high-elastic-modulus, unidirectional graphite fibers and polyimide resin. PRD-49-III is a DuPont unidirectional fiber that has twice the modulus of S-glass fibers at 45% less weight. S-glass-phenolic facing is made from unidirectional glass fibers and phenolic resin, and has twice the modulus of E-glass fabric at the same weight. E-glass-phenolic is a low-cost facing that uses woven glass fabric with phenolic resin. All of these materials were analyzed as 533°K (500°F) systems. Titanium was analyzed as a 533°K (500°F) system and as a 644°K (700°F) system. Aluminum was included as a facing material for a 422°K (300°F) system.

Table 21 lists the characteristics of the core materials that were considered. Glass-phenolic core was used for the 533°K (500°F) systems. Each facing material was studied in combination with three different honeycomb-core cell sizes. For the 421°K (300°F) system with aluminum facings, both aluminum core and glass-phenolic core were used. For the 644°K (700°F) systems, titanium core was used. Titanium was also studied as a 533°K (500°F) system with glass-phenolic core to determine what the weight penalty would be in order to provide a metallic face sheet that would be easier to refurbish. We feel that these combinations are representative of the range of potential subpanel materials.

Design.- For stress analysis, the basic concept that was considered is a 50.8x50.8-cm (20x20-in.) panel, simply supported by a frame on two sides and free on the remaining two sides. The panel is free to slide at the attachment points in order to avoid unnecessary loads in the plane of the panel.

Preliminary studies show that the most critical load is the air pressure load, which ranges from -19.3 kN/m^2 (-2.8 psi) to +19.3 kN/m^2 (+2.8 psi). The maximum negative load occurs just after launch. The maximum positive load occurs at maximum Q in the entry phase, at which point the heat pulse has not had sufficient time to reach the subpanel. This air pressure load causes a maximum bending moment at the center of the panel, midway between the support frames. In turn, this bending moment determines the facing and core thickness. For a detailed picture of the panel and edge members, see figures 47 and 48.

TABLE 20.- FACING MATERIALS

Material	Modulus, E_c		Density		Price	
	kN/m^2	$lb/in.^2$	g/cm^3	$lb/in.^3$	\$/kg	\$/lb
HTS-Gemon L	137×10^6	20.0×10^6	1.52	0.055	176.32	80.00
PRD-49-III	86	12.5	1.38	0.050	110.20	50.00
S-Glass-Phenolic	48	7.0	1.80	0.065	8.81	4.00
E-Glass-Phenolic	27	4.0	1.80	0.065	1.10	.50
Aluminum	69	10.1	2.79	0.101	2.20	1.00
Titanium Ti-6Aℓ-4V	110	16.0	4.42	0.160	44.08	20.00

TABLE 21.- CORE MATERIALS

Material	Cell size		Density		Modulus, E_c		Price	
	cm	in.	g/cm^3	lb/ft^3	kN/m^2	$lb/in.^2$	\$/kg	\$/lb
Glass Phenolic HRP Hexcel	0.476	3/16	0.064	4.0	393 000	57 000	55.10	25.00
	0.635	1/4	0.056	3.5	317 000	46 000		
	0.952	3/8	0.035	2.2	90 000	13 000		
Aluminum	0.317	1/8	0.049	3.1	641 000	93 000	55.10	25.00
	0.396	5/32	0.041	2.6	961 000	67 000		
	0.476	3/16	0.032	2.0	298 000	43 000		
	0.635	1/4	0.025	1.6	20 000	29 000		
	0.952	3/8	0.016	1.0	96 000	14 000		
Titanium	0.317	1/8	0.078	4.9	786 000	114 000	132.24	60.00
	0.635	1/4	0.038	2.4	379 000	55 000		
	0.952	3/8	0.027	1.7	268 000	39 000		

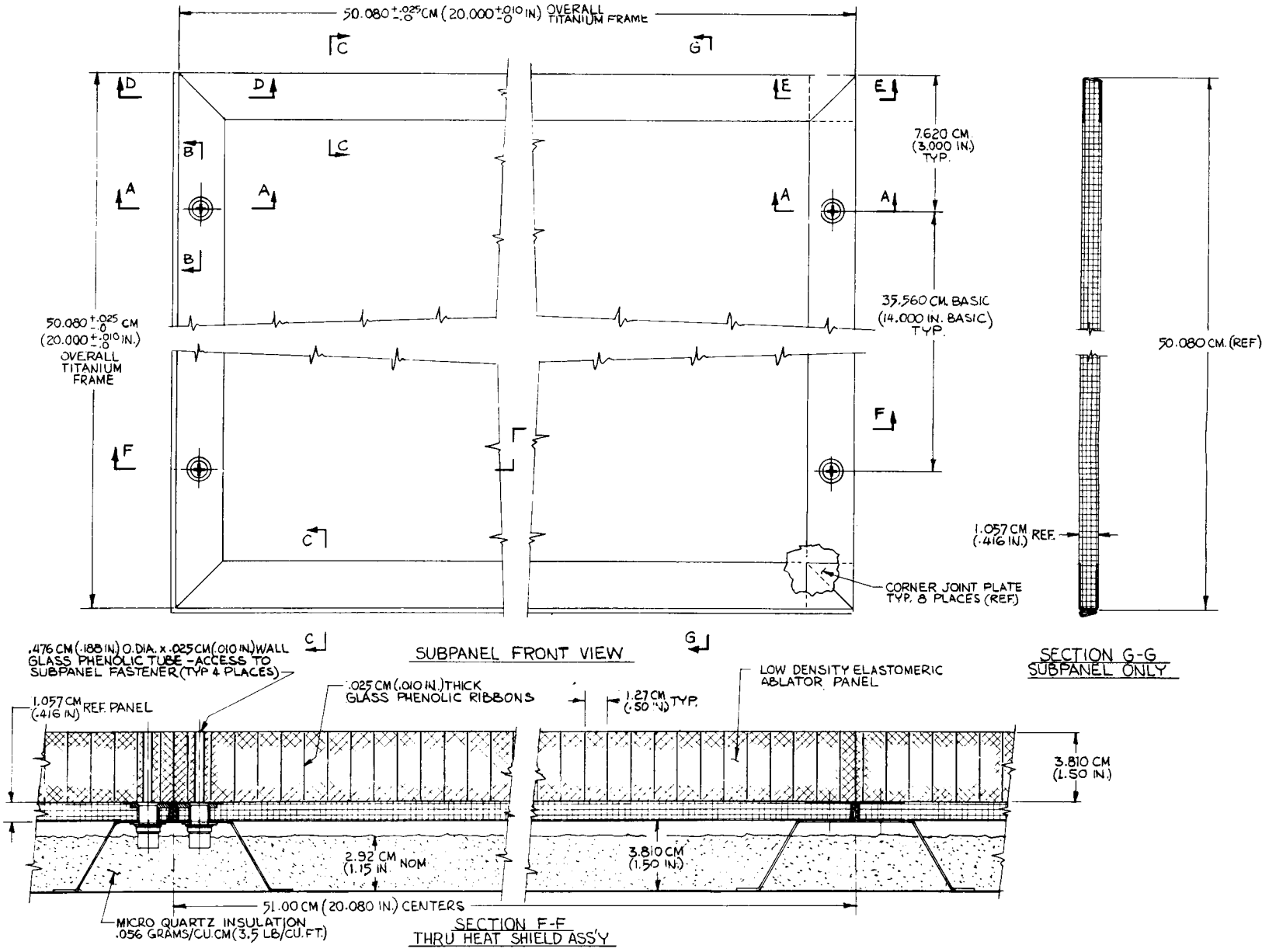

Figure 47.- Space Shuttle Heat Shield Reusable Subpanel

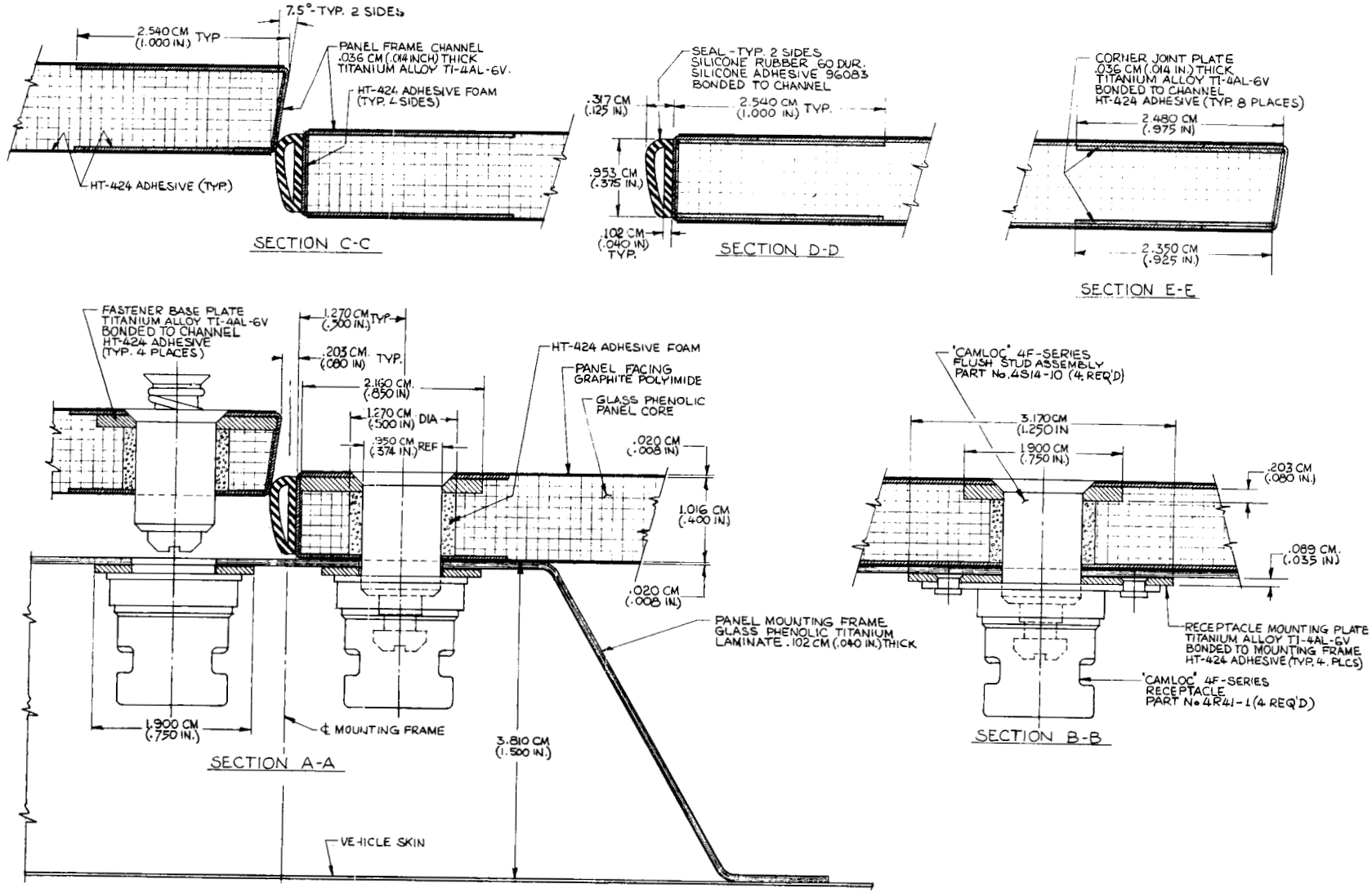

Figure 48.- Space Shuttle Heat Shield Reusable Subpanel

Analysis.- The panels were analyzed by calculating the bending moments that could be applied to the panel cross-section without causing failure. Three modes of failure were considered: (1) a strain of 1% in the outer fibers of the ablator; (2) failure of the facing by face wrinkling; and (3) failure of the facing by intracell buckling. The equations used to determine the allowable bending moments for these three modes of failure (ref. 6) are

$$MAS = \frac{(0.01)\ (IEO)\ (EF)}{(1 - CMU^2)\ (YBAR)}$$

$$MFW = 0.33\ [(EC)\ (EF)\ (TC)]^{1/2}\ (TT)^{3/2}$$

$$MIB = \frac{(2)\ (EF)\ (TC)\ (TT^3)}{(1 - CMU^2)\ (S^2)}$$

where MAS = moment allowable for 1% ablator strain, MFW = moment allowable for face wrinkling, MIB = moment allowable for intracell buckling, IEQ = moment of inertia of panel cross-section, EF = Young's modulus of elasticity of the facing in the direction of the bending stresses, CMU = Poisson's ratio, YBAR = distance from calculated neutral axis to outer fiber of ablator, EC = smeared-out compressive modulus of the core material, TC = thickness of the core, TT = thickness of the facing, and S = cell size of the honeycomb core.

To perform this tradeoff, we developed a computer optimization program to do a weight study of honeycomb sandwich-ablator thermal protection systems. The program determines the optimum honeycomb core thickness and edge frame thickness for a variety of different face thicknesses. The printout includes weights and material prices for each optimized configuration. A range of facing materials and core combinations was analyzed.

Results.- The results of this study have been plotted on three graphs that show how the design of the panel influences its weight. Each graph is based on a factor of safety of one, or a margin of safety of zero. Each panel has been optimized by holding the facing thickness, or cell size, or core thickness constant and changing the other variables to produce the lightest design possible.

The curves in figure 49 show that for each type of panel there is a minimum weight corresponding to a specific face thickness. If, for handling purposes or some other reason, a different facing thickness must be used, then the weight of the panel must be increased, as shown on the graph.

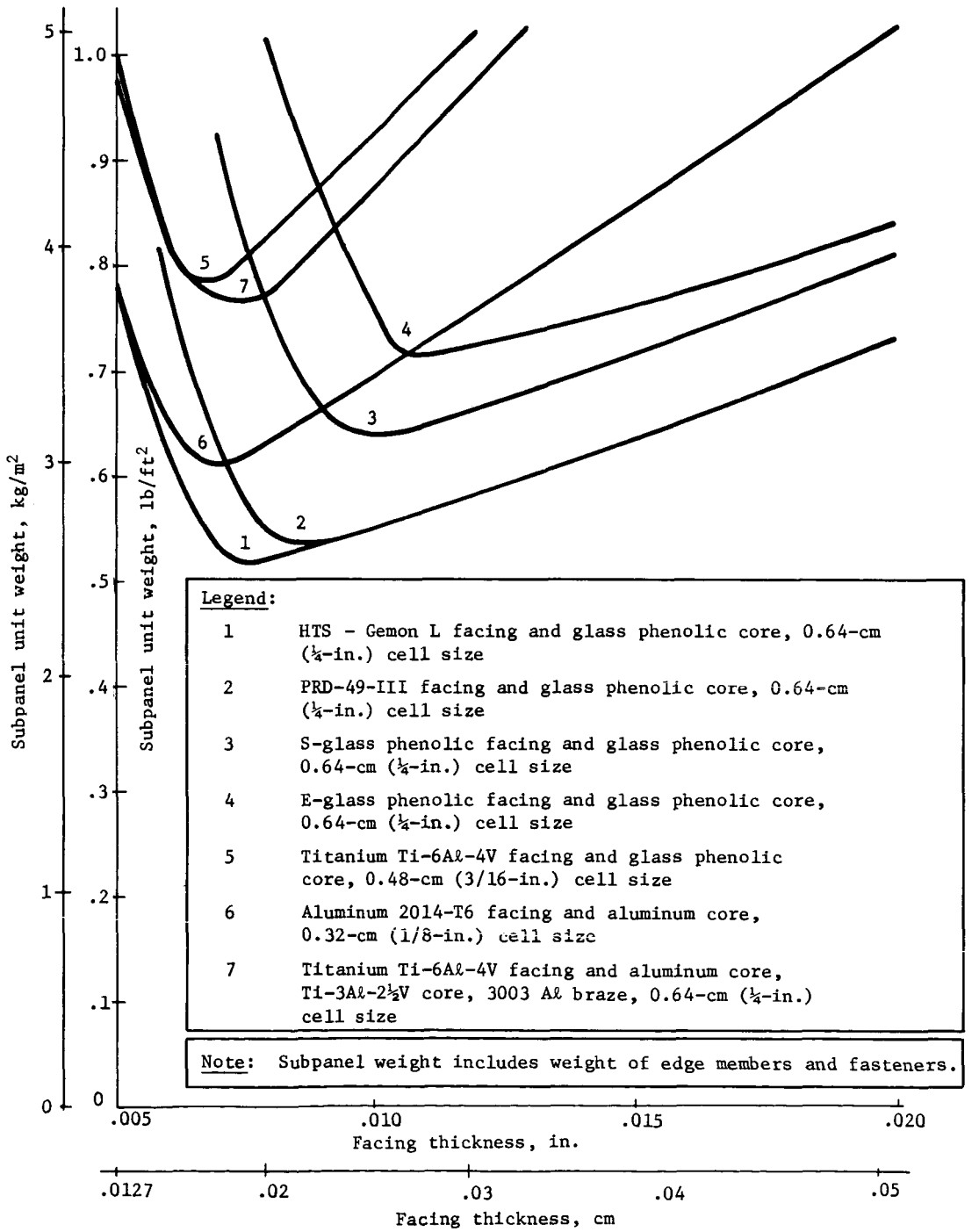

Figure 49.- Subpanel Weight vs Facing Thickness

Figure 50 shows that, for fibrous facings with a glass-phenolic core, the lightest panel can be obtained by using a 0.635-cm (1/4-in.) cell size. If aluminum or titanium metallic facings are used, the smallest cell size analyzed provides the lightest panel, under the conditions used.

The graph of subpanel weight versus core thickness (fig. 51) also shows that there is an optimum point for each type of panel. This core thickness corresponds to the optimum facing thickness discussed previously.

The data obtained from this study indicate that the lightest reusable panel would have graphite polyimide face sheets and glass-phenolic honeycomb core. Other face sheet materials with a lower modulus would require heavier panels to limit the allowable deflection. Since the panels are considered to be reusable, the raw material cost of the face sheet quickly amortizes over the panel life. Manufacturing labor costs, which would be similar for any face sheet material, will tend to even out the overall panel cost regardless of the raw materials used. Therefore, from an engineering standpoint, we recommend using the lightest panel design For this application. Our recommended design is shown in figures 47 and 48. The overall weight of the subpanel, including edge members, fasteners, and adhesive, is estimated to be about 2.54 kg/m^2 (0.52 lb/ft^2).

Integral Insulation

We had hoped that we could incorporate the required insulation inside the cells of the honeycomb core, since this would have provided a more convenient design. However, thermal analyses indicated that we would need at least 2.92 cm (1.15 in.) of insulation. Looking at figure 49, we find that panel weight increases sharply with thickness. For example, to use the large-cell-size, 9-mm (3/8-in.) core with graphite face sheets, the weight of the subpanel would have to be increased by 38% just to accommodate the insulation. Because of the imposed weight penalty, we used a design in which the insulation was behind the subpanel.

Fasteners

A test was run, under the Critical Defects Program, with holes drilled through the ablator to the back face sheet. These holes were not plugged, but left open. During the plasma arc test, the temperature of the back face was monitored by thermocouples under the holes and adjacent to the holes. There was no difference in

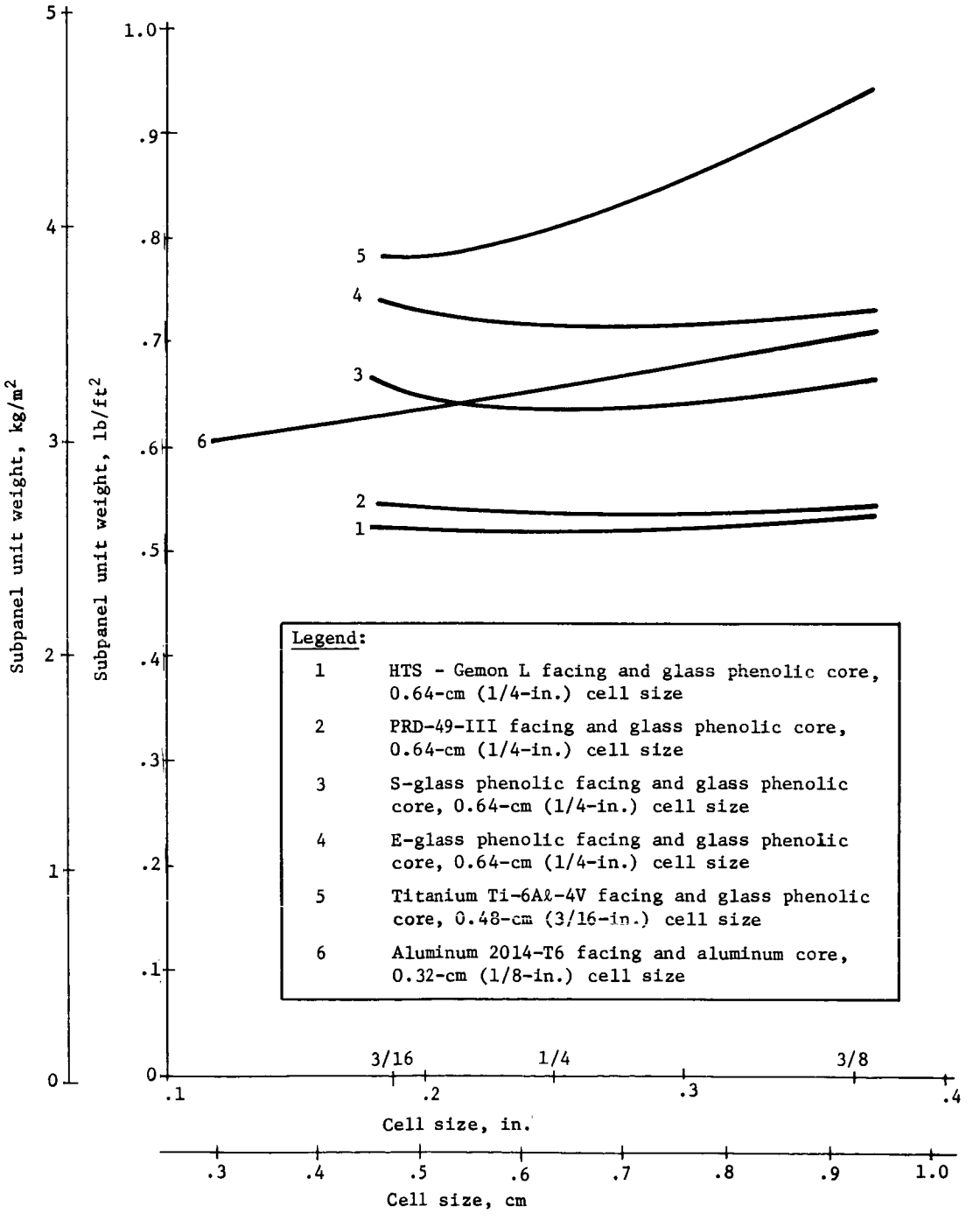

Figure 50.- Subpanel Weight vs Cell Size

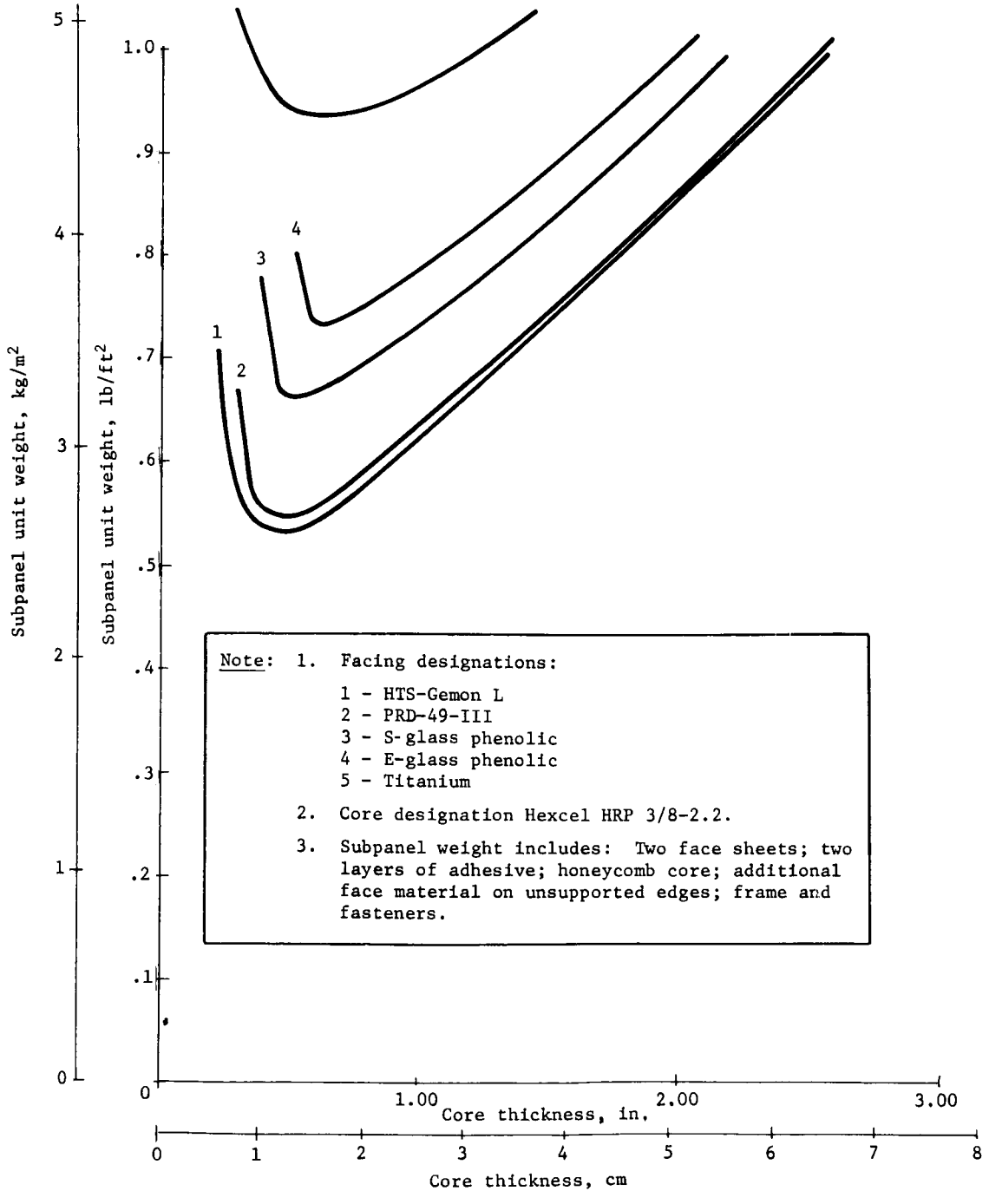

Figure 51.- Subpanel Weight vs Core Thickness

temperature for holes up to 4.8 mm (0.189 in.) in diameter. This concept is known to work on an ABM vehicle presently being flown. This means that, if a quick-disconnect fastener is used, only a small hole is required for activation, and the hole does not need to be plugged. This greatly simplifies field refurbishment and eliminates having to manufacture plugs. Our proposed panel incorporates this type of design. The present Camloc fastener has a Phillips head, but in production it would be redesigned to use an Allen head.

Refurbishment

Two 30.5x30.5-cm (12x12-in.) honeycomb panels were made. One panel had aluminum face sheets and the other panel has glass-phenolic face sheets. These two panels were used to determine if there was any difference in refurbishment time between panels with a metallic face sheet and those with a composite face sheet.

Ten ablative panels, each 2.5 cm (1 in.) thick, were then prepared using the 80/20 mixture and bonded to the subpanels. To simulate the condition of an ablative panel after flight, the panels were charred with an oxygen-acetylene torch (fig. 52). Next, the charred ablative material was removed down to the adhesive line with a modified commercial power plane (fig. 53) that could cut up to 1.3 cm (0.5 in.). To remove the remaining material, the panels were placed in an oven, heated to 422°K (300°F), and scraped with a plastic scraper. We found that heating aided the scraping operation.

Each subpanel was refurbished five times. The process plan and the direct times for each of the refurbishment operations are reported in Appendix B. These times represent the average times for the 10 refurbishments and have been factored to correspond to the refurbishment times for a 61x122x5.1-cm (2x4-ft x 2-in.) panel.

Using the data from this study we estimated the costs of refurbishing flat subpanels. These costs are itemized in tables 8 through 11, and are summarized below.

Process	Number of panels							
	1		10		100		1000	
	$/m^2	$/ft^2	$/m^2	$/ft^2	$/m^2	$/ft^2	$/m^2	$/ft^2
A, B, C, D, or E	174	16.13	148	13.73	110	10.22	73.40	6.82

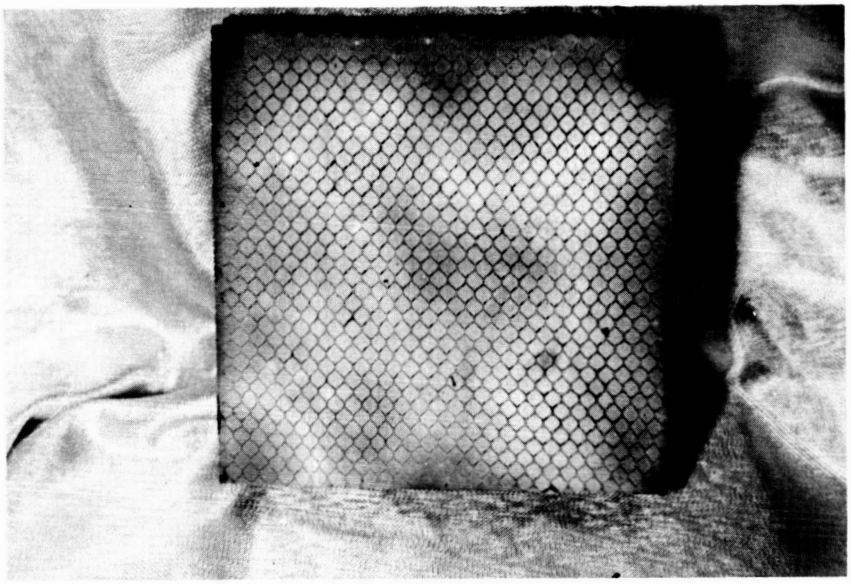

Figure 52.- Sample of Charred Ablative Panel

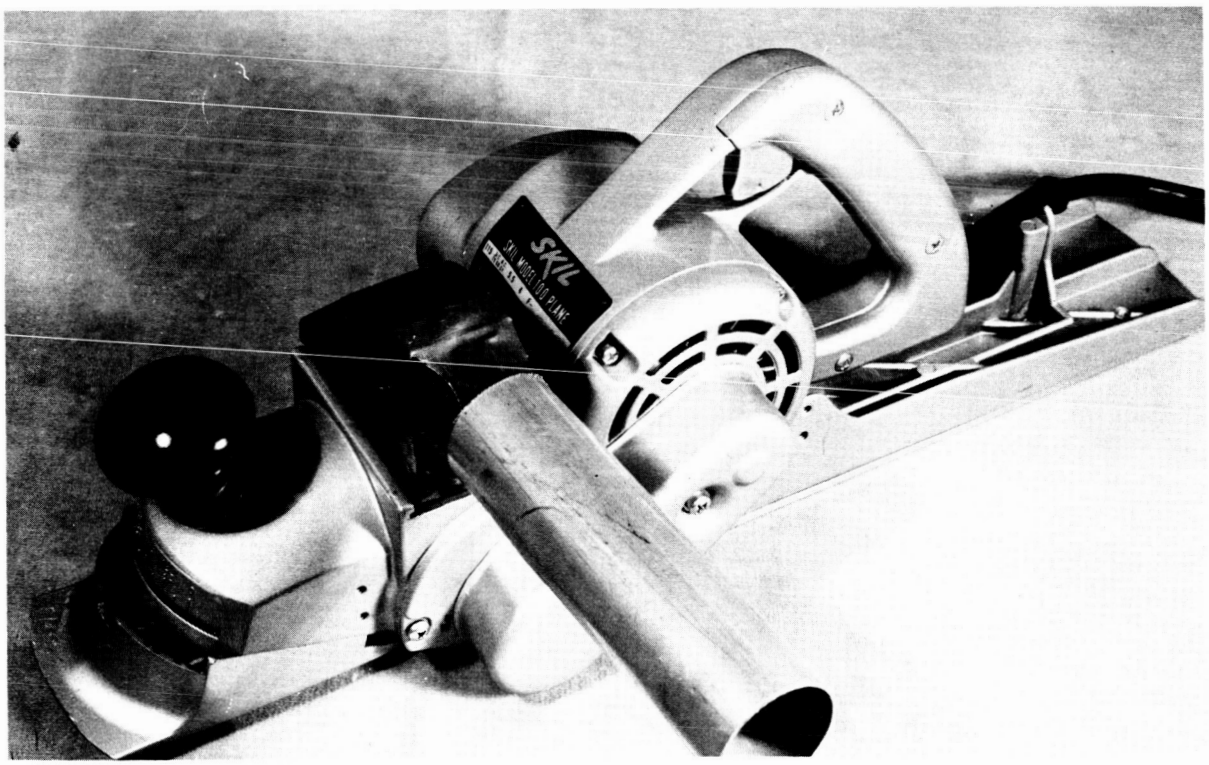

Figure 53.- Modified Commercial Plane

Bond Tensile Test

Considering the low tensile strength required between the ablator and the vehicle or subpanel, we felt that first bonding the core to a face sheet was not necessary. A test run using a silicone adhesive indicated that from 172°K (-150°F) to 533°K (500°F) the failure was in the ablator and core rather than in the bond. Above 533°K (500°F), the ablator and silicone adhesive are considered too weak; therefore, it would be necessary to first bond the reinforcement to a face sheet or subpanel with a high-temperature adhesive before loading and curing the ablative mixture. These adhesive are hard and difficult to remove for refurbishment purposes.

Therefore, to simplify refurbishment and provide adequate strength, we recommend using a secondary silicone bond to attach the ablator panel to the subpanel. The silicone bond used in this study exceeded the original NASA requirement of 6.9 kN/m^2 (1 psi) over the temperature range of 172°K (-150°F) to 533°K (500°F), as specified in RFP-L17-668.

CONCLUSIONS AND RECOMMENDATIONS

Conclusions

1. Panel costs can be substantially reduced if the honeycomb core presently being considered for the Shuttle is replaced with a lower-cost reinforcement.

2. The contractors working under previous Low-Cost Ablative Panel Fabrication contracts used similar fabrication times, but their quoted prices varied greatly.

3. The learning curve selected for the pricing estimates will greatly influence the quoted panel price. If the cost of the first panel is \$100, then the average cost for 100 panels could either be \$49.66, \$57.47, or \$71.12, depending on whether the 90%, 92%, or 95% curve were used.

4. The author believes that a 92% learning curve should be used.

5. Five different panel fabrication methods were experimentally evaluated and priced out. The most expensive method was the method developed under a previous Low-Cost Ablative Heat Shields for Space Shuttles contract (ref. 1); for 100 panels the average cost was \$963/m^2 (\$89.50/ft^2). The lowest average cost for 100 panels was \$569/m^2 (52.87/ft^2), and was obtained by using fiber reinforcement. Our recommended panel, which uses ribbon reinforcement, had an average cost of \$666/m^2 (\$61.86/ft^2) for 100 panels.

6. To eliminate the high costs involved in using honeycomb core, we developed a process for fabricating panels by using fiberglass ribbons for reinforcement instead of honeycomb core. Phenolic prepreg fiberglass ribbons using a primary bond consistently produced lighter panels than silicone prepreg ribbons.

7. Our studies showed that ablative panels containing up to 15% of 1.3-cm (0.5-in.) long fiberglass fibers could be made. This construction technique entirely eliminated the times and costs associated with using honeycomb core for reinforcement.

8. The high springback of the ablative material (up to 19%) after releasing the compacting pressure was attributed to the deformation of the microspheres.

9. The springback can be reduced by substituting glass microspheres for some of the phenolic microspheres.

10. The glass microspheres supplied by 3M contained sulfur, which inhibited the curing of the silicone resin. The glass microspheres supplied by Emerson & Cuming did not inhibit the cure.

11. Vibrating the material did not assist in moving it into the core. Impact loading was found to be a better loading method.

12. Centrifugal loading gave panels with the most uniform density from front to back, but gave a lower-density panel [0.221 gm/cm^3 (13.8 lb/ft^3), compared with the normal 0.256 gm/cm^3 (16 lb/ft^3)] for the SS-41 panels.

13. Isostatic pressure loading proved the least time-consuming method of all the techniques that were investigated.

14. Large-celled [1.9-cm (0.75-in.)] core took less time to load than the conventional 0.95-cm (3/8-in.) core. In the plasma arc tests, no difference in thermal performance could be found from using the two cell sizes.

15. Of all the filler additives tested in the plasma arc, fibers were the most beneficial in stabilizing the ablative char. These also improved the char's thermal efficiency.

16. Adding glass microspheres to the phenolic microspheres strengthened the char; but at levels above 25%, they lowered its thermal efficiency.

17. Graphite-filament face sheet composites gave the lightest subpanels. Their unit weight was only 2.54 kg/m^2 (0.52 lb/ft^2), compared with a weight of 3.52 kg/m^2 (0.72 lb/ft^2) for subpanels with a glass face sheet.

18. The test program definitely proved the feasibility of refurbishing structural subpanels combined with ablative panels. The projected average cost for 100 reusable panels was estimated to be \$110/m^2 (\$10.22/ft^2).

Recommendations

1. Continue to optimize both the ribbon-reinforced and the fiber-reinforced ablative panels. This should be done through a material charring program and an extensive plasma arc evaluation.

2. Use a refurbishable subpanel with an operating back face temperature of 533°K (500°F) for the Space Shuttle TPS.

3. Continue the subpanel design evaluations and conduct a structural test on the chosen design.

Martin Marietta Corporation
Denver, Colorado
April 24, 1972

APPENDIX A

MANUFACTURING PLAN AND TIME STUDY
FOR
FABRICATION METHOD FOR
ABLATIVE HEAT SHIELD

APPENDIX A

Materials:

A 90 pbw Phenolic Microspheres; 10 pbw Silicone Resin; standard core with Face sheet

B 50 pbw Phenolic Microspheres; 15 pbw Glass Microspheres; 10 pbw nylon powder; 25 pbw Silicone Resin; standard core with porous Face sheets

C. 50 pbw Phenolic Microspheres; 15 pbw Glass Microspheres; 10 pbw nylon powder, 25 pbw Silicone Resin; Large cell core/no Face sheet

D 50 pbw Phenolic Microspheres; 15 pbw Glass Microspheres; 10 pbw powder; 25 pbw Silicone Resin; 15 pbw glass fibers

E. 35 pbw Phenolic Microspheres; 25 pbw Glass Microspheres; 10 pbw nylon powder; 10 pbw glass fibers; 20 pbw Silicone Resin; Ribbon reinforcement construction.

Method	Setup time		Run time		A Baseline	B Update	C Pressurized core, large cell	D No core, small glass fibers	E Ribbon construction
	sec	minutes	sec	minutes					
Bond facesheet to phenolic glass (honeycomb) core, flat contoured panels, core material purchased with formed radius or flat as required									
Lay out outer surface profile of core material and holes per drawing	3.6×10^2	6.00	7.8×10^2	13.00	X	X	X		
Hand-cut core to layout using dough cutter and punch holes using (rubber type) hand punch	3.6	6.00	7.8	13.00	X	X	X		
Clean core material by blowing with dry nitrogen or filtered air.	1.8	3.00	3.6	6.00	X	X	X		
Vapor degrease core material, - submerge in vapors only			11.4	19.00	X	X	X		
Wrap core material in poly bag until use.	2.4	4.00	3.6	6.00	X	X	X		
Wipe tools with safety solvent to clean and prepare for bond, apply release agent to tool, mold tools required			67.8	113.00	X	X			
Remove prepreg from refrigerator			3.6	6.00	X	X			
Let warm to room temperature, hand cut 2 pieces of prepreg to suit mold tool (2 thickness required)	3.6	6.00	22.8	38.00	X				
Warm up prepreg, cut 1 ply	3.0	5.00	3.0	5.00		X			
Start panel layup, lay prepreg on tool, roll out wrinkles, strip protective film from prepreg and apply second layer same as first.	7.8	13.00	11.4	19.00	X				
Layout prepreg on tool and smooth out wrinkles	.6	1.00	1.2	2.00		X			
Install mold on top of prepreg layup	.6	1.00	.6	1.00	X	X			
Install clean honeycomb core material on prepreg layup on tool		6.00	3.6	6.00	X	X			
Place bleeder cloth (fiberglass) over core material			3.6	6.00	X	X			
Apply vacuum bag over assembly, seal with tape and pull full vacuum	3.6	6.00	22.8	38.00	X	X			
Place vacuum sealed assembly into oven	3.0	5.00	3.0	5.00	X	X			
Cure at 436°K (325°F) for 7200 sec (2 hr) at temperature					X	X			

APPENDIX A

Method	Setup time		Run time		A Baseline	B Update	C Pressurized core large cell	D No core, small glass fibers	E Ribbon construction
	sec	minutes	sec	minutes					
Remove assembly from oven and let cool under vacuum to 338°K (150°F) minimum before removing assembly to cool			7.8×10^2	13.00	X	X			
Hand drill 0.0031 m (1/8 in.) dia. holes thru face sheet at (approx.) center of each honeycomb cell, approximatly 7000 holes in panel, require special carbide drills, plus 6 attachment holes, 0.0015 m (1/16 in. holes at 1/sec)	3.6×10^2	6.00	87.0	145.00	X				
Wrap subassembly in kraft paper until used	2.4	4.00	3.6	6.00	X	X			
Dry phenolic microspheres material 7200 sec (2 hr) at 355°K (180°F) under vacuum in a solids processor	3.6	6.00	7.8	13.00	X	X	X	X	X
Allow material to cool to 333°K (140°F) under vacuum before removing from processor			7.8	13.00	X	X	X	X	X
Screen phenolic microspheres to remove conglomerates.	1.8	3.00	3.0	5.00	X	X	X	X	X
Store phenolic microspheres material in a desiccated sealed container when not used immediately				5.00	X	X	X	X	X
Measure tool to determine volume in cubic inches	1.2	2.00	3.0	5.00	X	X	X	X	X
Determine total material required to fill mold	.6	1.00	3.0	5.00	X	X	X	X	X
Break total material figure down into required percentages for appropriate panel formulation.	.6	1.00	3.0	5.00	X	X	X	X	X
Weigh out appropriate materials	3.0	5.00	12.0	20.00	X	X	X	X	X
Weigh silicone resin and catalyst into a small planetary mixer	7.8	13.00	11.4	19.00	X	X	X	X	X
Add equal amount of heptane to mixer as silicone resin and catalyst	7.8	13.00	7.8	13.00	X				
Mix for 600 sec (10 minutes)			7.8	13.00	X	X	X	X	X
Place weighed amount of dry phenolic microspheres into large planetary vacuum mixer, add half of mixed resin and catalyst mixture to phenolic microspheres and mix 120 sec (2 minutes)	3.6	6.00	22.8	38.00	X				
Add remainder of resin and catalyst mix to phenolic microspheres	3.6	6.00 mix	7.8 22.8	13.00 38.00	X				
Apply full vacuum to mixer and mix for additional 2700 sec (45 minutes)	7.8	13.00	37.8	63.00	X				
(This operation flashes off solvent)									
Slowly add dry phenolic microspheres to resin catalyst mixture until small planetary is full	1.2	2.00	7.8	13.00		X	X	X	X
Place remaining phenolic microspheres into large Hobart planetary along with resin/catalyst/wetted phenolic microspheres mixture; be sure to scrape small planetary beater and pot, mix for 300 sec (5 minutes)	1.2	2.00	6.00	10.00		X	X	X	X
Add fibers to mixer and mix for 300 sec (5 minutes)	.6	1.00	3.0	5.00				X	X

APPENDIX A

Method	Setup time		Run time		A Baseline	B Update	C Pressurized core large core	D No core, small glass fibers	E Ribbon construction
	sec	minutes	sec	minutes					
Add appropriate amount of glass bubbles to mixer and mix for 300 sec (5 minutes)						X	X	X	X
Add appropriate amount of nylon powder to mixer and mix for 300 sec (5 minutes)	0.6×10^2	1.00	3.0×10^2	5.00		X	X	X	X
After ingredients are mixed, check for excess conglomerates in mix, fibers gathered on pot wall or on beater, resin/catalyst concentration on bottom of mixer pot.	.6	1.00	.6	1.00		X	X	X	X
Blow panel subassembly clean with dry nitrogen or filtered air.	1.8	3.00	3.6	6.00	X	X	X		
Remove wrappings from core							X		
Spray primed panel and core with DC1200 silicone primer	7.8	13.00	15.0	25.00	X				
Allow primer to dry 7200 sec (2 hr) minimum to 43,200 sec (12 hr) maximum					X				
Record data and time panel was primed	1.8	3.00	7.8	13.00	X				
Mix wet coat, mix 90% silicone resin, 10% catalyst and heptane equal to 10% of resin and catalyst in a small planetary mixer for 600 sec (10 minutes)	7.8	13.00	15.0	25.00	X				
Spray wet coat mixture on inside of honeycomb core, four coats required, two cross coats each direction	3.6	6.00	22.8	38.00	X				
Dip panel with phenolic, allow to drain, place in 338°K (150°F) oven for 1800 sec (30 minutes)	3.6	6.00				X	X		
Clean panel, cure, frame tool			15.0	25.00	X	X	X	X	X
Apply fiberglass bleeder cloth on tool (2-ply)	1.8	3.00	3.6	6.00	X	X	X	X	X
Spray bleeder cloth with Teflon release agent	1.8	3.00	7.8	13.00	X				
Place mold on top of bleeder cloth	1.2	2.00	3.0	5.00	X	X	X	X	X
Position core panel with face sheet on bleeder cloth on tool			3.6	6.00	X	X			
Install picture frame part of tool	1.8	3.00	3.6	6.00	X	X	X	X	X
Weigh out appropriate amount of material for given panel	2.4	4.00	2.4	4.00			X	X	X
Place all material into mold and spread evenly, lightly hand pack with wooden tamper	.6	1.00	2.4	4.00				X	X
Place ablative material between side frame of tool and panel edge; pack ablative material around attachment holes	5.4	9.00	15.0	25.00	X	X			
Place trap door over layup	.6	1.00	.6	1.00	X	X			
Weigh mixture out and place amount of mix on assembly to fill core and extend above core approximatly 0.012 m (½ in) after spreading evenly inside picture frame part of tool	7.8	1.00	.6	1.00	X	X			
Remove trap door and press material into honeycomb by hand with wooden tamper	.6	1.00	3.0	5.00	X	X			

APPENDIX A

Method	Setup time		Run time		A Baseline	B Update	C Pressurized core large core	D No core, small glass fibers	E Ribbon construction
	sec	minutes	sec	minutes					
Place an additional 0.012 m (½ in) material into picture frame, spread evenly and press into honeycomb with wooden tamper until all cells are filled tightly and evenly compacted	0.6×10^2	1.00	3.0×10^2	5.00	X	X			
Fill mold (not picture frame) with material, spread evenly and lightly handpack with wooden tamper	.6	1.00	1.8	3.00			X		
Place honeycomb on top of material and place layup onto a hydraulic press	.6	1.00	1.2	2.00			X		
Using hydraulics, slowly press honeycomb into ablative material until flush with top of mold	.6	1.00	9.0	15.00			X		
Remove layup from press and install top picture frame onto mold	.6	1.00	.6	1.00			X		
Add balance of mixture and spread evenly over area of assembly	1.8	3.00	7.8	13.00	X	X	X		
Remove top picture frame part of tool and cover mixture with (1 ply 181 glass cloth, 1 ply bleeder cloth, in that order), cloths to extend over edges of mixture and assembly down to and mate with bottom bleeder cloth	7.8	13.00	18.6	31.00	X	X	X	X	X
Place vacuum bag over assembly, seal and pull full vacuum	3.6	6.00	22.8	38.00	X	X	X		
Place vacuum bag over assembly, seal and pull 50 640 n/m^2 15 in. Hg (½ vacuum)	3.6	6.00	22.8	38.00				X	X
Vibrate assembly to settle mixture into or 0.0015 m (1/16 in.) above core material using rivet bucking air tool with a large head	1.8	3.00	11.4	19.00	X		X		
Apply 6.89×10^5 n/m^2 100 psi autoclave pressure to part while under full vacuum	3.0	5.00	6.0	10.00		X			
Caution--do not crush core.									
Place assembly and tool into oven and cure 57 600 sec (16 hr) at 394°K (250°F) under full vacuum			7.8	13.00	X	X	X		
Cure assembly 57 600 sec (16 hr) @394°K (250°F) under 50 640 n/m^2 15 in. Hg								X	X
Remove assembly from oven and cool under vacuum to 340°K (150°F) minimum before removing assembly from tool			7.8	13.00	X	X	X	X	X
Use wood hand plane and remove excess material down to core 0.0508 m (2 in.), finish by sanding with 80-grit emery cloth	2.4	4.00	48.6 45.6	(C) 81.00 (F) 75.00	X	X	X	X	X
Saw periphery of assembly per layout on band saw and take density			22.8 30.0	(F) 38.00 (C) 50.00	X	X	X	X	X
Slice trimmed panel into 0.013 m (½ in.) strips, using band saw	1.2	2.00	6.0	10.00					X
Air clean 0.013 m (½ in.) ablator strips	.6	1.00	6.0	10.00					X
Cut required number of 91 ld strips to fit laminating tool	3.0	5.00	18.0	30.00					X
Lay up billet in side laminating tool: (a) ablator strip, (b) 91 ld strip, (c) ablator strip, (d) 91ld strip, etc.	.6	1.00	18.0	30.00					X

APPENDIX A

Method	Setup time		Run time		A Baseline	B Update	C Pressurized core large core	D No core, small glass fibers	E Ribbon construction
	sec	minutes	sec	minutes					
Install spacers at each end of tool, and wrap entire tool in bleeder cloth. Bag entire assembly and pull vacuum ensuring that spacers push billet into tool from each end.	1.8×10^2	3.00	15.0×10^2	25.00					X
Place layup into autoclave and cure under full vacuum for 7200 sec (2 hr) @ 436°K (325°F) with 35 psi additional autoclave pressure	3.0	5.00	3.0	5.00					X
Allow to cool for 3600 sec (1 hr) after cure is complete	.6	1.00	3.0	5.00					X
Remove cured panel from tool, trim to desired dimensions and take density record	1.8	3.00	36.0	60.00					X
Carbide tipped saw blades required and dust collector equipment saw									
Remove Teflon tooling plugs from assembly			7.8	13.00	X	X			
Open pilot holes at plug locations to drawing dimensions through face	1.8	3.00	3.6	6.00	X	X			
Drill attachment holes	3.6	6.00	10.8	18.00			X	X	X
Spray one coat of silicone dispersion (DC92007) on complete assembly	1.8	3.00	15.0	25.00	X	X	X	X	X
Allow assembly to air dry at room temperature for 86.4×10^{-3} sec (24 hr)					X	X	X	X	X
Place assembly in plastic bag and identify	3.6	6.00	11.4	19.00	X	X	X	X	X
Fabricate a small section of material along with flat panel for making plug fillers for shipping with assemblies to fill tooling plug holes on installation	7.8	13.00	22.8	38.00	X	X	X	X	X
Grind or plane to core material thickness	2.4	4.00	30.0	50.00	X	X	X	X	X
Saw outer surface 0.019 m (0.75 in.) dia x core thickness for turning to size on lathe			7.8	13.00	X	X	X	X	X
Make setup on lathe to grind outside diameter to drawing diameters or fit of panel holes (use live center one end and sandpaper opposite end to hold in lathe)	22.8	38.00	45.0	75.00	X	X	X	X	X
One plug required for each hole on panel									
Spray sealer on plugs same as panel assembly	1.8	3.00	11.4	19.00 (16 plugs)	X	X	X	X	X
Place plugs into plastic bag, seal and identify with type of plug material or type assembly	3.6	6.00	11.4	19.00	X	X	X	X	X
			Total setup hrs. panel-----		5.1	3.8	3.0	2.5	2.9
			Total setup sec x 10^{-3}		18.4	13.7	10.8	9.0	10.44
			Total run hrs. ----------		24.6	16.6	12.9	10.9	13.8
			Total run sec x 10^{-3} ------		88.6	59.8	46.4	39.2	49.7

APPENDIX B

FABRICATION METHOD FOR REFURBISHING ABLATIVE HEAT SHIELD, 61x122x5.1 cm (2x4 ft x 2 in.) FLAT PANEL

Method	Limited tooling				Optimum tooling			
	Panel setup time		Panel run time		Panel setup time		Panel run time	
	sec	minutes	sec	minutes	sec	minutes	sec	minutes
Get and position used panel, pick up planer tool and make three cuts 1.3 cm (0.5 in.) deep	3.6×10^{-2}	6.00	15.6×10^{-2}	26.00	27×10^{-2}	45.00	1.2×10^{-2}	2.00
Pick up planer tool and make one cut 0.64 cm (0.25 in.) deep	1.2	2.00	5.3	8.80	1.2	2.00	4.2	7.04
Pick up planer tool and make one cut >0.64 cm (0.25 in.) deep	1.2	2.00	8.7	14.51	1.2	2.00	7	11.68
Place panel into oven. Bake for 30 minutes and remove from oven	2.4	4.00	3.7	6.25	2.4	4.00	3	5.00
Hand scrape remaining ablative material from aluminum structure	1.2	2.00	16.2	27.00	1.2	2.00	13	21.60
Rebond. Weigh and mix adhesive, spread adhesive, place new ablative panel onto aluminum structure frame, bag panel, pull vacuum, seal, place panel into oven, bake 394°K (250°F) for 3600 sec (1 hr), cool oven to 322°K (120°F), remove panel from oven, remove bag, clean panel and place finished panel into temporary storage	9	15.00	48	80.00	9	15.00	41	68.00
TOTAL SETUP TIME		1800 sec (30 min)				4320 sec (1.2 hr)		
TOTAL RUN TIME		9720 sec (2.7 hr)				6840 sec (1.9 hr)		

REFERENCES

1. Chandler, Huel H.: Low-Cost Ablative Heat Shields for Space Shuttles. NASA CR-111800, October 1970.

2. Norwood, L. B.; and Cuzzupoli, J.: Low-Cost Ablative Heat Shield for Space Shuttles. NASA CR-111795, November 1970.

3. Dulak, R. E.; and Cecka, A. M.: Low-Cost Ablative Heat Shields for Space Shuttles. NASA CR-111814, 1970.

4. Abbott, Harry T.: Low-Cost Fabrication Method for Ablative Heat Shield Panels for Space Shuttles. NASA CR-111835, 1970.

5. Freeder, Herman; and Smith, W. N.: Low-Cost Ablative Heat Shields for Space Shuttles. NASA CR-111874, 1970.

6. Sullins, R. T.: Manual for Structural Stability Analysis of Sandwich Plates and Shells. NASA CR-1457, 1962.

N72-23499

THIS PAGE IS UNCLASSIFIED

ERRATA

NASA Contractor Report 112045

INVESTIGATION OF LOW-COST ABLATIVE HEAT SHIELD FABRICATION FOR SPACE SHUTTLES

By Huel H. Chandler
February 1972

Page 2: In line 4 of paragraph 3, change "hogh-elastic-modulus" to read "high-elastic-modulus".

Page 4: In line 1 of paragraph 1, change "Leaf Shields" to read "Heat Shields".

Page 23: In line 5 of the last paragraph, change "1.3-cm (0.5-in.) E-glass fibers" to read "0.65-cm (0.25-in.) E-glass fibers".

Page 40: In the first column, headed "Model data", change the description of the eighth composition from "1.3-cm glass fibers, type E, pbw" to read "0.65-cm (0.25-in.) glass fibers, type E, pbw".

Page 41: In the first column, headed "Model data", change the description of the eighth composition from "1.3-cm glass fibers, type E, pbw" to read "0.65-cm (0.25-in.) glass fibers, type E, pbw".

Page 58: Under "Cross-Sectional View", change General Comments from "very distinctive (1/2-in. thick)" to read "very distinctive [1.3-cm (1/2-in.) thick]".

Page 61: Under "Cross-Sectional View", change the second line of the General Comments from "a very low temperature (below 1500°F)" to read "a very low temperature [below 1090°K (1500°F)]".

Page 94: In line 2 of conclusion 7, change "1.3-cm (0.5-in.) long fiberglass fibers" to read "0.65-cm (0.25-in.) long fiberglass fibers".

Issue date: 9-14-72

THIS PAGE IS UNCLASSIFIED